FOREWORD

This research program was initiated 1 February 1960 by the Flight Control Laboratory, Aeronautical Systems Division. The work reported herein has been supported primarily under Contract AF 33(616)-6846, Project No. 8219, Task No. 821901. Mr. H. Max Davis is the cognizant Air Force Project Engineer. The authors wish to express their gratitude to Mr. Davis for his encouragement throughout this research effort, and to Mr. Charles Miller and Dr. Richard Oman of Grumman for their aid in the development of the instrumentation. In addition, the authors gratefully acknowledge the assistance of Mr. Richard Jenkins of Grumman in all phases of this project.

ABSTRACT

An experimental program was undertaken in the Grumman Hypersonic Shock Tunnel at nominal Mach numbers of 12 and 19 to measure the changes in the pressure distributions on two basic wing planforms due to distortions in their profile shape. The models included three rectangular planform wings with a flat profile, a circular-arc cambered profile, and a profile with symmetrical linear twist, and three 70° delta planform wings with a flat profile, a circular-arc cambered profile, and a sine-wave cambered profile. Angle of attack was varied from 0 to 15°. Data are presented in both tabular and graphical form.

Appended to this report is a description of the tunnel calibration procedures, and a description of the development of a Grumman-designed piezoelectric pressure transducer employed in obtaining the data.

PUBLICATION REVIEW

This report has been reviewed and is approved.

FOR THE COMMANDER:

Charles B. Westbrook
Branch Chief
Flight Control Laboratory

TABLE OF CONTENTS

LIST OF ILLUSTRATIONS

LIST OF ILLUSTRATIONS (Cont.)

LIST OF ILLUSTRATIONS (Cont.)

LIST OF ILLUSTRATIONS (Cont.)

LIST OF ILLUSTRATIONS (Cont.)

LIST OF ILLUSTRATIONS (Cont.)

LIST OF ILLUSTRATIONS (Cont.)

LIST OF ILLUSTRATIONS (Cont.)

LIST OF TABLES

INTRODUCTION

A vehicle traveling at very high speeds in the earth's atmosphere experiences heating and high aerodynamic forces which may distort the vehicle structure sufficiently to produce a significant change in the aerodynamic loading. The program reported herein was undertaken to obtain experimental hypersonic pressure data on a variety of distorted thin wings.

The tests were carried out in the Grumman Hypersonic Shock Tunnel. Because of the extremely short testing times generally available in shock tunnels, standard pressure instrumentation could not be used. Sufficiently sensitive transducers were not commercially available in a size small enough so that 20 or more could be placed within a thin wing. To our knowledge no one had attempted to measure the static pressure on thin wings in a shock tunnel at the time this program was initiated. It was necessary to design and develop a transducer capable of doing the job.

This program, therefore, had a twofold purpose: to advance the state-of-the-art in shock tunnel testing so that many static pressures could be obtained simultaneously over thin wings, and to obtain data of sufficient accuracy with these transducers to determine the effects of basic distortions of the wings at hypersonic speeds.

Six models were constructed, three of rectangular planform, and three of delta planform with a leading edge sweep angle of 70°. The rectangular wings included a basic flat wing, a symmetrical linear twist, and a circular-arc camber. The delta wings included a basic flat wing, a circular-arc camber, and a sine-wave camber. All wings were tested at nominal Mach numbers of 12 and 19 at two Reynolds numbers. Twenty pressure transducers were located within each rectangular wing and 16 within each delta wing to measure pressures over the lower wing surfaces only.

Manuscript released by the authors February 15, 1962 for publication as an ASD Technical Documentary Report.

TEST PROGRAM

Models

Two basic planforms were chosen for this investigation: a rectangular wing with a 6" span and a 4-1/2" chord, and a 70° delta wing with a 6" span. Three models of each planform were constructed.

Rectangular Wings

The three rectangular models included a flat profile, Fig. 1, p. 82, a symmetrical linear twist with 5° twist at the tips, Fig. 2, p. 82, and a circular-arc cambered profile with a maximum camber of 5° at the leading edge, Fig. 3, p. 84. A plot of the spanwise variation of angle of attack for the twisted wing is shown in Fig. 2b, p. 83. Ordinates of the cambered wing are tabulated in Fig. 3a, p. 84, and the chordwise variation of angle of attack due to camber is plotted in Fig. 3b, p. 85. The leading edge was originally a symmetrical wedge with a 25° semiwedge angle, and the total wing thickness was 3/8". Twenty pressure transducers were located within each model, as shown in Fig. 4, p. 86. Pressures were measured on the bottom surfaces only as explained under Instrumentation. A removable cover plate 1/32" thick extended over the upper surfaces to provide access to the gauges. Initial runs showed that the wing flexure under load was picked up by the transducers. The models were stiffened by increasing the thickness of the cover plate to 1/4", resulting in a total model thickness of 19/32". The wings as finally tested were therefore unsymmetrical about the chordal plane. Photographs of the three rectangular models as tested are shown in Figs. 5 through 7, pp.87 through 89.

70° Delta Wings

The three delta wings included a flat, undistorted profile, a circular-arc profile, with 5° maximum camber, and a sine-wave cambered profile also with 5° maximum camber. Figures 8 through 10, pp. 90 through 92, show sketches of these wings along with ordinates of the cambered profiles. The chordwise variation of angle of attack due to the circular arc camber is the same as shown in Fig. 3b, p. 85 for the rectangular wing. Figure 10b, p. 93 shows this variation for the sine-wave cambered wing. The

location of the 16 pressure transducers in these models is shown in Fig. 11, p. 94, and photographs of the three models are shown in Figs. 12 through 14, pp. 95 through 97. These models also were stiffened by increasing the cover plate thickness. As a result, the leading edges, originally constructed with a 25° semi-wedge angle normal to the leading edge, were unsymmetrical about the chordal plane.

The triangular pieces at the trailing edges of all six models are fairings to cover the special low-noise cables from the pressure transducers as they enter the sting. A total of 40 cables had to be taken from each rectangular model, and 32 from each delta wing model through these fairings. All of the leading edges were removable to facilitate replacement in the event of damage, and to allow different leading-edge configurations to be tested at a later date. The chordal plane of the wings was displaced 1/8" below the sting centerline to reduce the possibility of sting interference on the lower surfaces. The tunnel angle of attack was taken as the angle between the horizontal plane and the chordal plane of the undistorted wings. For each model, algebraic addition of the angle of attack due to the distortion and the tunnel angle will therefore yield the local angle of attack at any point.

Tunnel Test Conditions

All tests were performed in the Grumman Hypersonic Shock Tunnel. This tunnel has a steel driver section 20' long, with a 5" inside diameter and a 16" outside diameter. The steel driven section is 100' long with a 3" inside diameter and a 9-1/4" outside diameter, terminated by a converging-diverging conical nozzle with a 25° total angle and an exit diameter of 18". The nozzle throat section is replaceable in order to vary the Mach number. The test section is at the forward end of a 20" square, 15' long dump tank. Figure 15, p. 98, is a photograph showing the downstream end of the driven section, the nozzle, the dump tank, and some of the instrumentation.

In operation, a thin copper wire crimped every 12" is mounted along the centerline of the driver tube. The driver is then loaded with a stoichiometric mixture of hydrogen and oxygen diluted with 80 per cent helium. A capacitor bank charged to 9000 volts is discharged, sending 632 joules through the wire and "exploding" it simultaneously at each crimp. The resulting

combustion builds up the driver pressure and temperature until a metal diaphragm, separating the driver and driven tubes, bursts sending a strong shock wave through air originally contained in the driven tube. The shock-processed air expands through the nozzle producing hypersonic conditions in the test section for 2 to 4 milliseconds. The dump tank is evacuated prior to each run to below 10 microns to facilitate nozzle starting.

A complete description of the tunnel and associated equipment may be found in Ref. 1. A description of the tunnel calibration procedure and the results obtained for M=12 and M=19 are given in Appendix I. The results are summarized in Table I, p. 22.

An accurate survey of the flow angularity in the test section has not been made. However, we have taken schlieren photographs of a rake consisting of several parallel rods aligned with the centerline of the nozzle, with small spheres mounted on the ends. Analysis of the unsymmetrical shock wave angles from these spheres indicates the angularity 2" from the nozzle exit to be approximately 1.4° per inch normal to the tunnel centerline. The symmetry of the tunnel flow was investigated by measuring pressures on a 70° cone at two points located symmetrically above and below the tunnel centerline. The measured pressure coefficients agreed within 2 per cent. Pressure on a flat plate at angle of attack also agreed when the model was inverted.

Instrumentation

Because of the extremely short times available to obtain reliable data in the shock tunnel, all of the instrumentation must have a rise time of less than 1 millisecond. For these tests the instrumentation both for the tunnel and the models consisted of piezoelectric pressure transducers, whose outputs were recorded on electronic oscilloscopes.

Tunnel Instrumentation

Speed of the shock wave in the driven tube, tunnel stagnation pressure, driver pressure, and test section pitot pressure were recorded for each run using commercially available Kistler SLM quartz pressure transducers.

Several of these gauges are mounted at known intervals near the nozzle end of the driven section. The output for each is differentiated and displayed on a Tektronix 535 oscilloscope programmed to provide a raster giving an extended time interval at a high rate of sweep. Accurate timing marks are also displayed on the raster from a Tektronix Type 181 Time Mark generator. By this system we are able to determine the shock wave speed to an accuracy of ±1 per cent. The most upstream gauge is used as a trigger source for all scopes. A typical record is shown in Fig. 16, p. 99. The trace starts in the lower left-hand corner, and sweeps alternately from left to right then right to left. The large pips in the down direction are 100 microsecond time marks and the small pips are 10 microsecond marks. The pips in the upward direction are the differentiated outputs from the time-of-arrival gauges in the tube.

One Kistler gauge is located 2-3/4" upstream of the nozzle throat to record the tunnel stagnation pressure. Its output is recorded along with the pitot pressure in the test section as shown in the typical record of Fig. 17, p. 99. From the known shock speed, stagnation pressure, and pitot pressure, the conditions for each run may be calculated (see Appendix I). The driver pressure is monitored on another oscilloscope in order to determine the smoothness of combustion, and the diaphragm bursting pressure.

Model Instrumentation

Although the Kistler gauge is quite adequate for use in the high-pressure sections of the tunnel and for measurements of the test section pitot pressure and tunnel stagnation pressure, its sensitivity is not sufficient nor is its size small enough to be used to measure static pressures on slender models. As no commercial gauge was available to fill our particular needs, a satisfactory gauge was necessarily developed. Details of the development program and the calibration procedures employed are given in Appendix II.

Figure 18, p. 100 is a photograph of one of the transducers used and Fig. 19, p. 100 shows some of the gauges mounted in the flat 70° delta wing model. The output of each of the transducers mounted in a model was fed through special low-noise cables to a Tektronix 122 preamplifier modified to have an input impedance of 100 megohms. From the preamps each output was fed to one channel

of a four-channel Model ES-142 Newton Co. electronic switch. Each switch has two output channels, carrying two signals each, which are fed to the two beams of a Tektronix 502 oscilloscope, thus displaying four data traces per scope. Therefore, for the 20 data channels, 5 oscilloscopes, 5 electronic switches, and 20 preamplifiers were required. Each channel was filtered between the preamp and switch by specially built fourth-order 3000 cps filters. All transducers were calibrated through the same preamp and switch as used during the runs. The over-all accuracy of the recording system is within ±2 per cent as specified by the manufacturer.

Schlieren System

Schlieren photographs of each run were taken with a Grumman designed, double-pass system. The use of a spherical mirror (of 12" diameter) with a 33' radius of curvature reduces parallax to satisfactory proportions. Both black and white and color schlierens were obtained on 35 mm film by use of a 1000 mm lens. The light source is a high-pressure mercury vapor lamp with a flash duration of about 10 microseconds.

Run Schedule

The schedule of runs at M=12 and M=19 is given in the list of test conditions of Table II, p. 23. Many of the runs were repeated when results indicated this to be desirable.

Data Reduction

The measured value of the tunnel stagnation pressure, p_5, was used to obtain the variation in free stream static pressure from the nozzle calibration curve of p_∞/p_5 vs. the distance along the tunnel centerline, (Appendix I). The data were then corrected to the leading edge conditions by the method of Ref. 2, which is essentially a buoyancy correction:

$$\left(\frac{p_{meas.}}{p_\infty}\right)_{corrected} = \frac{p_{meas.}}{p_{\infty_{L.E.}}} + \frac{\left[p_{\infty_{L.E.}} - p_{\infty_{local}}\right]}{p_{\infty_{L.E.}}}$$

where $p_{\infty_{local}}$ is the free stream static pressure at the given tap location. The corrected pressure ratios were then converted to standard pressure coefficients:

$$c_p = \frac{2}{\gamma_\infty (M_{\infty_{L.E.}})^2} \left[\frac{p_{meas.}}{p_\infty \text{ corrected}} - 1 \right] .$$

The free stream ratio of specific heats, γ_∞, was taken to be 1.4.

DESCRIPTION OF TESTS AND PRESENTATION OF DATA

Initial Runs and Mounting Problems

During the initial runs, many problems developed, necessitating changes in gauge mounting in the thin models. At first, the gauges were rigidly mounted in the flat rectangular wing. The lower copper ring of the gauge was in direct contact with the model, and the gauge was held in place by metal washers as shown in the sketch below. We had expected that the large mass of the

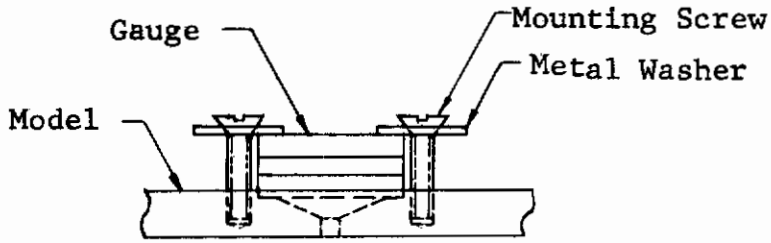

sting and sector and its inherent stiffness would prevent noticeable vibration or acceleration signals below the 3000 cps range (all frequencies above 3000 cps were filtered out). In fact, this mounting had been tested successfully in a prototype model. However, the results of the first runs, employing the thin rectangular wing, were highly erratic, and we discovered that the flexing of the model under load was introducing mechanical strain in the transducers. A sample record showing four traces is shown in Fig. 20, p.101. This did not occur in the prototype model since it was smaller, thicker, and hollowed out only in the immediate vicinity of the transducer.

After a considerable amount of experimenting, two major changes were made. A heavier cover plate was built to add stiffness to the model and thus reduce the amount of flexure, and the gauge mounting was changed in order to decouple the gauges from the model. Several different schemes were investigated with regard to the latter change with the result that half of a rubber "O"-ring was placed between the gauge and the model, and the metal hold-down washers were replaced with thin plastic. These changes resulted in a decided improvement, as can be seen from the sample traces in Fig. 21, p.101, and all of the models and transducers were modified accordingly.

An extensive recalibration then took place to determine the effects of the new mounting arrangement on gauge response. During this time, the calibration procedure described in Appendix II was worked out and refined, and the isolation of the test section from the shock tube recoil was improved.

All gauges were then remounted in the flat rectangular wing using the new mounting scheme and runs began. The improved isolation had a decided improvement on the high frequency noise, as shown in Fig. 22, p.102. Some of the gauges still showed some unwanted acceleration effects, notably a low-frequency (600 cps), high-amplitude signal superimposed on the pressure trace, also apparent on the traces shown in Fig. 22. After further experimentation, we replaced the half "O"-ring under each gauge with a soft rubber washer 1/32" thick. This virtually eliminated the low-frequency signal, and all tests were run with this mounting. An example of the gauge response with this final mounting is shown in Fig. 23, p.102.

Over 60 runs were made with the flat rectangular wing to develop the final improvements to the pressure measuring system and to explore repeatability. Before pulling the model, we mounted tip extensions which increased the model span by 3" at each tip in order to obtain additional information pertaining to the pressure distribution in the region of the tip. Figure 24, p.103 shows a photograph of the model with the extensions in place. We also interchanged transducers in the leading edge region to explore more fully some of the differences in pressures measured there. Other models were tested less extensively.

A photograph of the 70° delta sine-wave wing mounted in the test section is shown in Fig. 25, p.104. The pitot probe is visible in the upper part of the picture.

Presentation of Data

All data are tabulated as pressure coefficients in Tables III through VI beginning on p. 25. In the tables, the configuration, angle of attack, and tap location (given as per cent chord and per cent semispan) are indicated. Data points have been crossed out wherever they were considered to be in obvious error. Blank entries in the tables indicate that no data were obtained for those points. The double entry in the tables for the rectangular wings is for the two tip points nearest the leading edge and serve as a check on the symmetry of the pressures about the wing centerline.

Plots of C_p vs. x/c for various spanwise stations and at various angles of attack for the rectangular wings, and plots of C_p against x/c_{Root} where c_{Root} is the chord at the model centerline for the delta wings are presented in Figs. 26 through 47 starting on p.105. Typical schlieren photographs are presented in Figs. 48 through 58, starting on p.147.

DISCUSSION OF EXPERIMENTAL RESULTS

This program has proven the feasibility of measuring the pressure distribution over thin wings in the short testing times available in a shock tunnel. There are certain refinements to the instrumentation techniques which should be made before completely satisfactory data can be obtained for all conditions. Most of these refinements concern the design of the pressure transducers and are discussed in Appendix II.

Data Accuracy

It is difficult to estimate the absolute accuracy of the data presented. The transducers and the technique used to mount them were such that uniformly noise-free outputs were not always possible, especially in the portions of the models where the gauges were crowded closely together. On the delta wing models it was virtually impossible to prevent some of the cables from touching portions of other gauges, thus adding to the noise problem. In fact, it was necessary to eliminate 4 of the gauges from the delta wing models in order to obtain acceptable data from the remaining 16.

The widest discrepancies in the data were obtained for the points nearest the leading edges of the models. As can be seen from the shock-expansion curve of Fig. 63, p.157 the pressures on the leading-edge-wedge surface are almost an order of magnitude greater than those back on the wing. Because the points near the leading edge are in a region of very steep pressure gradient, it can be expected that a wider variation in measured pressures might be obtained. In order to investigate this more fully and to ascertain whether gauge error was contributing to the problem, we made several runs at M=12 on the flat rectangular wing with the leading-edge gauges interchanged. The results presented in Fig. 59, p.153 show that these differences cannot be attributed to the transducers. In this figure, the pressure coefficients are plotted against the per cent semispan measured from the wing centerline. The square symbols show the data obtained with the original gauge mounting, and the circles show the results after interchanging the gauges. The scatter is about normal for the leading-edge gauges as can be seen from the repeated points for the original mounting.

The traces from the gauges mounted in the tip region of the rectangular wings contained more noise than the others in these wings. Because these gauges were mounted in extremely close proximity to the edge of the model, we wanted to determine whether the increased noise from the cramped mounting was causing an appreciable error in the pressure readings. We therefore mounted 3" extensions to the wing span at each tip so that the tip gauges would be in a region of two-dimensional flow. The pressures measured with these gauges could then be compared with results from the other two-dimensional wing regions. The data shown in Fig. 60, p.154, indicate that the tip gauges were responding correctly. A few points are missing from these runs because of instrumentation malfunction.

Except for the leading-edge gauges, the average scatter of the results was within ±5 per cent or less. Increased scatter was apparent at the low angles of attack (0° and 2°). At these angles the maximum scatter in pressure coefficient from repeat runs was about ±.005.

Reynolds Number Variation

In order to maintain as high a degree of confidence as possible in the data generated during the course of this experimental investigation, we established at the outset the ground rule that only those tunnel initial conditions producing substantially constant stagnation conditions for several milliseconds would be employed. At the time when it was necessary to fix these conditions, the state of development of the operating envelope for our tunnel was such that for the Mach numbers involved in this program, a somewhat smaller variation in Reynolds number than desired had to be accepted.

At both Mach 12 and 19, the Reynolds number was varied by a factor less than two. While for both the rectangular and the delta wings the level of the pressure data for the low Reynolds number runs was generally higher than for the high Reynolds number, the difference is usually quite small. Figure 61, p.155, shows a comparison for the flat rectangular wing at the nominal Mach number of 12 at 0° and 10° angle of attack. The circles are for a Re/ft of 2.13×10^5 and the squares for a Re/ft of 3.86×10^5. Similar comparisons are shown in Fig. 62, p.156, for the nominal Mach number of 19. Data are presented for the flat 70° delta wing at 0° angle of attack, and for the 70° delta wing with circular-arc camber at 10° angle of attack. The circles are for a Re/ft of 6.54×10^4 and the squares for a

Re/ft of 9.13×10^4. Because of the small differences, we did not run all of the models at both Reynolds numbers at all angles of attack. The run schedule presented in Table II lists actual test conditions.

Comparison of Data with Simple Calculations

No attempt has been made to predict the pressure distributions by any exact theories. We have made several checks on the over-all level of the data using inviscid shock-expansion values. Figure 63, p. 157 shows the data on the centerline and mid-semispan stations of the flat rectangular wing at M=12.8 and $\alpha = 10°$. The centerline distribution for this wing geometry and flow condition is also shown in Fig. 64, p.158, with the expanded vertical scale. In both of these instances, we have plotted the value of C_p predicted by ordinary shock-expansion theory (solid line) and the inviscid exact value for a $10°$ wedge (dashed line). The pressure on the rear of the wing can be expected to approach this latter value asymptotically. The data points generally lie between the two values as expected. At lower angles of attack, where the viscous effects become large, the data points are higher than the corresponding shock-expansion values for those angles.

In addition to the flat rectangular wing data presented in Fig. 64, p.158, as mentioned above, we have plotted measured centerline pressure distributions for the two distorted rectangular wings for the same flow conditions and angle of attack. Pressure distributions calculated by the ordinary shock-expansion method are also given; in the case of the twisted wing, this calculated result is identical to that for the flat wing. In Fig. 65, p.159, experimental data for the three delta wings at M=12.6 and $\alpha = 10°$ are compared with results from a simple modified Newtonian pressure law calculation. It should be noted that for this test condition, the shock is detached from the delta-wing leading edges. For both the rectangular and the delta wings, the trends indicated by the rather crude computations are reflected in the experimental data.

REFERENCES

1. Leng, Jarvis, Hopkins, Harold, and Scheuing, Richard, A., The Grumman Hypersonic Research Shock Tunnel, Grumman Research Department Report to be published.

2. Baradell, Donald L., and Bertram, Mitchel H., The Blunt Plate in Hypersonic Flow, NASA TN D-408, October 1960.

3. Hilsenrath, Joseph, and Beckett, Charles W., Tables of Thermodynamic Properties of Argon-Free Air to 15,000 °K, AEDC TN 56-12, September 1956.

APPENDIX I

TEST SECTION CALIBRATION

The shock tunnel test section was surveyed by means of a three-probed rake, each probe containing a Kistler Instrument Corp. PZ-6 quartz pressure transducer. These transducers were dynamically calibrated in a small shock tube in a manner similar to that used for the wing model transducers (see Appendix II).

During each tunnel run the stagnation pressure, p_5, the incident shock Mach number, M_s, and the three test section pitot pressures, p_{0_2}, were recorded. Assuming an isentropic expansion through the nozzle and ideal free stream conditions, $\gamma_\infty = 1.4$, real-gas calculations yield the test section free stream conditions. The tunnel calibration was checked by measuring static pressure on a $70°$ cone at several test section locations.

From the measured stagnation pressure an "equivalent" shock Mach number is calculated using the real-gas properties of air and the normal shock relationships. This calculation is necessary because the shock wave is attenuated, producing shock processed air with varying properties. When the incident shock wave reflects back up the driven tube, the pressure reaches some average value in the stagnation region. With properly chosen initial conditions, this value is constant for several milliseconds. From the "equivalent" shock Mach number the remaining properties of the air in the stagnation region are determined. The measured pressure turns out to be approximately equal to the value calculated for the average shock Mach number over the last twenty feet of the tube. In any event, the pressure coefficients on the models are relatively insensitive to the stagnation conditions, and the results from the models turn out to be the same regardless of the method used.

Results of Calibration for M=12 Nozzle

The M=12 nozzle has a throat 0.4" in diameter, and an exit of 18" in diameter. This area ratio gives an ideal ($\gamma = 1.4$) Mach number of about 13.2 at the nozzle exit. Measurements were taken longitudinally 1/2", 2", 3-1/2", and 5" from the nozzle exit, and at positions on the nozzle centerline, and 2-1/2" and 5" above and below the centerline at these stations.

Mach number vs. longitudinal position is plotted in Fig. 66, p. 160, for the 600 psi initial driven pressure and 1 atmosphere driven pressure, in Fig. 67, p. 160, for a 1200 psi driver and 2 atmosphere driven pressure. No Mach number gradient normal to the centerline is apparent (Ref. 1). The position of the leading edge of the rectangular and delta wing models is shown for reference. Figs. 68 and 69, p. 161 show the ratio of free stream static pressure to tunnel stagnation pressure for the above initial conditions. A summary of the results of the calibration are tabulated in Table I.

Results of Calibration for M=19 Nozzle

This nozzle has a throat 0.125" in diameter giving an ideal Mach number of about 21.3. The calibration procedure was similar to that for the M=12 nozzle, and the results are also summarized in Table I. Mach number vs. longitudinal position is plotted in Fig. 70, p. 162 for a 1300 psi initial driver pressure and 1.33 atmosphere driven pressure, and in Fig. 71, p. 162 for a 2000 psi initial driver pressure and 2 atmosphere driven pressure. The corresponding ratios of free stream static pressure to tunnel stagnation pressure are shown in Figs. 72 and 73, p. 163.

APPENDIX II

SURFACE PRESSURE INSTRUMENTATION AND CALIBRATION

Pressure Transducer Design

Before this program was initiated, it was apparent that no pressure transducers were available commercially to fulfill our requirements of high sensitivity and small size. We therefore set out to develop a suitable gauge with the following design objectives in mind:

1. An over-all size small enough to permit mounting several gauges within a thin wing model

2. Sensitivity sufficiently high to measure static pressures of the order encountered at altitudes of 200,000-250,000 feet

3. Rise time no greater than approximately 100 microseconds in order that gauge response would not limit the over-all response time of the final system

4. A high resonant frequency so that a low-pass filter could be used effectively

5. Freedom from pyroelectric effects (temperature response) during the time required to obtain pressure data in the shock tunnel (up to 5 milliseconds)

Because the piezoelectric crystal had previously been used successfully for pressure measurements in shock tubes and tunnels, we decided to concentrate on this type of gauge. Two disadvantages of piezoelectric crystals had to be overcome: 1) sensitivity to temperature, and 2) sensitivity to acceleration. Crude initial attempts proved how serious the acceleration problem was to be.

To familiarize ourselves with the problems likely to be encountered, we fashioned a rather primitive gauge by soldering leads directly to a barium titanate crystal and imbedding the crystal in beeswax. Beeswax was chosen as an easily workable

mounting material serving also as a shock absorber and as an electrical insulator. This gauge, when mounted in a model in the tunnel, produced a trace full of hash and unreadable. At that time the sting mounting system in the tunnel test section was a temporary and somewhat flimsy setup. It was obvious that the accelerations of the model produced by tunnel recoil, etc. were rendering any pressure signal completely unintelligible.

Although we planned to improve the sting-sector arrangement so that its inherent design would reduce the amount of tunnel recoil and vibration reaching the models, we felt that it would be wise to concentrate on some type of electrical compensation to minimize the acceleration output of the gauge. The means for accomplishing "acceleration compensation" was conceptually rather simple. A second piezoelectric element similar to the first but shielded from any pressure signal was to be mounted within the transducer envelope. Hopefully, the "pressure" element would respond to pressure plus any acceleration present while the acceleration element would respond to acceleration only. Subtraction of the two signals would then yield a pure pressure output. In practice we found that the difficulties in obtaining crystals exactly matched and in mounting them in an identical manner made the ideal result difficult to attain.

Several prototype gauges were built and tested with limited success. The degree of acceleration compensation of each gauge was determined by subjecting the gauge, installed in a model, to accelerations over a wide frequency range by means of a standard "shaker." The output of the two elements in the gauge were recorded and compared. The design finally chosen for use in the present program did provide a reasonable degree of compensation, and when properly mounted in a model of sufficient stiffness, gave a pressure signal sufficiently free from acceleration "noise." (The final mounting problems of the transducer are discussed under Description of Tests and Presentation of Data in the main body of the report.) The design was not felt to be optimum, and the more experience we had with the gauge, the more we felt it could be improved. However, any significant improvements at this stage would have required an extensive redesign, which could not have been accomplished in time to produce useful information for the present program.

The sketch on the following page shows the general arrangement of the pressure transducer used for these tests. The thin covering of Scotch Brand Pressure Sensitive Tape No. 810 (Minnesota Mining and Manufacturing Company) over the pressure crystal provided sufficient thermal insulation to prevent any pyroelectric response during the run period.

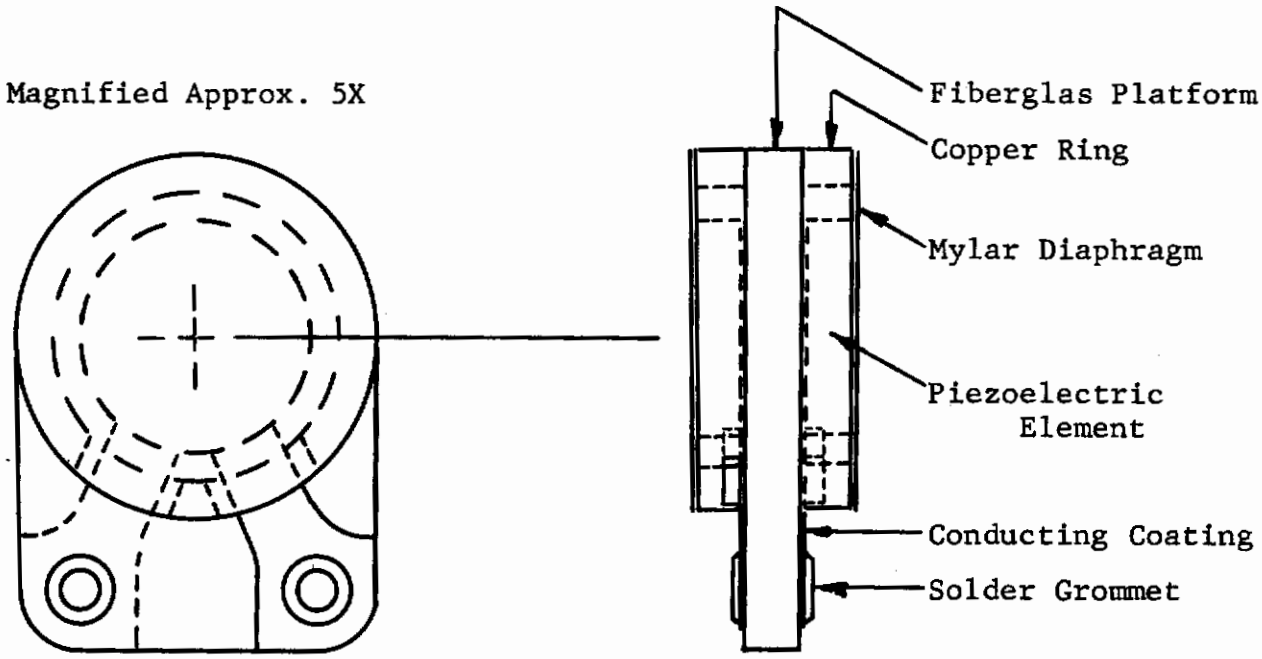

The gauges were mounted within the model beneath an orifice cavity combination (see sketch below), so they would be measuring pressure essentially at a point. The orifice cavity acts as an

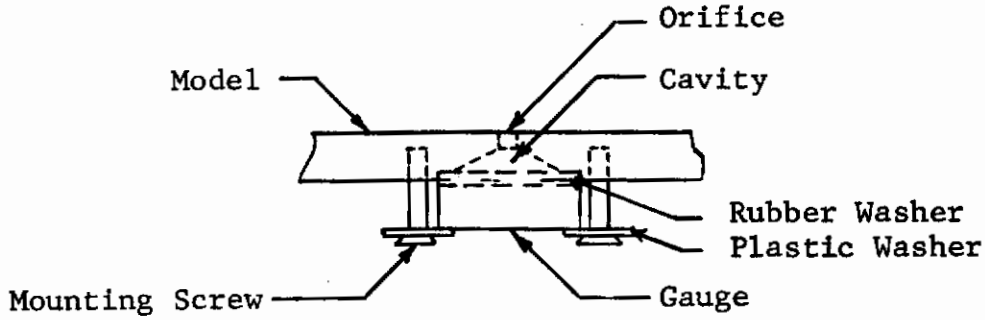

aerodynamic filter, similar in effect to an electronic RC-network. During the calibration development, the final sizes of the orifice and cavity (within limits) were determined not to have too noticeable an influence on the response time of the system, although the effect was measurable.

Calibration

Because piezoelectric crystals have a short time constant, the calibration device must provide a dynamic calibration, supplying an accurately known pressure step to the gauge for a period of a few milliseconds. The pressures at which the gauge is calibrated should also be within the range of pressures to be measured by the gauge in the tunnel.

Our first attempt consisted of a large "can" covered by a cellophane diaphragm at one end. Its prime advantage was that the entire model could be mounted within the can, along with a "standard" Statham P-81 pressure gauge, a d-c gauge whose calibration was known. In operation, the can was evacuated to a few millimeters below one atmosphere and the diaphragm was ruptured. An organ pipe effect resulted in a relatively low-frequency, sinusoidal pressure wave resonating within the cavity. Although this device proved useful in the early evaluation of the transducers, it had serious disadvantages which we felt prohibited its employment as an accurate calibration device. Among these were: the pressures measured were small differences from one atmosphere, rather than from a vacuum as in the case in the tunnel; the "standard" gauge and the transducers were not necessarily all located in a region of uniform pressure, and the output of the Statham gauge had to be filtered to remove high frequency diaphragm resonances within the gauge making its calibration doubtful. The results obtained with this method were erratic and therefore we started to look elsewhere for a more accurate and reliable system.

We turned to the use of a small shock tube. Although, ideally, it would be far superior to calibrate all gauges while mounted within the model, the size of the models forced a compromise. The gauges were mounted in the sidewall of a 1-1/2" tube in a mounting identical in all respects to that in the model. Weak shock waves were passed over the gauges to provide a pressure step which could be calculated from the measured shock Mach number.

Shock tube driver pressures on the order of 50 mm. Hg. and initial driven pressures from 1 to 4 mm. Hg. provided shock Mach numbers from 1.4 to 1.8 and pressure steps from 0.01 psi to 0.1 psi. The transducers were mounted between two time-of-arrival gauges located 3-1/2" apart. The outputs of these gauges were fed to a scope sweeping at 25 microseconds per centimeter. Five microsecond time marks superimposed on the traces enabled us to obtain the shock Mach numbers to an accuracy of better than 1 per cent. Each transducer was calibrated through the preamplifier and electronic switch used during the subsequent actual tests. Cable

lengths and capacitances were duplicated as closely as possible.

A typical calibration is shown in Fig. 74, p.164. By mounting some of the gauges in the end of the tube and calibrating against the reflected shock stagnation pressure, we were able to determine the linearity of the transducers up to 1 psi. Effects of variables such as cavity and orifice sizes, tension of mounting screws, cable lengths, etc. were evaluated during the calibration period, and were found either to have no effect or to be controllable. The gauges in most cases were repeatable within 2 per cent, and all sensitivities were between 75 and 150 mv/psi.

TABLE I

RESULTS OF TEST SECTION CALIBRATION

M=12

Initial driver pressure	600 psig	1200 psig
Initial driven pressure	15 psia	30 psia
M_∞ at rectangular model L.E. 2-1/2" from nozzle	12.76	12.50
M_∞ gradient per inch	.115	.115
Re/ft. at model leading edge	2.14×10^5	3.86×10^5
Tunnel stagnation pressure	1400 psia	3500 psia
Tunnel stagnation temperature	3800 °R	4400 °R
Test section static temperature	131 °R	160 °R

M=19

Initial driver pressure	1300 psi	2000 psi
Initial driven pressure	20 psia	30 psia
M_∞ at rectangular model L.E. 2-1/2" from nozzle	19.16	18.80
M_∞ gradient per inch	.167	.160
Re/ft at model leading edge	$.65 \times 10^5$	$.91 \times 10^5$
Tunnel stagnation pressure	3500 psia	6000 psia
Tunnel stagnation temperature	5600 °R	5900 °R
Test section static temperature	94 °R	104 °R

TABLE II

TEST CONDITIONS

Wing	$M_{L.E.}$ *	Re/ft†	Angles of Attack
W_1	12.8	2.13×10^5	0,2,5,10,15
W_1	12.5	3.86×10^5	0,5,10
W_2	12.8	2.13×10^5	0,2,5,10,15
W_2	12.5	3.86×10^5	0,5,10
W_3	12.8	2.13×10^5	0,2,5,10,15
W_3	12.5	3.86×10^5	0,5,10
W_4	12.6	2.13×10^5	0,2,5,10,15
W_4	12.3	3.86×10^5	0
W_5	12.6	2.13×10^5	0,2,5,10,15
W_5	12.3	3.86×10^5	0,5,10
W_6	12.6	2.13×10^5	0,2,5,10,15
W_6	12.3	3.86×10^5	0,5,10
W_1	19.2	$.65 \times 10^5$	0,2,5,10,15
W_1	18.8	$.91 \times 10^5$	0
W_2	19.2	$.65 \times 10^5$	0,2,5,10,15
W_3	19.2	$.65 \times 10^5$	0,2,5,10,15
W_4	18.9	$.65 \times 10^5$	0,2,5,10,15
W_4	18.6	$.91 \times 10^5$	0

TABLE II (Cont.)

Wing	$M_{L.E.}$*	Re/ft†	Angles of Attack
W_5	18.9	$.65 \times 10^5$	0,2,5,10,15
W_5	18.6	$.91 \times 10^5$	10
W_6	18.9	$.65 \times 10^5$	0,2,5,10,15
W_6	18.6	$.91 \times 10^5$	0

WING IDENTIFICATION

W_1 - flat rectangular

W_2 - twisted rectangular

W_3 - cambered rectangular

W_4 - flat 70° delta

W_5 - sine-wave cambered 70° delta

W_6 - circular arc cambered 70° delta

*For 70° delta wings Mach number is given at apex of wing.

†Re/ft is the nominal value 2-1/2" from the nozzle exit at a point coinciding with the rectangular wing leading edge and 1-1/2" back from the delta wing apex.

TABLE III

PRESSURE COEFFICIENTS ON FLAT RECTANGULAR WING
LEADING EDGE M= 12.8

ALPHA = 0 DEG., RUN = 672 P5 = 1801. PSI

X/C	2Y/B = 0	.25	.5	.708	.917
.149	0.043	0.051	0.055	0.027	0.030 , 0.027
.260	0.022		0.036		0.027
.371	0.020		0.027		0.015
.482			0.021		0.015
.593	0.016				~~0.023~~
.704	0.023		0.026		0.016

ALPHA = 0 DEG., RUN = 673 P5 = 1613. PSI

X/C	2Y/B = 0	.25	.5	.708	.917
.149	0.043	0.053	0.061	0.029	0.036 , 0.028
.260	0.021		0.036		0.027
.371	0.019		0.028		0.020
.482			0.021		0.016
.593	0.015				~~0.025~~
.704	0.022				0.017

TABLE III (Cont.)

PRESSURE COEFFICIENTS ON FLAT RECTANGULAR WING
LEADING EDGE M= 12.8

ALPHA = 2 DEG., RUN = 677 P5 = 1707. PSI

X/C	2Y/B 0	.25	.5	.708	.917
.149	0.058	0.069	0.076	0.041	0.047 , 0.040
.260	0.032		0.049		0.029
.371	0.030		0.038		0.028
.482			0.035		0.017
.593	0.027				~~0.034~~
.704	0.037		0.039		0.029

ALPHA = 2 DEG., RUN = 678 P5 = 1519. PSI

X/C	2Y/B 0	.25	.5	.708	.917
.149	0.059	0.074	0.076	0.041	0.049 , 0.042
.260	0.035		0.053		0.027
.371	0.030		0.038		0.026
.482			0.034		0.015
.593	0.026				~~0.030~~
.704	0.037		0.038		0.027

TABLE III (Cont.)

PRESSURE COEFFICIENTS ON FLAT RECTANGULAR WING
LEADING EDGE M= 12.8

ALPHA = 5 DEG., RUN = 674 P5 = 1707. PSI

X/C	2Y/B	0	.25	.5	.708	.917
.149		0.083	0.087	0.111	0.059	0.065 , 0.056
.260		0.051		0.073		0.047
.371		0.052		0.058		0.037
.482				0.056		0.021
.593		0.044				~~0.036~~
.704		0.053		0.054		0.027

ALPHA = 10 DEG., RUN = 670 P5 = 1705. PSI

X/C	2Y/B	0	.25	.5	.708	.917
.149		0.126	0.106	0.190	0.101	0.102 , 0.085
.260		0.101		0.127		0.099
.371		0.105		0.109		0.068
.482				0.101		0.051
.593		0.085				~~0.068~~
.704		0.090		0.098		

TABLE III (Cont.)

PRESSURE COEFFICIENTS ON FLAT RECTANGULAR WING
LEADING EDGE M= 12.8

ALPHA = 15 DEG., RUN = 680 P5 = 1660. PSI

X/C	2Y/B	0	.25	.5	.708	.917
.149		0.196	0.194	0.291	0.131	0.176 , 0.139
.260		0.181		0.239		0.138
.371		0.170		0.180		
.482				0.165		
.593		~~0.142~~				~~0.118~~
.704				0.154		0.083

ALPHA = 15 DEG., RUN = 679 P5 = 1660. PSI

X/C	2Y/B	0	.25	.5	.708	.917
.149		0.210	0.197	0.294	0.143	0.166 , 0.136
.260		0.181		0.243		0.138
.371		0.176		0.182		0.122
.482				0.174		0.079
.593		~~0.144~~				~~0.110~~
.704		0.176		0.158		0.083

TABLE III (Cont.)

PRESSURE COEFFICIENTS ON FLAT RECTANGULAR WING
LEADING EDGE M= 12.5

ALPHA = 0 DEG., RUN = 684 P5 = 4720. PSI

X /C	2Y /B	0	.25	.5	.708	.917
.149		0.025	0.045	0.040		0.026 , 0.024
.260		0.017		0.044		0.018
.371		0.013		0.013		0.017
.482				0.016		0.009
.593		0.013				~~0.021~~
.704		0.018		0.019		0.013

ALPHA = 5 DEG., RUN = 685 P5 = 4385. PSI

X /C	2Y /B	0	.25	.5	.708	.917
.149		0.058	0.053	0.089	0.036	0.053 , 0.032
.260		0.045		0.073		0.038
.371		0.045		0.041		0.036
.482				0.050		~~0.025~~
.593		0.045				0.039
.704		0.046		0.047		0.034

TABLE III (Cont.)

PRESSURE COEFFICIENTS ON FLAT RECTANGULAR WING
LEADING EDGE M= 12.5

ALPHA = 10 DEG., RUN = 681 P5 = 4125. PSI

X/C	2Y/B	0	.25	.5	.708	.917	
.149		0.114	0.091	0.160	0.055		~~0.054~~
.260		0.091		0.122			
.371		0.097		0.088		0.073	
.482				0.089		~~0.047~~	
.593		0.080				0.070	
.704		~~0.101~~		0.080		0.052	

ALPHA = 10 DEG., RUN = 682 P5 = 4215. PSI

X/C	2Y/B	0	.25	.5	.708	.917	
.149		0.113	0.081	0.159	0.045	0.100	~~0.057~~
.260		0.090		0.160		0.080	
.371		0.094		0.088		0.070	
.482				0.091		~~0.047~~	
.593		0.082				0.067	
.704		~~0.104~~		0.081		0.054	

TABLE III (Cont.)

PRESSURE COEFFICIENTS ON TWISTED RECTANGULAR WING
LEADING EDGE M= 12.8

ALPHA = 0 DEG., RUN = 706 P5 = 1836. PSI

X/C	2Y/B 0	.25	.5	.708	.917
.149	0.044	0.050	0.058	0.043	0.066 , 0.062
.260	0.024		0.043		0.053
.371	0.029		0.037		0.043
.482	~~0.038~~		0.032		0.030
.593	0.025				~~0.041~~
.704	0.024				~~0.049~~

ALPHA = 2 DEG., RUN = 707 P5 = 1790. PSI

X/C	2Y/B 0	.25	.5	.708	.917
.149	0.053	0.062	0.065	0.052	0.080 , 0.071
.260	0.035		0.054		0.065
.371	0.036		0.049		0.054
.482	~~0.044~~		0.040		0.039
.593	0.031				~~0.055~~
.704	0.029		0.046		~~0.046~~

TABLE III (Cont.)

PRESSURE COEFFICIENTS ON TWISTED RECTANGULAR WING
LEADING EDGE M= 12.8

ALPHA = 5 DEG., RUN = 705 P5 = 1715. PSI

X/C	2Y/B	0	.25	.5	.708	.917
.149		0.077	0.086	0.090	0.067	0.113 , 0.094
.260		0.056		0.080		0.100
.371		0.052		0.074		0.087
.482		~~0.065~~		0.059		0.070
.593		~~0.041~~				~~0.075~~
.704		0.054		0.054		0.028

ALPHA = 5 DEG., RUN = 704 P5 = 1696. PSI

X/C	2Y/B	0	.25	.5	.708	.917
.149		0.081	0.086	0.094	0.086	0.110 , ~~0.100~~
.260		0.061		0.078		0.102
.371		0.052		0.079		0.089
.482		~~0.067~~		0.066		0.078
.593		~~0.041~~				~~0.082~~
.704		0.050				

TABLE III (Cont.)

PRESSURE COEFFICIENTS ON TWISTED RECTANGULAR WING
LEADING EDGE M= 12.8

ALPHA = 10 DEG., RUN = 702 P5 = 1696. PSI

X/C	2Y/B = 0	.25	.5	.708	.917
.149	0.131	0.140	0.132	0.134	0.179 , ~~0.136~~
.260	0.108		~~0.138~~		0.160
.371	0.097		~~0.124~~		0.150
.482	~~0.128~~		0.099		0.110
.593	~~0.068~~				~~0.137~~
.704	0.097		0.077		

ALPHA = 10 DEG., RUN = 703 P5 = 2257. PSI

X/C	2Y/B = 0	.25	.5	.708	.917
.149	0.123	0.133	0.133	0.119	0.177 , ~~0.149~~
.260	0.107		~~0.137~~		0.170
.371	0.095		~~0.134~~		0.140
.482	~~0.127~~		0.098		0.114
.593	~~0.057~~				~~0.120~~
.704	0.092		0.077		

TABLE III (Cont.)

PRESSURE COEFFICIENTS ON TWISTED RECTANGULAR WING
LEADING EDGE M= 12.8

ALPHA = 15 DEG., RUN = 708 P5 = 1790. PSI

X/C	2Y/B	0	.25	.5	.708	.917
.149		0.208	0.223	0.242	0.205	0.255 , ~~0.211~~
.260		0.188		0.212		0.252
.371		0.157		0.193		0.213
.482		~~0.199~~		0.152		0.165
.593						~~0.197~~
.704		0.148				

ALPHA = 15 DEG., RUN = 709 P5 = 1602. PSI

X/C	2Y/B	0	.25	.5	.708	.917
.149		0.210	0.236	0.240	0.199	0.260 , ~~0.198~~
.260		0.191		0.214		0.249
.371		0.146		0.204		0.191
.482		~~0.205~~		0.151		0.161
.593						~~0.191~~
.704		0.146				

TABLE III (Cont.)

PRESSURE COEFFICIENTS ON TWISTED RECTANGULAR WING
LEADING EDGE M= 12.5

ALPHA = 0 DEG., RUN = 711 P5 = 4271. PSI

X/C (2Y/B)	0	.25	.5	.708	.917	
.149	0.036	0.046	0.047	0.036		, 0.057
.260	0.023		0.042			
.371	0.024		0.038			
.482	~~0.036~~		0.030			
.593	0.029				~~0.043~~	
.704	0.031					

ALPHA = 0 DEG., RUN = 712 P5 = 4271. PSI

X/C (2Y/B)	0	.25	.5	.708	.917	
.149	0.037	0.046	0.050	0.033	0.058	, ~~0.051~~
.260	0.020		0.036		0.050	
.371	0.026		0.039		0.041	
.482	0.018		0.030		0.034	
.593	0.029				~~0.040~~	
.704	0.025					

TABLE III (Cont.)

PRESSURE COEFFICIENTS ON TWISTED RECTANGULAR WING
LEADING EDGE M= 12.5

ALPHA = 5 DEG., RUN = 710 P5 = 4186. PSI

X/C	2Y/B	0	.25	.5	.708	.917
.149		0.068	0.078	0.087	0.072	0.111 , ~~0.092~~
.260		0.053		0.077		0.108
.371		0.050		0.071		0.086
.482		~~0.068~~		0.060		0.068
.593		0.040				0.084
.704		0.047		0.054		

ALPHA = 10 DEG., RUN = 714 P5 = 4186. PSI

X/C	2Y/B	0	.25	.5	.708	.917
.149		0.126	0.149	0.152	0.132	0.186 , ~~0.143~~
.260		0.115		0.144		
.371		0.116				
.482		0.098		0.101		0.122
.593						0.127
.704		0.099				

TABLE III (Cont.)

PRESSURE COEFFICIENTS ON TWISTED RECTANGULAR WING
LEADING EDGE M= 12.5

ALPHA = 10 DEG., RUN = 7-15 P5 = 4016. PSI

X/C	2Y/B	0	.25	.5	.708	.917
.149		0.124	0.166	0.157	0.128	0.179 , ~~0.142~~
.260		0.116		0.143		~~0.191~~
.371		0.107		0.128		0.137
.482		~~0.143~~		0.103		0.115
.593						0.129
.704		0.107				

TABLE III (Cont.)

PRESSURE COEFFICIENTS ON CAMBERED RECTANGULAR WING
LEADING EDGE M= 12.8

ALPHA = 0 DEG., RUN = 726 P5 = 1393. PSI

X/C	2Y/B = 0	.25	.5	.708	.917
.149	0.071	0.095	0.090	0.057	, 0.062
.260	0.042		0.052		
.371	0.036		0.044		
.482	~~0.041~~		0.034		
.593	0.023				~~0.027~~
.704	0.018		0.031		0.014

ALPHA = 0 DEG., RUN = 727 P5 = 1720. PSI

X/C	2Y/B = 0	.25	.5	.708	.917
.149	0.065	0.088	0.077	0.055	0.058 , 0.064
.260	0.036		0.058		0.038
.371	0.033		0.041		0.022
.482	~~0.037~~		0.032		0.014
.593	0.021				~~0.022~~
.704	0.018		0.032		0.012

TABLE III (Cont.)

PRESSURE COEFFICIENTS ON CAMBERED RECTANGULAR WING
LEADING EDGE M= 12.8

ALPHA = 2 DEG., RUN = 733 P5 = 1626. PSI

X/C	2Y/B = 0	.25	.5	.708	.917
.149	0.086	0.095	0.101	0.074	0.072 , 0.075
.260	0.052		0.064		0.049
.371	0.045		0.053		0.029
.482	~~0.053~~		0.045		0.019
.593	0.029				~~0.029~~
.704	0.021		0.037		0.014

ALPHA = 5 DEG., RUN = 720 P5 = 1650. PSI

X/C	2Y/B = 0	.25	.5	.708	.917
.149	0.135	0.132	0.145	0.107	0.102 , 0.099
.260	0.089		0.098		0.080
.371	0.073		0.075		0.048
.482	~~0.082~~		0.076		0.031
.593	0.046				~~0.042~~
.704	0.034		0.047		0.026

TABLE III (Cont.)

PRESSURE COEFFICIENTS ON CAMBERED RECTANGULAR WING
LEADING EDGE M= 12.8

ALPHA = 5 DEG., RUN = 722 P5 = 1556. PSI

X/C (2Y/B)	0	.25	.5	.708	.917	
.149	0.124	0.125	0.120	0.092	0.098	0.102
.260	0.088		0.100		0.074	
.371	0.074		0.077		0.046	
.482	~~0.083~~		0.064		0.031	
.593	0.052				~~0.037~~	
.704	0.031		0.073		0.023	

ALPHA = 5 DEG., RUN = 723 P5 = 1930. PSI

X/C (2Y/B)	0	.25	.5	.708	.917	
.149	0.117	0.132	0.133	0.096		0.096
.260	0.086		0.094			
.371	0.069		0.070			
.482	~~0.085~~		0.067			
.593	0.044				~~0.043~~	
.704	0.034		0.047		0.023	

TABLE III (Cont.)

PRESSURE COEFFICIENTS ON CAMBERED RECTANGULAR WING
LEADING EDGE M= 12.8

ALPHA = 10 DEG., RUN = 734 P5 = 1612. PSI

X/C	2Y/B 0	.25	.5	.708	.917
.149	0.198	0.190	0.239	0.173	0.160 , 0.151
.260	0.157		0.159		0.133
.371	0.120		0.128		0.076
.482	~~0.153~~		0.114		0.052
.593	~~0.075~~				~~0.068~~
.704	0.099		0.074		0.044

ALPHA = 15 DEG., RUN = 731 P5 = 1486. PSI

X/C	2Y/B 0	.25	.5	.708	.917
.149	0.325	0.330	0.380	0.262	0.246 , 0.231
.260	0.249		0.261		0.203
.371	0.197		0.201		0.124
.482	~~0.262~~		0.178		0.089
.593	0.123				~~0.104~~
.704	0.093		0.161		0.079

TABLE III (Cont.)

PRESSURE COEFFICIENTS ON CAMBERED RECTANGULAR WING
LEADING EDGE M= 12.8

ALPHA = 15 DEG., RUN = 730 P5 = 1883. PSI

X /C	2Y /B	0	.25	.5	.708	.917
.149		0.300	0.280	0.362		0.236 , 0.236
.260		0.243		0.259		0.196
.371		0.175		0.178		0.112
.482		~~0.244~~		0.178		0.078
.593		0.113				~~0.106~~
.704		0.084		~~0.119~~		0.061

TABLE III (Cont.)

PRESSURE COEFFICIENTS ON CAMBERED RECTANGULAR WING
LEADING EDGE M= 12.5

ALPHA = 0 DEG., RUN = 732 P5 = 3761. PSI

X/C	2Y/B = 0	.25	.5	.708	.917
.149	0.059	0.076	0.072	0.050	0.054 , 0.053
.260	0.039		0.048		0.037
.371	0.032		0.040		0.026
.482	0.017		0.029		0.016
.593	~~0.010~~				~~0.026~~
.704	0.018		0.029		0.017

TABLE III (Cont.)

PRESSURE COEFFICIENTS ON CAMBERED RECTANGULAR WING
LEADING EDGE M= 12.5

ALPHA = 5 DEG., RUN = 736 P5 = 3675. PSI

X/C (2Y/B)	0	.25	.5	.708	.917
.149	0.112	0.116	0.137	0.104	0.099 , 0.089
.260	0.087		0.093		0.078
.371	0.074		0.079		0.046
.482	~~0.138~~		0.069		0.032
.593	0.042				~~0.045~~
.704	0.031		0.059		0.025

ALPHA = 10 DEG., RUN = 719 P5 = 3846. PSI

X/C (2Y/B)	0	.25	.5	.708	.917
.149	0.182	0.182	0.224	0.158	0.158 , 0.145
.260	0.159		0.158		0.131
.371	0.115		0.121		0.079
.482	~~0.165~~		0.119		0.054
.593	0.073				~~0.067~~
.704	0.051		0.090		0.039

TABLE IV

PRESSURE COEFFICIENTS ON FLAT 70 DEGREE DELTA WING
APEX M= 12.6

ALPHA = 0 DEG., RUN = 831 P5 = 1351. PSI

X /C ROOT	2Y /B 0	.147	.295	.442	.590	.738
.237	0.018					
.384	0.009					
.532	0.008		0.008			
.585			0.004			
.679	0.011			0.009		
.827	0.007				0.017	
.880					0.018	
.974			0.008			0.005

ALPHA = 2 DEG., RUN = 833 P5 = 1351. PSI

X /C ROOT	2Y /B 0	.147	.295	.442	.590	.738
.237	0.021					
.384	0.016	0.013				
.532	0.016		0.016			
.585			0.003			
.679	0.013		0.010	0.015		
.827	0.015				0.021	
.880					0.019	
.974			0.007		0.006	0.014

TABLE IV (Cont.)

PRESSURE COEFFICIENTS ON FLAT 70 DEGREE DELTA WING
APEX M= 12.6

ALPHA = 5 DEG., RUN = 832 P5 = 1635. PSI

X/C ROOT	2Y/B	0	.147	.295	.442	.590	.738
.237							
.384		0.032					
.532		0.025		0.045			
.585				0.019			
.679		0.018		0.022	0.024		
.827		0.025				0.028	
.880						0.022	
.974				0.013		0.006	0.032

ALPHA = 10 DEG., RUN = 829 P5 = 1241. PSI

X/C ROOT	2Y/B	0	.147	.295	.442	.590	.738
.237		0.067					
.384		0.059	0.075				
.532		0.054		0.069			
.585				0.051			
.679		0.039		0.035	0.047		
.827		~~0.068~~		0.037		0.053	
.880						0.039	
.974				0.022		0.029	0.046

TABLE IV (Cont.)

PRESSURE COEFFICIENTS ON FLAT 70 DEGREE DELTA WING
APEX M= 12.6

ALPHA = 15 DEG., RUN = 834 P5 = 1307. PSI

X /C ROOT	2Y /B	0	.147	.295	.442	.590	.738
.237							
.384		0.142					
.532		0.124		0.192			
.585				0.130			
.679					0.129		
.827		0.045				0.091	
.880						0.085	
.974				0.095		0.044	0.147

TABLE IV (Cont.)

PRESSURE COEFFICIENTS ON FLAT 70 DEGREE DELTA WING
APEX M= 12.3

ALPHA = 0 DEG., RUN = 835 P5 = 3848. PSI

X /C ROOT	2Y /B	0	.147	.295	.442	.590	.738
.237		0.008					
.384		0.005					
.532		0.004		0.006			
.585				0.003			
.679		~~-0.016~~		0.005	0.017		
.827		0.003				0.015	
.880						0.014	
.974				0.005		0.011	

TABLE IV (Cont.)

PRESSURE COEFFICIENTS ON SINE WAVE CAMBERED 70 DEGREE DELTA WING
APEX M= 12.6

ALPHA = 0 DEG., RUN = 784 P5 = 1701. PSI

X /C	2Y /B	0	.147	.295	.442	.590	.738
	ROOT						
.237		0.020					
.384		0.004	0.009				
.532		0.006		0.001			
.585				-0.005			
.679		0.005			0.004		
.827		0.001				0.018	
.880						0.019	
.974				0.016		0.021	0.022

ALPHA = 2 DEG., RUN = 783 P5 = 1592. PSI

X /C	2Y /B	0	.147	.295	.442	.590	.738
	ROOT						
.237		0.026					
.384		0.005	0.010				
.532		0.004		0.004			
.585				0.006			
.679		0.008		0.000	0.010		
.827		0.010				0.028	
.880						0.029	
.974				0.021		0.035	0.048

TABLE IV (Cont.)

PRESSURE COEFFICIENTS ON SINE WAVE CAMBERED 70 DEGREE DELTA WING
APEX M= 12.6

ALPHA = 5 DEG., RUN = 782 P5 = 1504. PSI

X /C	2Y /B	0	.147	.295	.442	.590	.738
	ROOT						
	.237	0.047					
	.384	0.018	0.051				
	.532	0.008		0.011			
	.585			0.005			
	.679	0.011		0.011	0.025		
	.827	0.034				0.035	
	.880					0.048	
	.974			0.040		0.077	0.098

ALPHA = 5 DEG., RUN = 781 P5 = 1767. PSI

X /C	2Y /B	0	.147	.295	.442	.590	.738
	ROOT						
	.237	0.042					
	.384	0.012	0.051				
	.532	0.005		0.008			
	.585			0.005			
	.679	0.011		0.011	0.021		
	.827	0.031				0.031	
	.880					0.045	
	.974			0.041		0.074	0.100

TABLE IV (Cont.)

PRESSURE COEFFICIENTS ON SINE WAVE CAMBERED 70 DEGREE DELTA WING
APEX M= 12.6

ALPHA = 10 DEG., RUN = 780 P5 = 1504. PSI

X /C ROOT	2Y /B	0	.147	.295	.442	.590	.738
.237		0.115					
.384		0.040	0.130				
.532		0.023		0.030			
.585				0.033			
.679		0.038		0.044	0.071		
.827		0.083				0.061	
.880						0.100	
.974				0.102		0.156	0.144

ALPHA = 15 DEG., RUN = 785 P5 = 1679. PSI

X /C ROOT	2Y /B	0	.147	.295	.442	.590	.738
.237		0.153					
.384		0.070	0.250				
.532		0.061		0.069			
.585				0.063			
.679		0.060		0.080	0.103		
.827		0.152				0.131	
.880						0.181	
.974				0.212		0.298	

TABLE IV (Cont.)

PRESSURE COEFFICIENTS ON SINE WAVE CAMBERED 70 DEGREE DELTA WING
APEX M= 12.6

ALPHA = 15 DEG., RUN = 786 PS = 1438. PSI

X /C ROOT	2Y /B	0	.147	.295	.442	.590	.738
.237		0.152					
.384		0.079	0.196				
.532		0.063		0.048			
.585				0.055			
.679		0.071		0.086	0.115		
.827		0.154				0.120	
.880						0.161	
.974				0.213		0.280	0.330

TABLE IV (Cont.)

PRESSURE COEFFICIENTS ON SINE WAVE CAMBERED 70 DEGREE DELTA WING
APEX M= 12.3

ALPHA = 0 DEG., RUN = 789 P5 = 3528. PSI

X /C ROOT	2Y /B 0	.147	.295	.442	.590	.738
.237	0.020					
.384	-0.008	0.011				
.532	-0.007		0.002			
.585			-0.007			
.679			-0.003	-0.007		
.827	0.002				0.021	
.880					0.019	
.974			0.016		0.025	0.024

TABLE IV (Cont.)

PRESSURE COEFFICIENTS ON SINE WAVE CAMBERED 70 DEGREE DELTA WING
APEX M= 12.3

ALPHA = 5 DEG., RUN = 787 P5 = 3688. PSI

X /C ROOT	2Y /B	0	.147	.295	.442	.590	.738
.237		0.038					
.384		0.008	0.048				
.532		0.009		0.022			
.585				0.003			
.679		0.012		0.008	0.011		
.827		0.027				0.030	
.880						0.045	
.974				0.042		0.078	0.085

ALPHA = 10 DEG., RUN = 791 P5 = 3848. PSI

X /C ROOT	2Y /B	0	.147	.295	.442	.590	.738
.237		0.127					
.384		0.028	0.078				
.532		0.017		0.015			
.585				0.015			
.679		0.026		0.033	0.023		
.827		0.078				0.062	
.880						0.095	
.974				0.091		0.156	0.098

TABLE IV (Cont.)

PRESSURE COEFFICIENTS ON CIRCULAR ARC CAMBERED 70 DEGREE DELTA WING
APEX M= 12.6

ALPHA = 0 DEG., RUN = 815 P5 = 1416. PSI

X /C	2Y /B	0	.147	.295	.442	.590	.738
ROOT							
.237							
.384		0.017	0.014				
.532		0.011		0.018			
.585				-0.001			
.679		0.010		0.007	0.016		
.827		0.009				0.006	
.880							
.974				0.005		0.004	0.004

ALPHA = 2 DEG., RUN = 812 P5 = 1548. PSI

X /C	2Y /B	0	.147	.295	.442	.590	.738
ROOT							
.237							
.384		0.031	0.029				
.532		0.017		0.026			
.585				0.000			
.679		0.010		0.005	0.010		
.827		0.011				0.008	
.880						0.003	
.974				0.008		0.007	0.003

TABLE IV (Cont.)

PRESSURE COEFFICIENTS ON CIRCULAR ARC CAMBERED 70 DEGREE DELTA WING
APEX M= 12.6

ALPHA = 5 DEG., RUN = 811 P5 = 1592. PSI

X /C ROOT	2Y /B	0	.147	.295	.442	.590	.738
.237							
.384		0.043	0.029				
.532		0.026		0.052			
.585				0.010			
.679		0.021		0.013	0.021		
.827		0.019				0.011	
.880						0.019	
.974				0.007		0.013	0.009

ALPHA = 10 DEG., RUN = 809 P5 = 1504. PSI

X /C ROOT	2Y /B	0	.147	.295	.442	.590	.738
.237							
.384		0.090	0.092				
.532		0.052		0.061			
.585				0.047			
.679		0.041		0.029	0.041		
.827		0.036				0.025	
.880						0.050	
.974				0.021		0.029	0.018

TABLE IV (Cont.)

PRESSURE COEFFICIENTS ON CIRCULAR ARC CAMBERED 70 DEGREE DELTA WING
APEX M= 12.6

ALPHA = 10 DEG., RUN = 808 P5 = 1504. PSI

X /C	2Y /B	0	.147	.295	.442	.590	.738
ROOT							
.237		0.091					
.384		0.086	0.102				
.532		0.055		0.050			
.585				0.058			
.679		0.025		0.029	0.052		
.827		0.037		0.033		0.025	
.880						0.049	
.974				0.028		0.028	0.018

ALPHA = 15 DEG., RUN = 810 P5 = 1460. PSI

X /C	2Y /B	0	.147	.295	.442	.590	.738
ROOT							
.237							
.384		0.170	0.145				
.532		0.103		0.105			
.585				0.107			
.679		0.085		0.070	0.088		
.827		0.079				0.063	
.880						0.095	
.974				0.054		0.071	0.053

TABLE IV (Cont.)

PRESSURE COEFFICIENTS ON CIRCULAR ARC CAMBERED 70 DEGREE DELTA WING
APEX M= 12.3

ALPHA = 0 DEG., RUN = 816 P5 = 3768. PSI

X /C	2Y /B	0	.147	.295	.442	.590	.738
ROOT							
.237							
.384		0.017	0.008				
.532		0.008		0.011			
.585				-0.001			
.679		0.010		-0.002	0.004		
.827		0.007				0.003	
.880							
.974				0.004		0.000	-0.003

ALPHA = 5 DEG., RUN = 817 P5 = 3688. PSI

X /C	2Y /B	0	.147	.295	.442	.590	.738
ROOT							
.237							
.384		0.042	0.044				
.532		0.024		0.037			
.585				0.006			
.679		0.020		0.012	0.007		
.827		0.015				0.006	
.880						0.009	
.974				-0.001		0.007	0.007

TABLE IV (Cont.)

PRESSURE COEFFICIENTS ON CIRCULAR ARC CAMBERED 70 DEGREE DELTA WING
APEX M= 12.3

ALPHA = 10 DEG., RUN = 819 P5 = 3528. PSI

X /C ROOT	2Y /B	0	.147	.295	.442	.590	.738
.237							
.384		0.075	0.099				
.532		0.054		0.077			
.585				0.023			
.679		0.037		0.028	0.045		
.827		0.035				0.030	
.880						0.041	
.974				0.025		0.029	0.020

TABLE V

PRESSURE COEFFICIENTS ON FLAT RECTANGULAR WING
LEADING EDGE M= 19.2

ALPHA = 0 DEG., RUN = 846 P5 = 3608. PSI

X/C	2Y/B 0	.25	.5	.708	.917
.149	0.099	0.123	0.040	0.090	~~0.032~~ , 0.047
.260	0.056				0.025
.371	0.051		0.053		0.040
.482	0.035		0.032		0.024
.593	0.034				0.012
.704	~~0.055~~				0.008

ALPHA = 2 DEG., RUN = 847 P5 = 3688. PSI

X/C	2Y/B 0	.25	.5	.708	.917
.149	0.112	0.148	0.067	0.082	~~0.039 , 0.079~~
.260	0.071				
.371	0.063		0.064		0.052
.482	0.052		0.039		~~0.022~~
.593	0.037				0.036
.704	~~0.064~~				

TABLE V (Cont.)

PRESSURE COEFFICIENTS ON FLAT RECTANGULAR WING
LEADING EDGE M= 19.2

ALPHA = 5 DEG., RUN = 848 P5 = 3528. PSI

X /C	2Y /B	0	.25	.5	.708	.917
.149		0.134	0.178	0.106	0.116	~~0.060~~ , 0.090
.260		0.089				
.371		0.082		0.070		
.482		~~0.087~~		0.054		~~0.025~~
.593		0.057				0.033
.704		0.058		0.049		0.020

ALPHA = 10 DEG., RUN = 844 P5 = 3528. PSI

X /C	2Y /B	0	.25	.5	.708	.917
.149		0.201	0.274	0.266	0.160	~~0.112~~ , 0.136
.260		0.141				~~0.078~~
.371		0.141		0.123		0.094
.482		~~0.156~~		0.095		~~0.044~~
.593		0.082				0.066
.704		~~0.092~~		0.094		0.053

TABLE V (Cont.)

PRESSURE COEFFICIENTS ON FLAT RECTANGULAR WING
LEADING EDGE M= 19.2

ALPHA = 15 DEG., RUN = 849 P5 = 3528. PSI

X /C	2Y /B	0	.25	.5	.708	.917
.149		0.253	0.387	0.232	0.019	0.227 , ~~0.018~~
.260		0.193				0.142
.371		0.205		0.176		0.139
.482		~~0.254~~		0.123		0.058
.593		0.127				~~0.007~~
.704		~~0.176~~		0.133		0.026

TABLE V (Cont.)

PRESSURE COEFFICIENTS ON FLAT RECTANGULAR WING
LEADING EDGE M= 18.8

ALPHA = 0 DEG., RUN = 845 P5 = 5764. PSI

X /C	2Y /B	0	.25	.5	.708	.917
.149		0.093	0.108	0.076	0.080	~~0.020~~ , 0.052
.260		0.055				~~0.010~~
.371		0.046		0.058		0.038
.482		0.029		0.032		0.023
.593		0.033				
.704		0.046		0.037		0.029

TABLE V (Cont.)

PRESSURE COEFFICIENTS ON TWISTED RECTANGULAR WING
LEADING EDGE M= 19.2

ALPHA = 0 DEG., RUN = 856 P5 = 3368. PSI

X/C	2Y/B	0	.25	.5	.708	.917
.149		0.072	0.073	0.074	0.015	0.070 , 0.091
.260		0.052				0.051
.371		0.050		0.052		0.036
.482		0.045		0.042		0.021
.593		0.039				0.031
.704		0.029		0.071		

ALPHA = 2 DEG., RUN = 857 P5 = 3688. PSI

X/C	2Y/B	0	.25	.5	.708	.917
.149		0.078	0.072	0.076	0.013	0.087 , 0.105
.260		0.052				0.073
.371		0.052		0.062		0.047
.482		0.050		0.049		0.033
.593		0.043				0.040
.704		0.025		0.071		0.051

TABLE V (Cont.)

PRESSURE COEFFICIENTS ON TWISTED RECTANGULAR WING
LEADING EDGE M= 19.2

ALPHA = 2 DEG., RUN = 854 P5 = 3848. PSI

X/C	2Y/B	0	.25	.5	.708	.917
.149		0.069	0.071	0.068	0.019	0.081 , 0.099
.260		0.048				0.066
.371		0.048		0.055		0.045
.482		0.045		0.049		0.028
.593		0.042				0.039
.704		0.025		0.079		0.053

ALPHA = 5 DEG., RUN = 853 P5 = 3448. PSI

X/C	2Y/B	0	.25	.5	.708	.917
.149		0.101	0.090	0.108	0.013	0.121 , 0.136
.260		0.067				0.091
.371		0.068		0.078		0.073
.482		0.061		0.067		0.045
.593		0.036				0.054
.704		0.026		0.063		

TABLE V (Cont.)

PRESSURE COEFFICIENTS ON TWISTED RECTANGULAR WING
LEADING EDGE M= 19.2

ALPHA = 10 DEG., RUN = 851 P5 = 3448. PSI

X /C	2Y /B	0	.25	.5	.708	.917
.149		0.138	0.145	0.168	0.027	0.196 , 0.187
.260		0.109				0.145
.371		0.111		0.140		0.107
.482		0.121		0.105		0.071
.593		0.084				0.078
.704		0.047		0.097		

ALPHA = 15 DEG., RUN = 852 P5 = 3608. PSI

X /C	2Y /B	0	.25	.5	.708	.917
.149		0.215	0.204	0.240	0.039	0.297 , 0.264
.260		0.177				0.207
.371		0.185		0.214		0.172
.482		0.186		0.165		0.122
.593		0.093				0.126
.704		0.076		0.136		

TABLE V (Cont.)

PRESSURE COEFFICIENTS ON CAMBERED RECTANGULAR WING
LEADING EDGE M= 19.2

ALPHA = 0 DEG., RUN = 863 P5 = 3608. PSI

X/C	2Y/B = 0	.25	.5	.708	.917
.149	0.093	0.062	0.116	0.109	0.078 , 0.102
.260	0.053				0.041
.371	0.049		0.051		0.037
.482	0.042		0.033		0.015
.593	0.030				
.704	0.031		0.028		0.017

ALPHA = 2 DEG., RUN = 862 P5 = 3528. PSI

X/C	2Y/B = 0	.25	.5	.708	.917
.149	0.115	0.072	0.126	0.133	0.109 , 0.125
.260	0.092				0.060
.371	0.061		0.062		0.051
.482	~~0.003~~		0.046		0.025
.593	0.028				
.704	0.042				0.014

TABLE V (Cont.)

PRESSURE COEFFICIENTS ON CAMBERED RECTANGULAR WING
LEADING EDGE M= 19.2

ALPHA = 5 DEG., RUN = 861 P5 = 3528. PSI

X/C	2Y/B = 0	.25	.5	.708	.917
.149	0.161	0.121	0.159	0.174	0.147 , 0.157
.260	0.101				0.089
.371	0.087		0.081		0.073
.482	0.069		0.060		0.032
.593	~~0.044~~				
.704	0.062				0.020

ALPHA = 10 DEG., RUN = 859 P5 = 3528. PSI

X/C	2Y/B = 0	.25	.5	.708	.917
.149	0.220	0.184	0.270	0.185	0.195 , ~~0.293~~
.260	0.161				0.123
.371	0.141		0.134		0.109
.482	0.125		0.106		0.058
.593	~~0.068~~				~~0.083~~
.704	0.110				0.055

TABLE V (Cont.)

PRESSURE COEFFICIENTS ON CAMBERED RECTANGULAR WING
LEADING EDGE M= 19.2

ALPHA = 15 DEG., RUN = 860 PS = 3608. PSI

X/C	2Y/B	0	.25	.5	.708	.917
.149		0.305	0.258	0.364	0.354	0.310 , 0.322
.260		0.228				0.210
.371		0.195		0.203		0.179
.482		0.177		0.154		~~0.085~~
.593		~~0.111~~				0.087
.704		0.172				0.054

TABLE VI

PRESSURE COEFFICIENTS ON FLAT 70 DEGREE DELTA WING
APEX M= 18.9

ALPHA = 0 DEG., RUN = 836 P5 = 3448. PSI

X /C ROOT	2Y /B	0	.147	.295	.442	.590	.738
.237		0.031					
.384		0.026					
.532		0.018		0.025			
.585				0.015			
.679		0.026		0.021	0.028		
.827		0.009				0.030	
.880						0.028	
.974				0.017		0.033	0.009

ALPHA = 2 DEG., RUN = 841 P5 = 3209. PSI

X /C ROOT	2Y /B	0	.147	.295	.442	.590	.738
.237		0.034					
.384		0.028					
.532		0.020		0.021			
.585				0.010			
.679		0.019		0.010	0.024		
.827		0.020				0.031	
.880						0.022	
.974				0.014		0.014	0.017

TABLE VI (Cont.)

PRESSURE COEFFICIENTS ON FLAT 70 DEGREE DELTA WING
APEX M= 18.9

ALPHA = 5 DEG., RUN = 837 P5 = 3289. PSI

X /C	2Y /B	0	.147	.295	.442	.590	.738
ROOT							
.237		0.047					
.384		0.046					
.532		0.041		0.045			
.585				0.024			
.679		0.017		0.021	0.031		
.827		0.038				0.033	
.880						0.023	
.974				0.023		0.028	0.042

ALPHA = 10 DEG., RUN = 838 P5 = 3688. PSI

X /C	2Y /B	0	.147	.295	.442	.590	.738
ROOT							
.237							
.384		0.080					
.532		0.087		0.092			
.585				0.043			
.679				0.044	0.048		
.827		0.092				0.063	
.880						0.048	
.974				0.046		0.035	

TABLE VI (Cont.)

PRESSURE COEFFICIENTS ON FLAT 70 DEGREE DELTA WING
APEX M= 18.9

ALPHA = 15 DEG., RUN = 840 P5 = 3688. PSI

X /C ROOT	2Y /B	0	.147	.295	.442	.590	.738
.237		0.138					
.384		0.132					
.532		0.141		0.155			
.585				0.075			
.679		0.075		0.089	0.082		
.827		0.165				0.127	
.880						0.099	
.974				0.089		0.089	0.160

TABLE VI (Cont.)

PRESSURE COEFFICIENTS ON FLAT 70 DEGREE DELTA WING
APEX M= 18.5

ALPHA = 0 DEG., RUN = 842 P5 = 5604. PSI

X/C ROOT	2Y/B 0	.147	.295	.442	.590	.738
.237	0.020					
.384	0.019					
.532	0.010		0.016			
.585			0.012			
.679	0.024		0.017	0.028		
.827	0.003				0.025	
.880					0.026	
.974			0.012		0.022	0.004

TABLE VI (Cont.)

PRESSURE COEFFICIENTS ON SINE WAVE CAMBERED 70 DEGREE DELTA WING
APEX M= 18.9

ALPHA = 0 DEG., RUN = 800 P5 = 3528. PSI

X /C ROOT	2Y /B	0	.147	.295	.442	.590	.738
.237		0.031					
.384		0.018					
.532		0.015		0.012			
.585				0.014			
.679		0.015		0.002	0.015		
.827		0.018				0.026	
.880						0.024	
.974				0.020		0.029	0.028

ALPHA = 2 DEG., RUN = 797 P5 = 3528. PSI

X /C ROOT	2Y /B	0	.147	.295	.442	.590	.738
.237		0.041					
.384		0.024					
.532		0.013		0.012			
.585				0.011			
.679		0.017		0.010			
.827		0.021				0.036	
.880						0.030	
.974				0.022		0.039	0.042

TABLE VI (Cont.)

PRESSURE COEFFICIENTS ON SINE WAVE CAMBERED 70 DEGREE DELTA WING
APEX M= 18.9

ALPHA = 5 DEG., RUN = 795 P5 = 3688. PSI

X/C ROOT	2Y/B	0	.147	.295	.442	.590	.738
.237		0.057					
.384		0.025	~~-0.089~~				
.532		0.013		0.007			
.585				0.014			
.679		0.019		0.018	0.025		
.827		0.046				0.034	
.880						0.044	
.974				0.034		0.068	0.100

ALPHA = 10 DEG., RUN = 792 P5 = 3608. PSI

X/C ROOT	2Y/B	0	.147	.295	.442	.590	.738
.237		0.110					
.384		0.055	~~-0.184~~				
.532		0.031		0.026			
.585				0.025			
.679		0.036		0.050	0.065		
.827		0.090				0.070	
.880						0.108	
.974				0.082		0.159	0.207

TABLE VI (Cont.)

PRESSURE COEFFICIENTS ON SINE WAVE CAMBERED 70 DEGREE DELTA WING
APEX M= 18.9

ALPHA = 15 DEG., RUN = 794 P5 = 3528. PSI

X /C ROOT	2Y /B	0	.147	.295	.442	.590	.738
.237		0.196					
.384		0.084	~~0.329~~				
.532		0.079		0.069			
.585				0.078			
.679		0.093		0.112	0.125		
.827		0.217				0.139	
.880						0.194	
.974				0.219		0.329	0.403

ALPHA = 15 DEG., RUN = 793 P5 = 3289. PSI

X /C ROOT	2Y /B	0	.147	.295	.442	.590	.738
.237		0.188					
.384			~~0.381~~				
.532		0.067		0.074			
.585				0.084			
.679				0.114			
.827		0.240				0.136	
.880						0.200	
.974						0.329	0.407

TABLE VI (Cont.)

PRESSURE COEFFICIENTS ON SINE WAVE CAMBERED 70 DEGREE DELTA WING
APEX M= 18.5

ALPHA = 10 DEG., RUN = 801 P5 = 6083. PSI

X /C ROOT	2Y /B 0	.147	.295	.442	.590	.738
.237	0.102					
.384	0.038					
.532	0.021		0.013			
.585			0.016			
.679	0.033		0.048	0.043		
.827	0.083				0.076	
.880					0.098	
.974			0.089		0.164	0.201

TABLE VI (Cont.)

PRESSURE COEFFICIENTS ON CIRCULAR ARC CAMBERED 70 DEGREE DELTA WING
APEX M= 18.9

ALPHA = 0 DEG., RUN = 821 P5 = 4247. PSI

X /C ROOT	2Y /B	0	.147	.295	.442	.590	.738
.237							
.384		0.028	0.031				
.532		0.024		0.026			
.585				0.006			
.679		0.022		0.011	0.021		
.827		0.016				0.010	
.880							
.974				0.012		0.012	0.004

ALPHA = 2 DEG., RUN = 825 P5 = 3528. PSI

X /C ROOT	2Y /B	0	.147	.295	.442	.590	.738
.237							
.384		0.035	0.041				
.532		0.024		0.031			
.585				0.006			
.679		0.022		0.015	0.025		
.827		0.018				0.010	
.880						0.005	
.974				0.008		0.010	0.004

TABLE VI (Cont.)

PRESSURE COEFFICIENTS ON CIRCULAR ARC CAMBERED 70 DEGREE DELTA WING
APEX M= 18.9

ALPHA = 5 DEG., RUN = 823 P5 = 3528. PSI

X /C	2Y /B	0	.147	.295	.442	.590	.738
ROOT							
.237							
.384		0.066	0.083				
.532		0.045		0.046			
.585				0.021			
.679		0.035		0.021	0.031		
.827		0.030				0.013	
.880						0.027	
.974				0.013		0.023	0.009

ALPHA = 10 DEG., RUN = 820 P5 = 3528. PSI

X /C	2Y /B	0	.147	.295	.442	.590	.738
ROOT							
.237							
.384		0.116	0.143				
.532		0.082		0.083			
.585				0.039			
.679		0.058		0.039	0.046		
.827		0.048				0.032	
.880						0.058	
.974				0.018		0.041	0.021

TABLE VI (Cont.)

PRESSURE COEFFICIENTS ON CIRCULAR ARC CAMBERED 70 DEGREE DELTA WING
APEX M= 18.9

ALPHA = 15 DEG., RUN = 822 P5 = 3289. PSI

X /C ROOT	2Y /B	0	.147	.295	.442	.590	.738
.237							
.384		0.195	0.216				
.532				0.187			
.585				0.076			
.679		0.106			0.100		
.827		0.103				0.066	
.880							
.974				0.058		0.072	0.053

TABLE VI (Cont.)

PRESSURE COEFFICIENTS ON CIRCULAR ARC CAMBERED 70 DEGREE DELTA WING
APEX M= 18.5

ALPHA = 0 DLG., RUN = 827 P5 = 6722. PSI

X /C ROOT	2Y /B	0	.147	.295	.442	.590	.738
.237							
.384		0.018	0.023				
.532		0.015		0.020			
.585				0.006			
.679		0.015		0.013	0.016		
.827		0.014				0.010	
.880							
.974				0.007		0.006	0.002

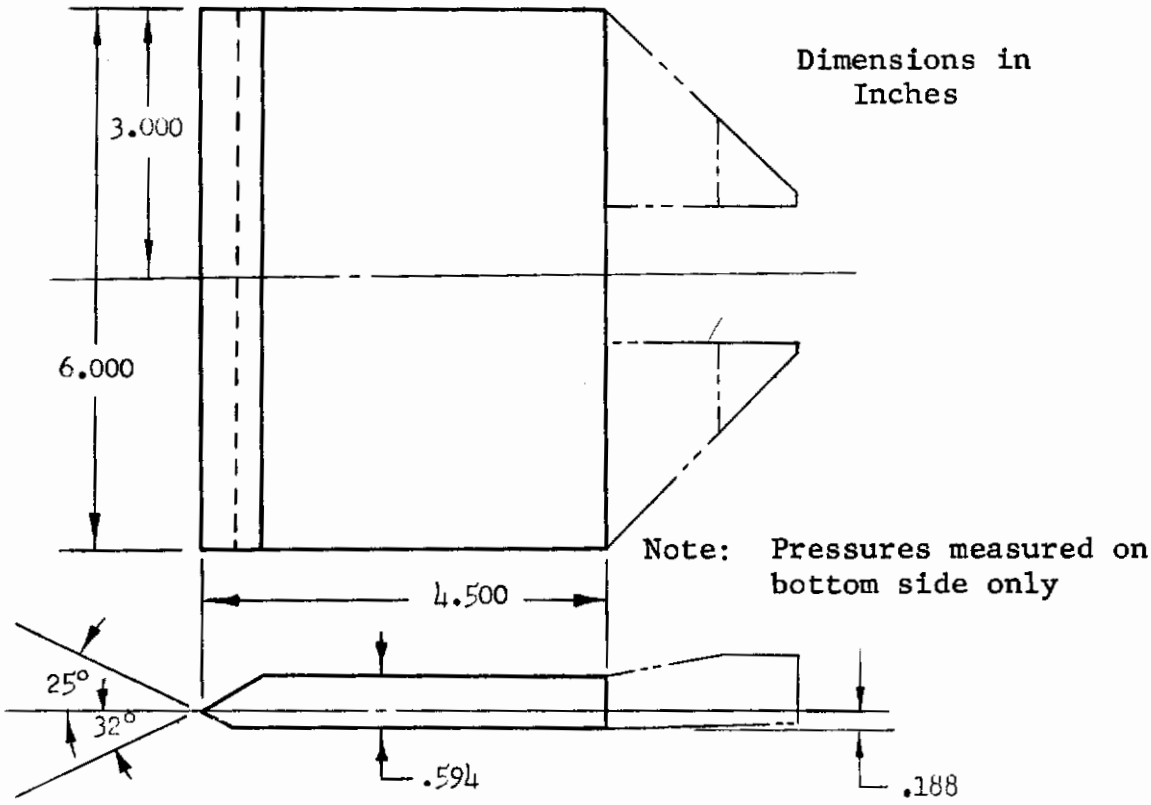

Fig. 1 - Sketch of Flat Rectangular Wing

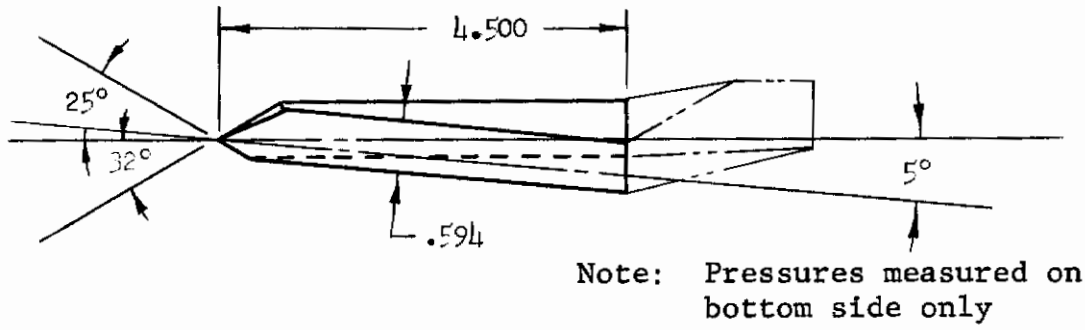

Fig. 2a - Profile of Rectangular Wing with Symmetrical Linear Twist

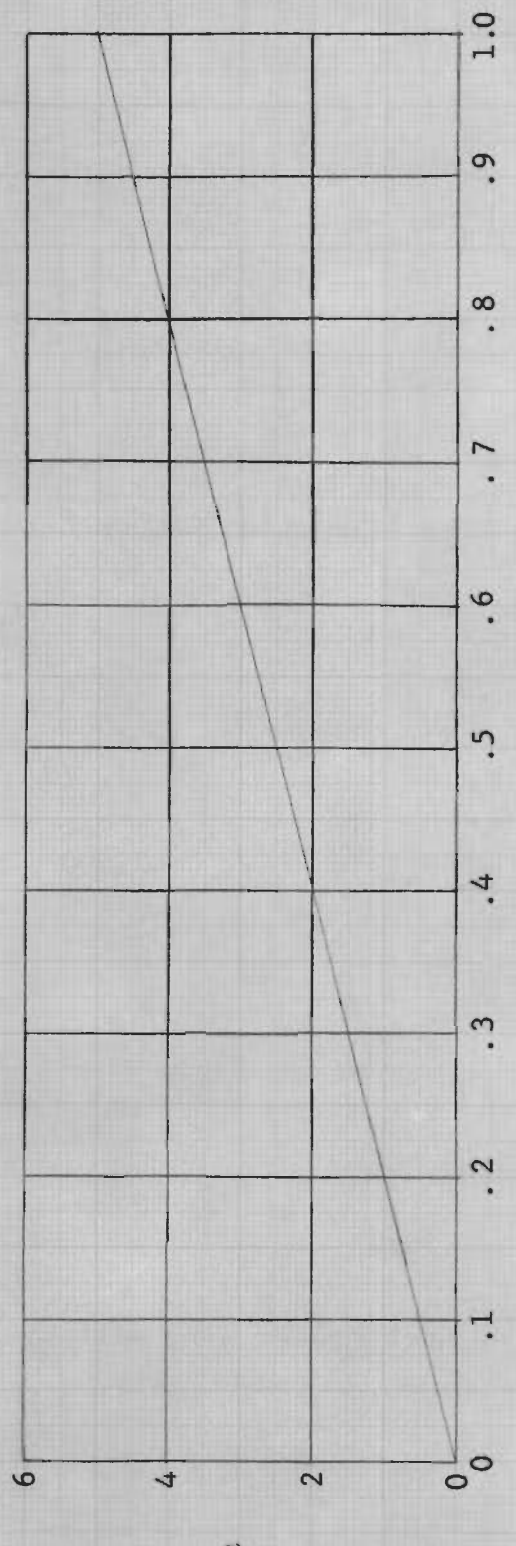

Fig. 2b - Spanwise Variation of Angle of Attack Due to Twist

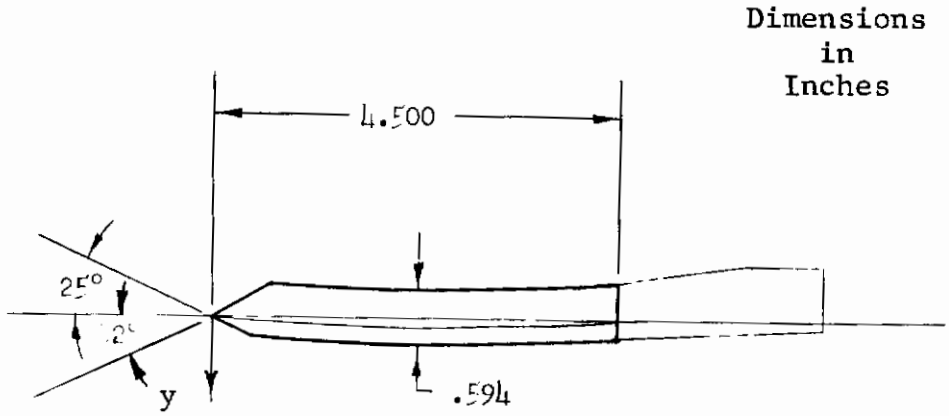

Note: Pressures measured on bottom side only

Ordinates of Section Camber Line

x	y	x	y
.188	.035	2.250	.098
.250	.039	2.500	.094
.500	.055	2.750	.088
.750	.069	3.000	.080
1.000	.080	3.250	.069
1.250	.088	3.500	.055
1.500	.094	3.750	.039
1.750	.098	4.000	.021
2.000	.099	4.250	0

Fig. 3a - Profile of Rectangular Wing with Circular-Arc Camber

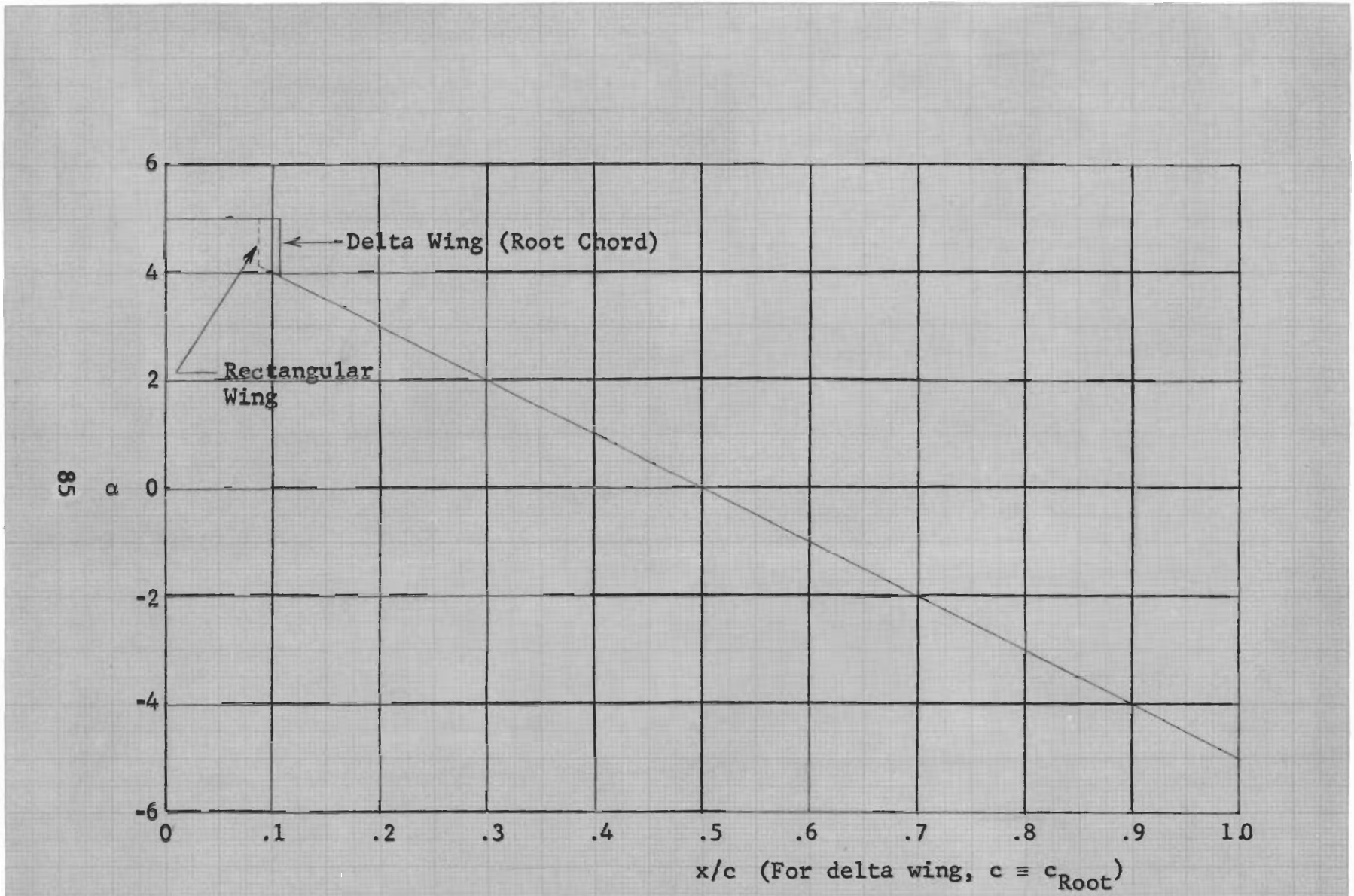

Fig. 3b - Chordwise Variation of Angle of Attack Due to Circular-Arc Camber

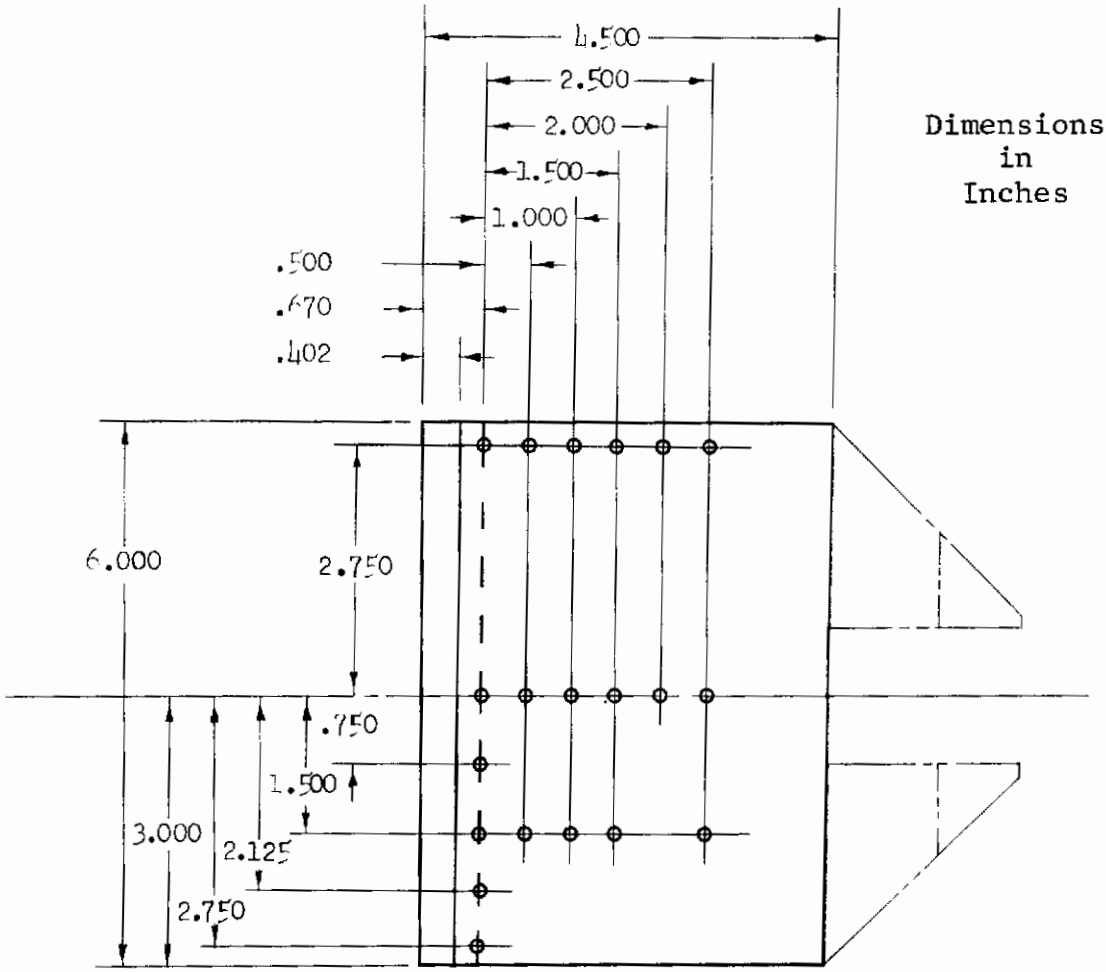

Fig. 4 - Location of Pressure Transducers in Rectangular Wings

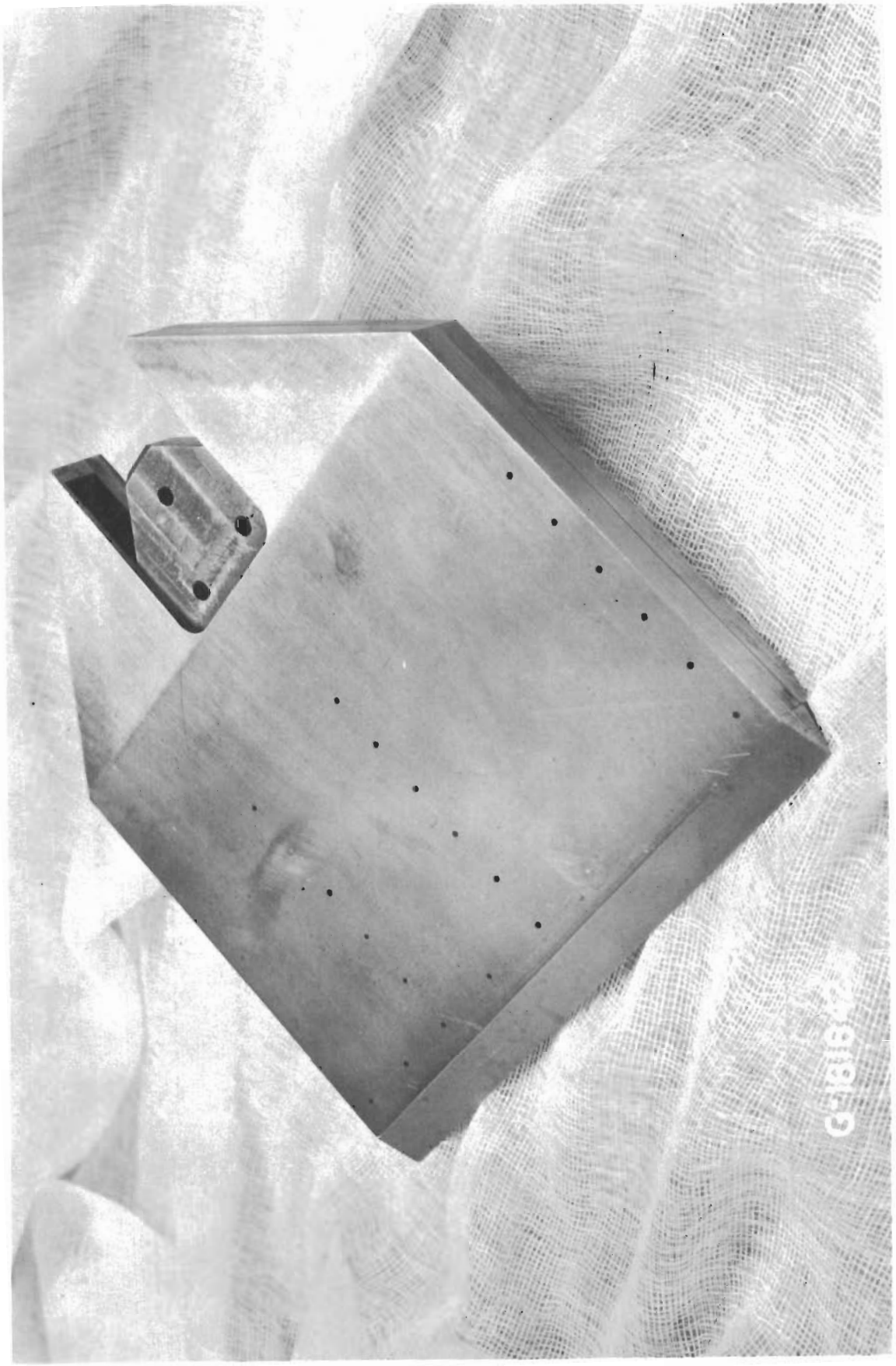

Fig. 5 - Photograph of Flat Rectangular Wing

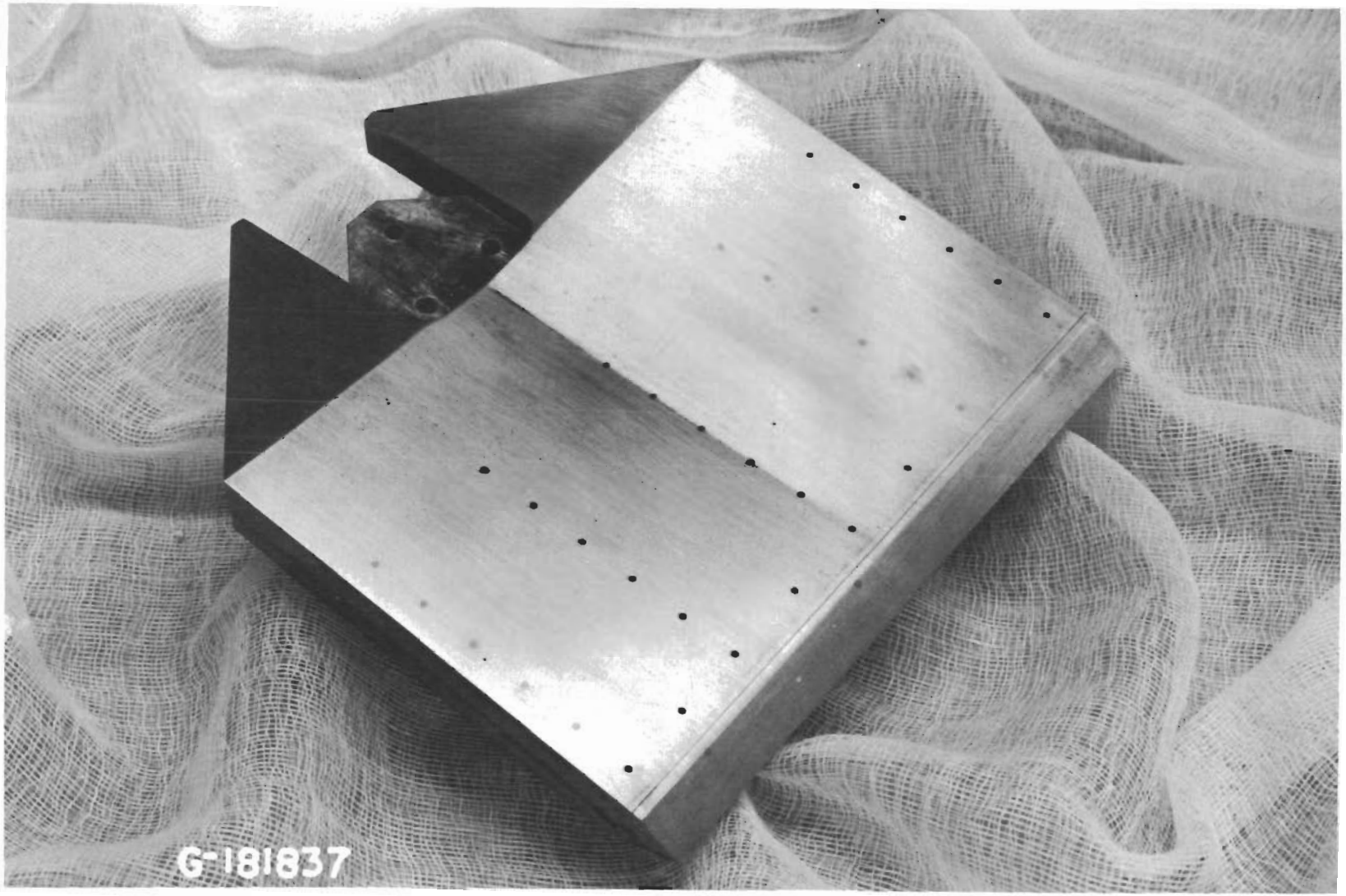

Fig. 6 - Photograph of Rectangular Wing with Symmetrical Linear Twist

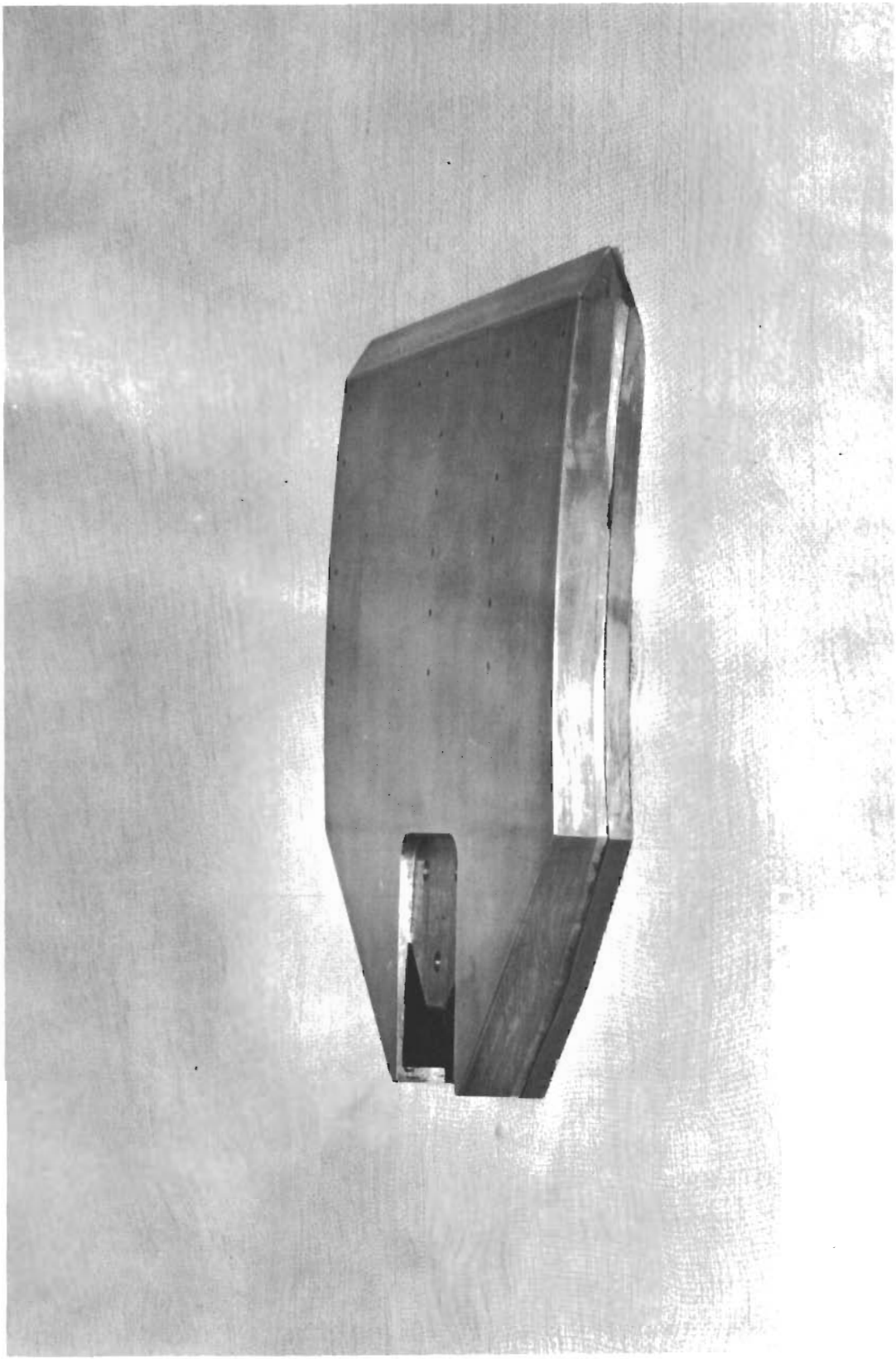

Fig. 7 - Photograph of Rectangular Wing with Circular-Arc Camber

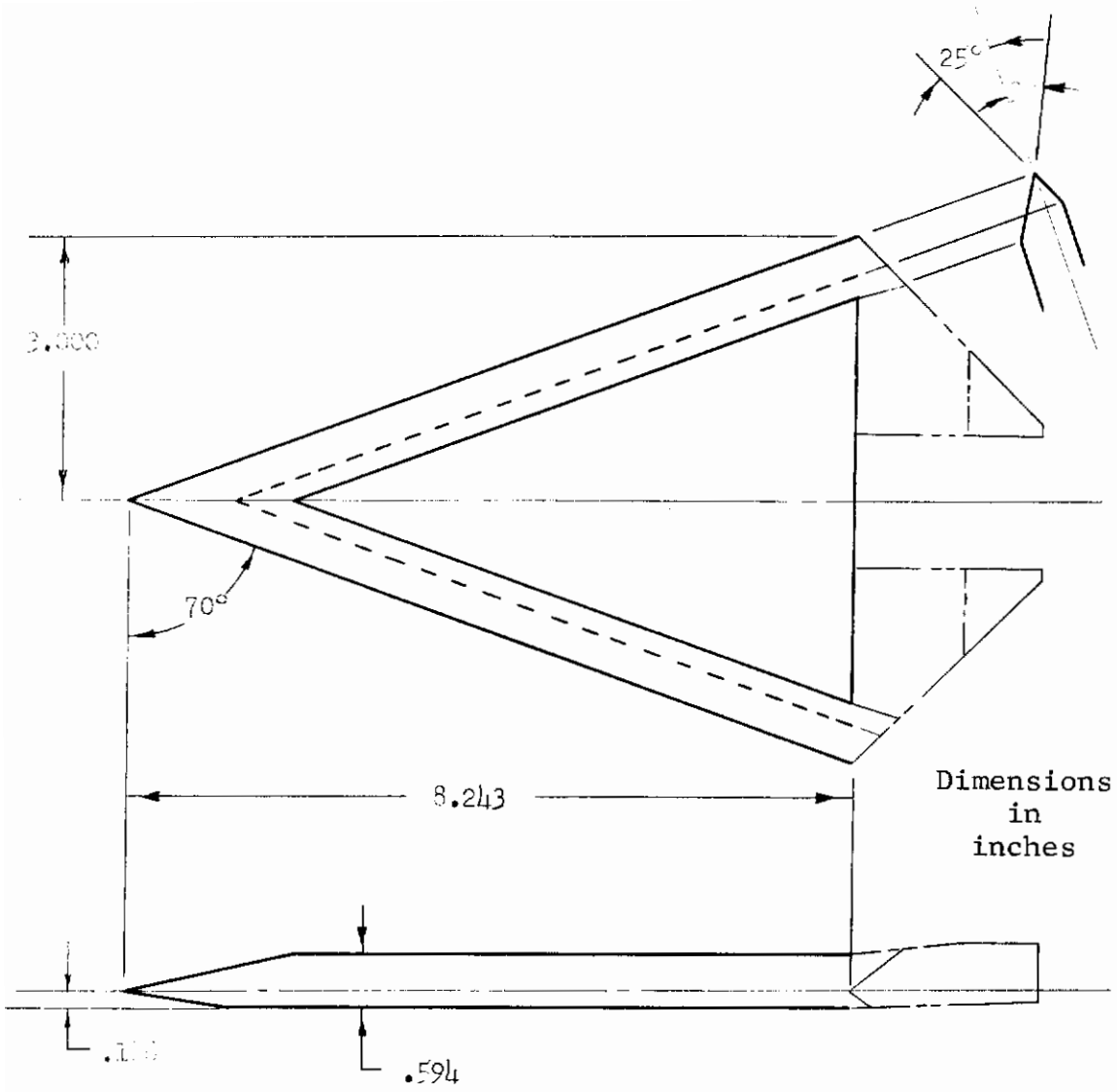

Note: Pressures measured on
bottom side only

Fig. 8 - Sketch of Flat 70° Delta Wing

Ordinates of Section Camber Line

x	y
0	0
.250	.021
.500	.041
.750	.060
1.000	.077
1.250	.093
1.500	.107
1.750	.121
2.000	.132
2.250	.143
2.500	.152
2.750	.160
3.000	.167
3.250	.172
3.500	.176
3.750	.179
4.000	.180
4.250	.180
4.500	.179
4.750	.176
5.000	.172
5.250	.167
5.500	.160
5.750	.152
6.000	.143
6.250	.132
6.500	.120
6.750	.107
7.000	.092
7.250	.076
7.500	.059
7.750	.041
8.000	.021
8.242	0

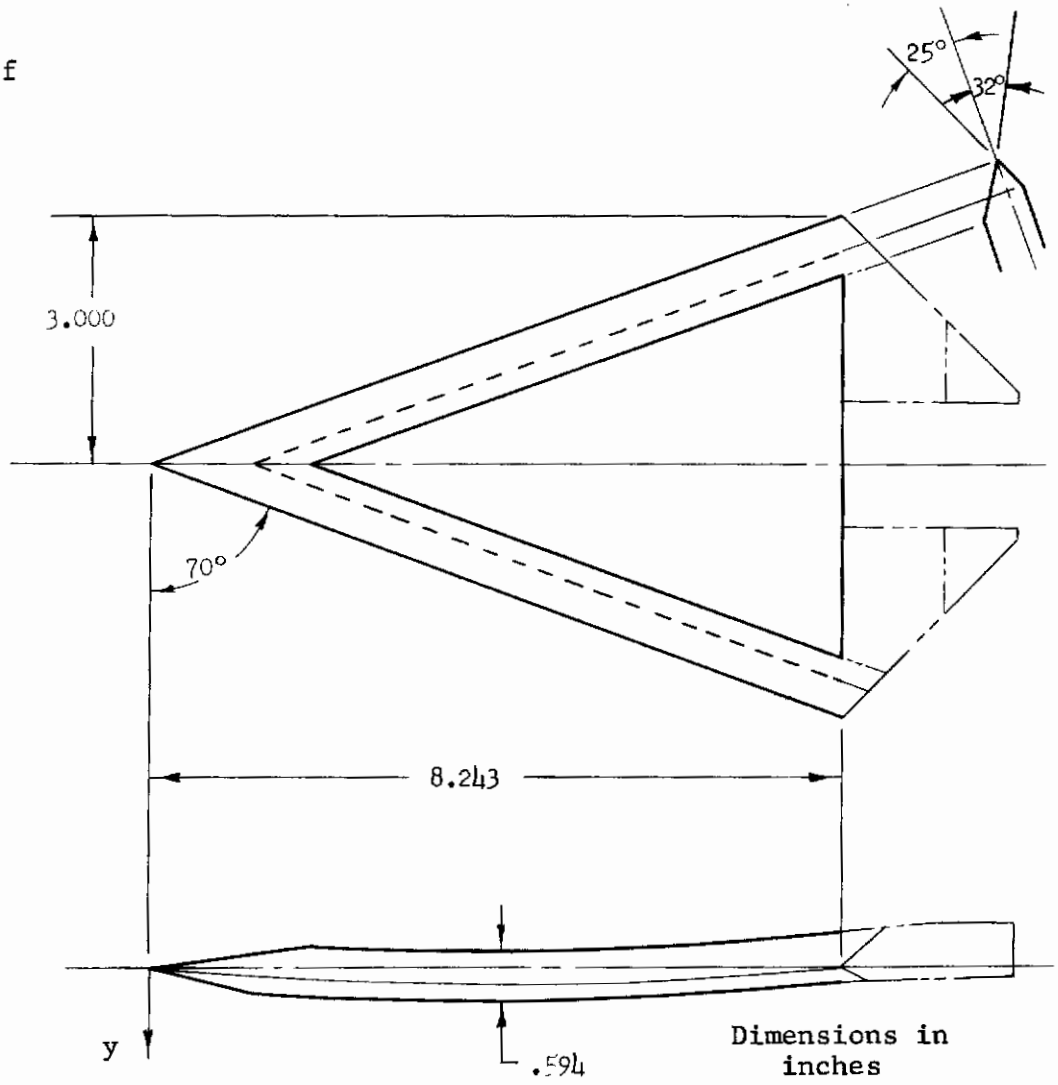

Note: Pressures measured on bottom side only

Fig. 9 - Sketch of 70° Delta Wing with Circular-Arc Camber

Ordinates of Section Camber Line

x	y
.000	.000
.250	+.022
.500	+.043
.750	+.062
1.000	+.079
1.250	+.094
1.500	+.104
1.750	+.112
2.000	+.115
2.250	+.114
2.500	+.108
2.750	+.099
3.000	+.087
3.250	+.071
3.500	+.052
3.750	+.032
4.000	+.011
4.250	-.011
4.500	-.033
4.750	-.053
5.000	-.071
5.250	-.087
5.500	-.100
5.750	-.109
6.000	-.114
6.250	-.115
6.500	-.111
6.750	-.104
7.000	-.093
7.250	-.079
7.500	-.062
7.750	-.042
8.000	-.021
8.2425	.000

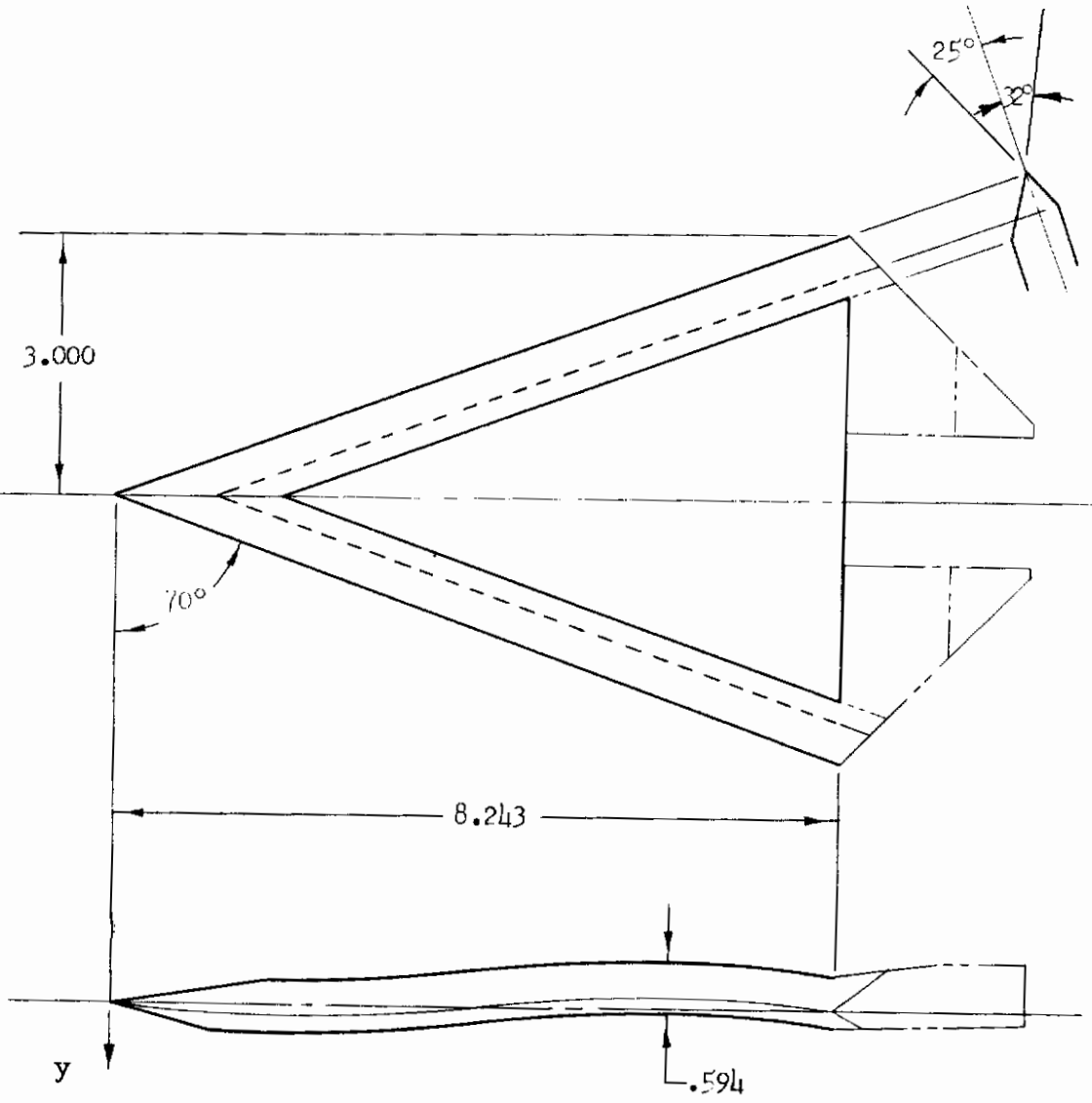

Dimensions in Inches

Fig. 10a - Sketch of 70° Delta Wing with Sine-Wave Camber

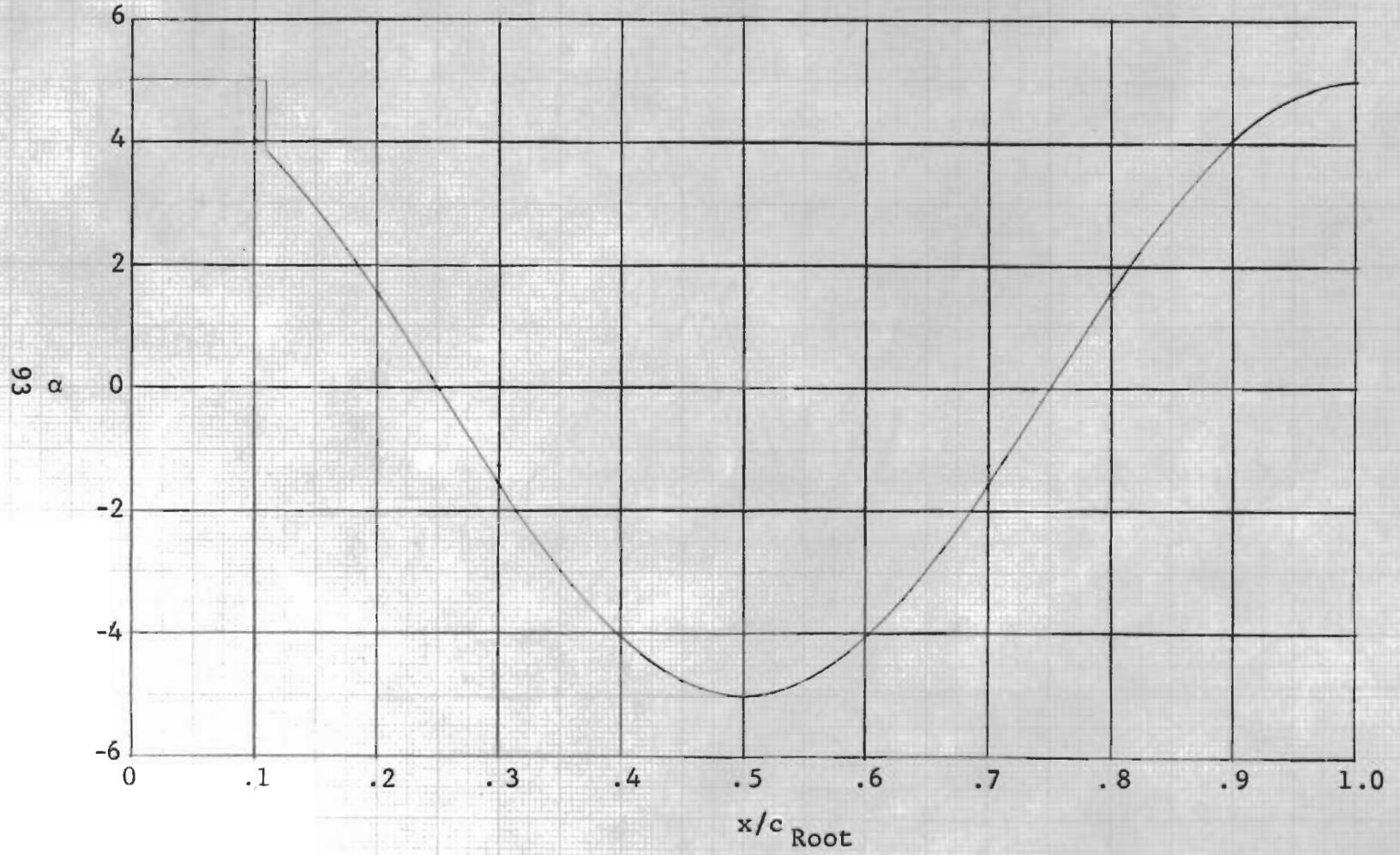

Fig. 10b - Chordwise Variation of Angle of Attack Due to Sine-Wave Camber

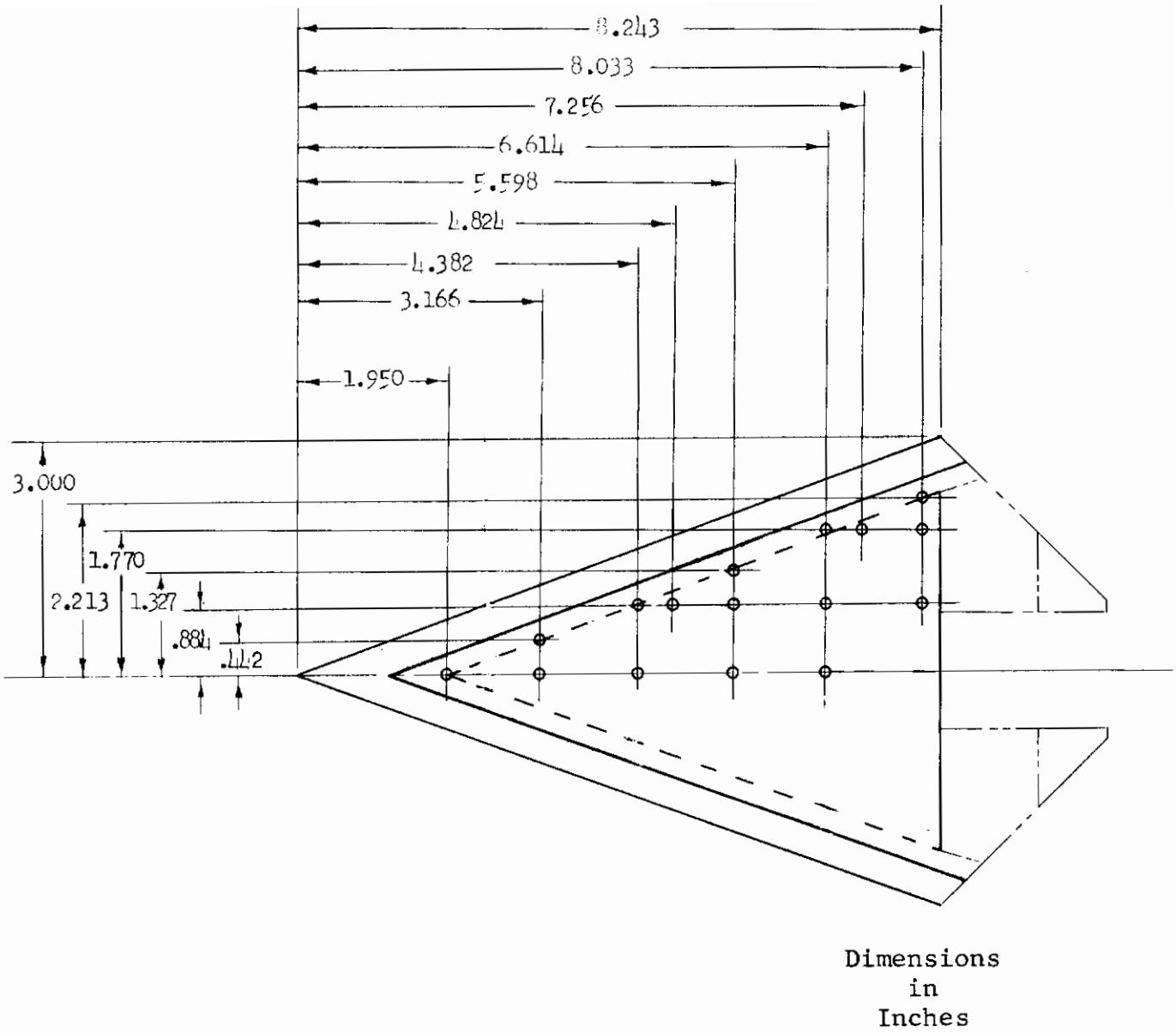

Fig. 11 - Location of Pressure Transducers in 70° Delta Wings

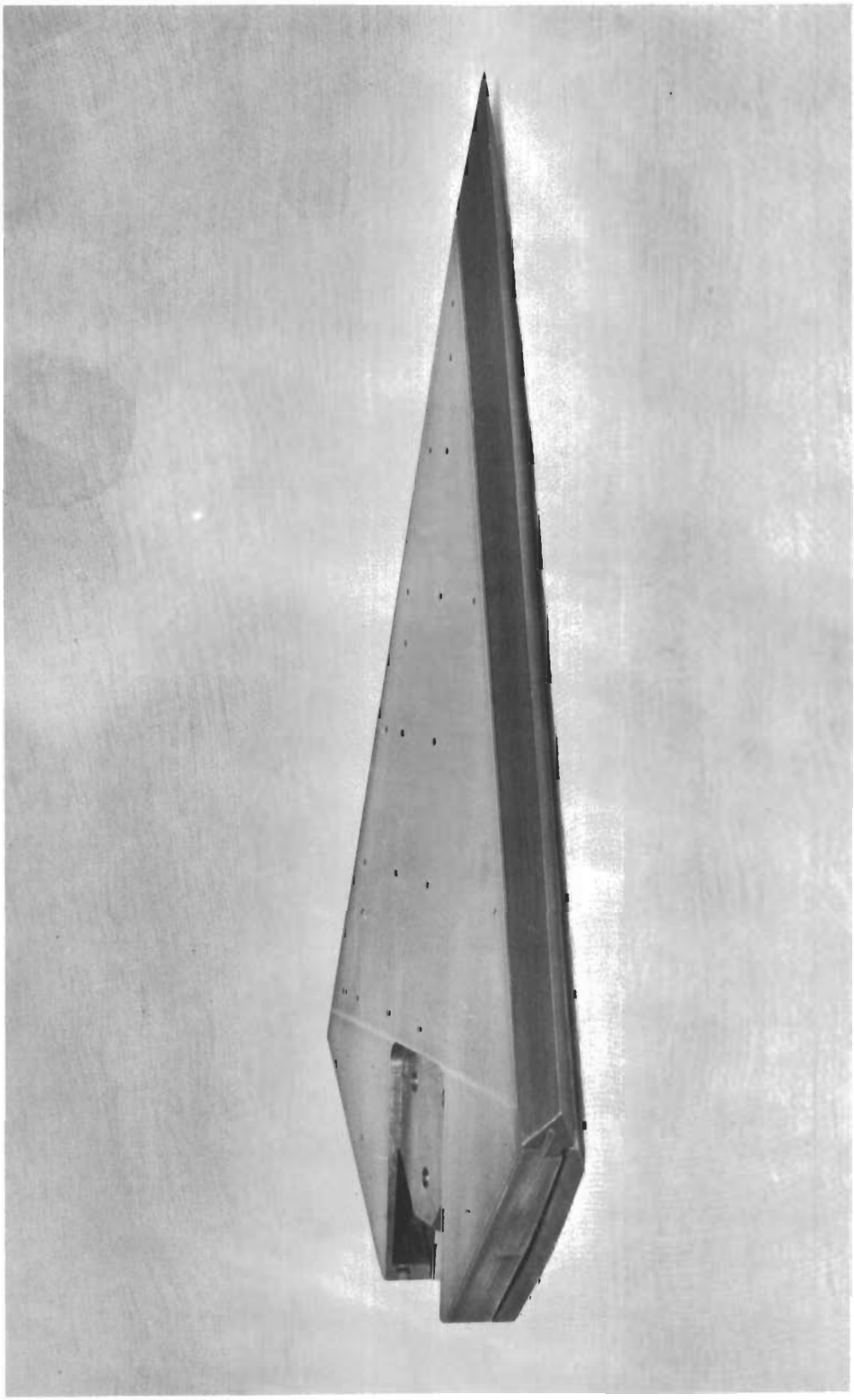

Fig. 12 - Photograph of Flat 70° Delta Wing

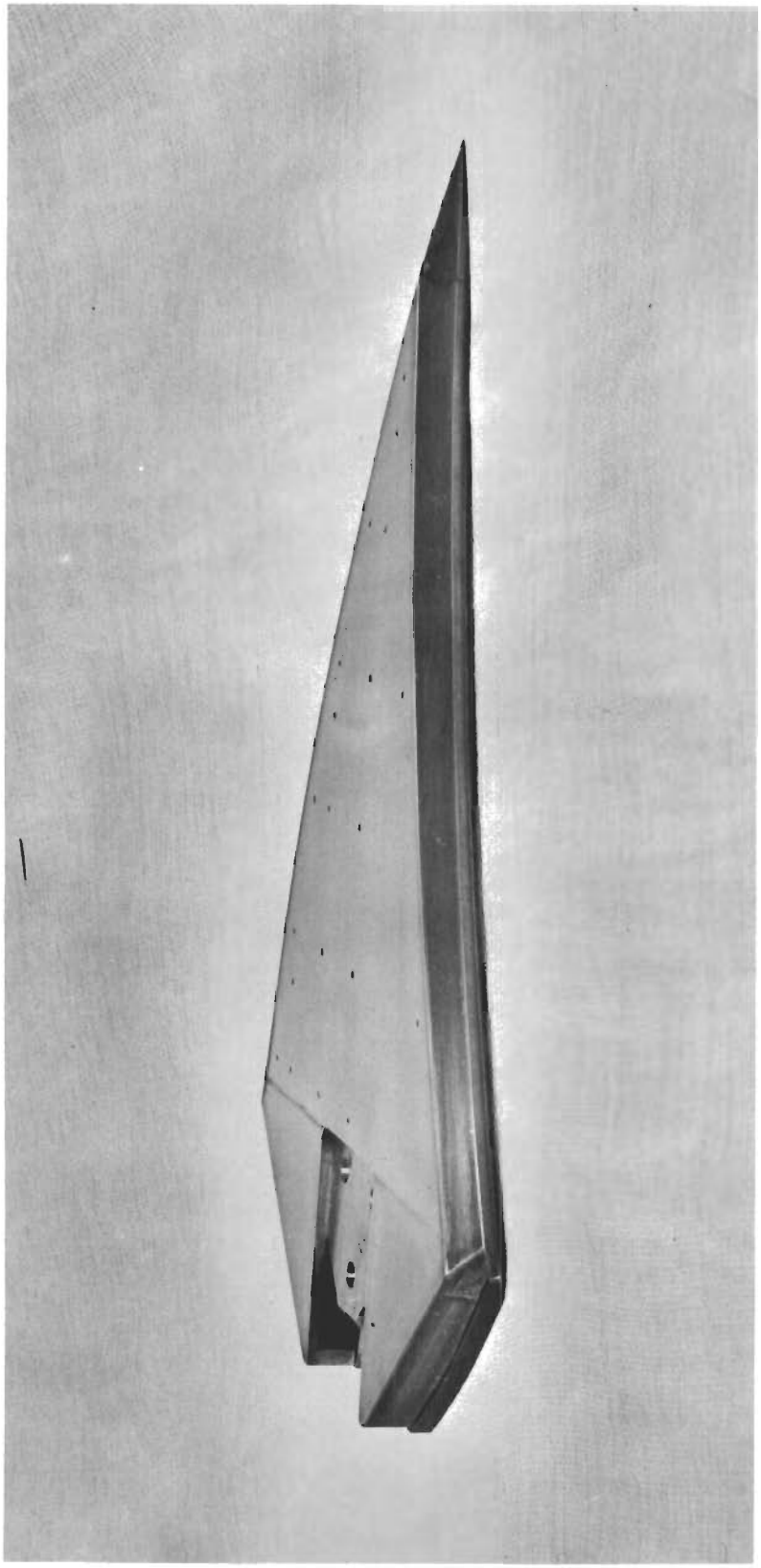

Fig. 13 - Photograph of 70° Delta Wing with Circular-Arc Camber

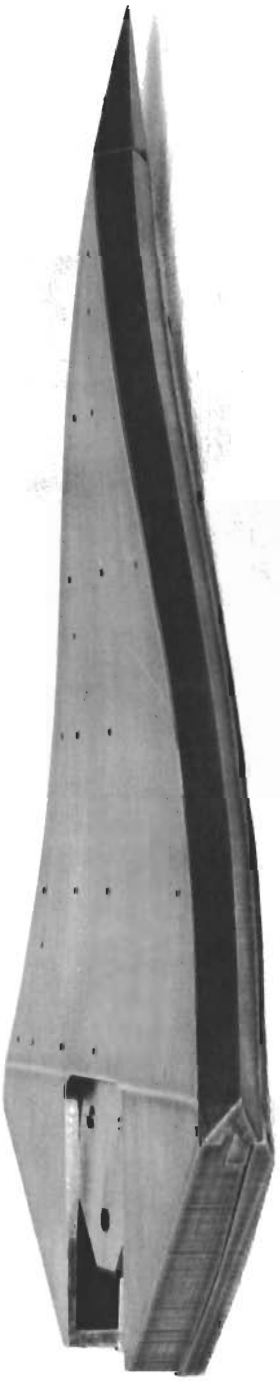

Fig. 14 - Photograph of 70° Delta Wing with Sine-Wave Camber

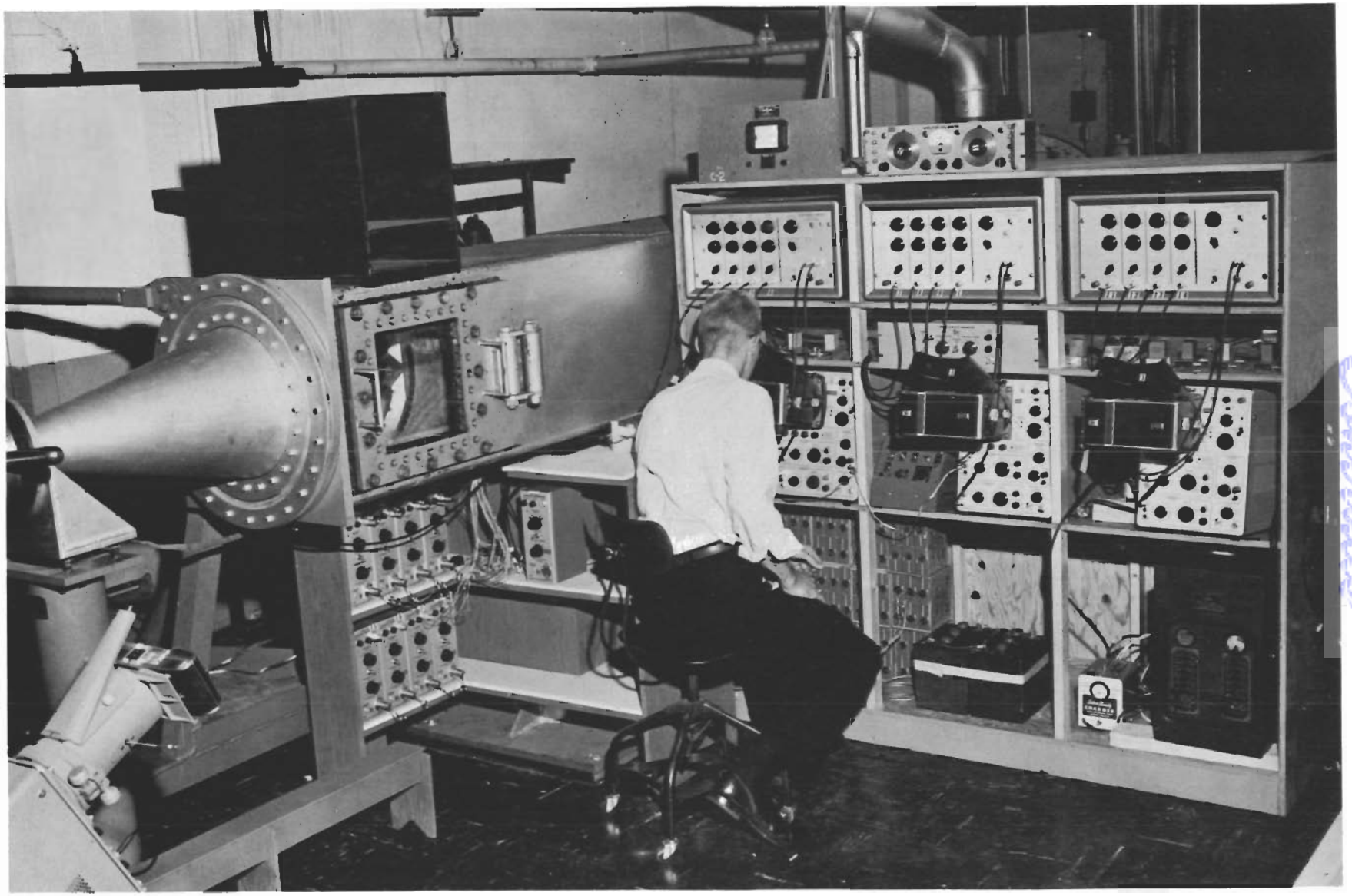

Fig. 15 - Photograph of Shock Tunnel Showing Nozzle, Dump Tank, and some Instrumentation

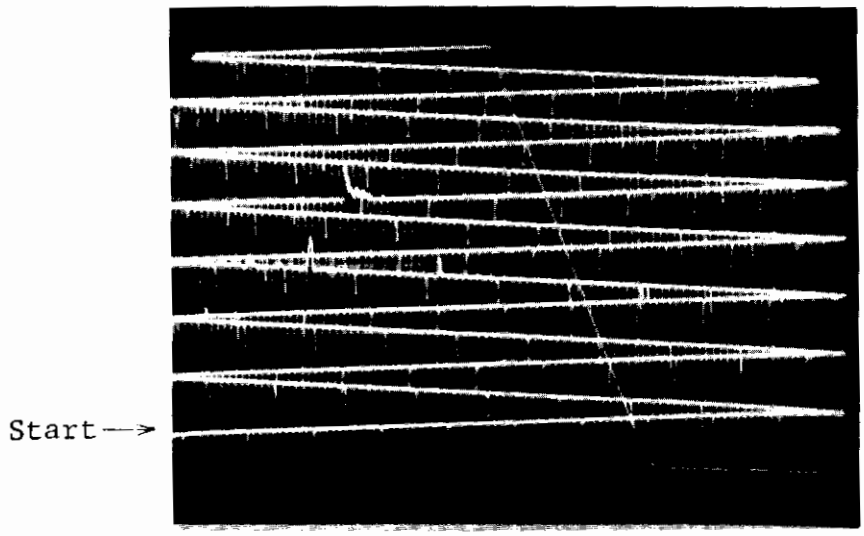

Fig. 16 - Typical Raster for Shock Time of Arrival Measurement. (Large time marks every 100 μ sec, small marks every 10 μ sec.)

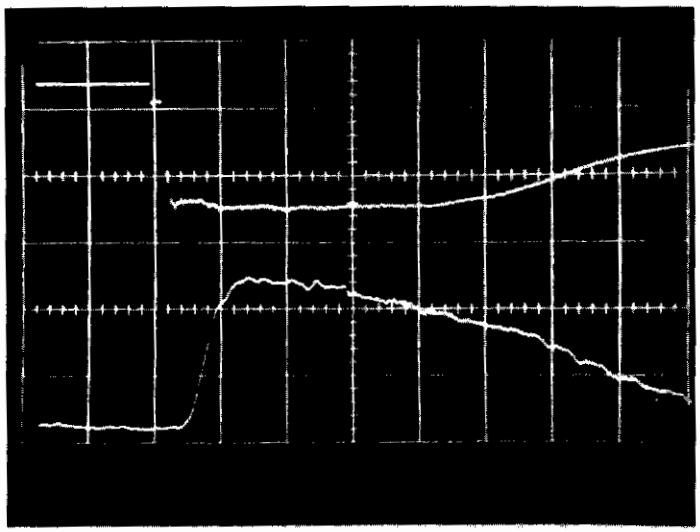

Fig. 17 - Typical Oscilloscope Record of Tunnel Stagnation Pressure, and Test Section Pitot Pressures. (Top trace - positive pressure down, bottom trace - positive pressure up, sweep speed 1 ms/cm from left to right.)

Fig. 18 - Photograph of Grumman Pressure Transducer

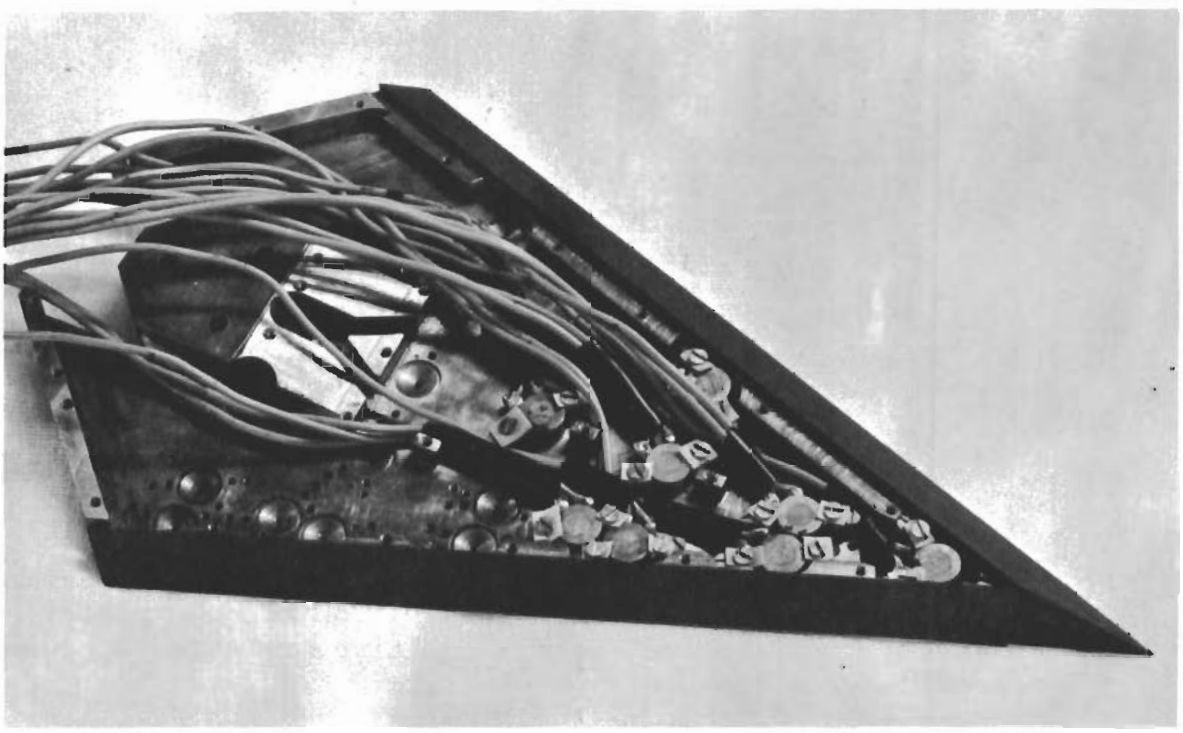

Fig. 19 - Photograph of Transducers Installed in Flat 70° Delta Wing

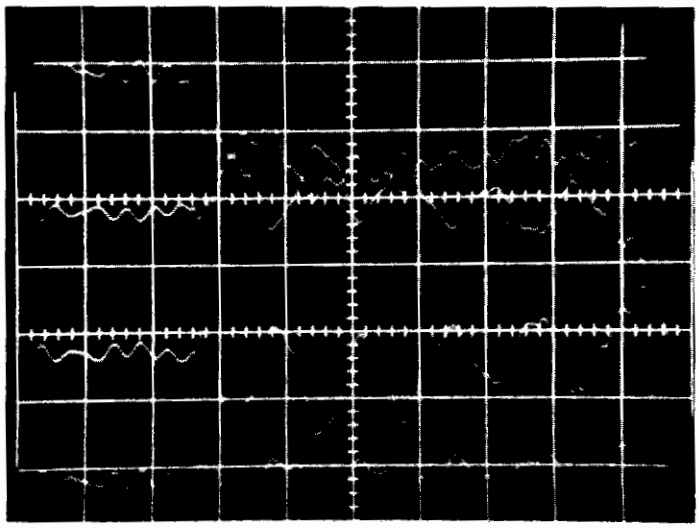

Fig. 20 - Output of Four Transducers when Rigidly Mounted in Model. (Sweep speed 1 ms/cm left to right.)

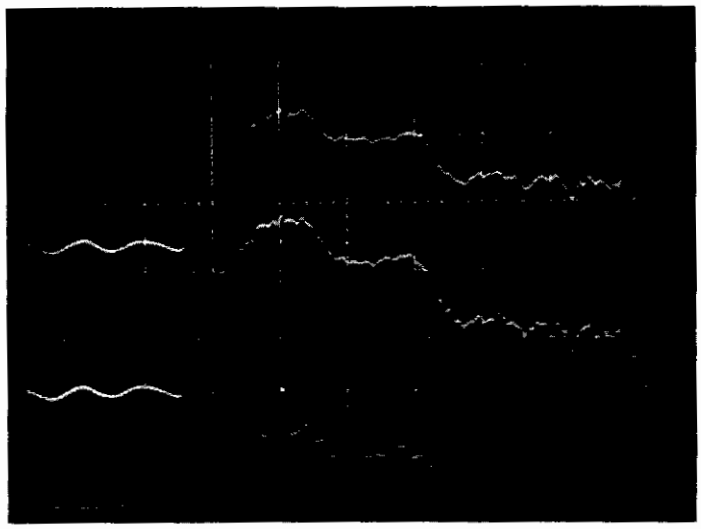

Fig. 21 - Output of Three Transducers Mounted on 1/2 "O"-Ring. (Positive pressure up, sweep speed 1 ms/cm left to right.)

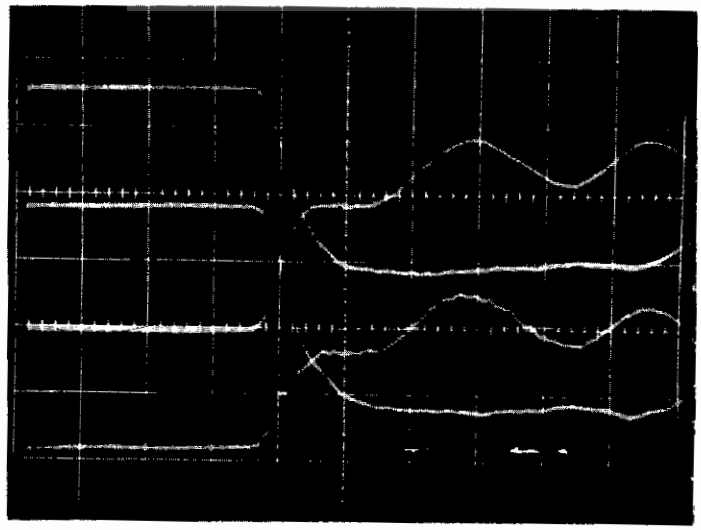

Fig. 22 - Output of Four Transducers Mounted on 1/2 "O"-Ring, after Improvement in Isolation of Test Section. (Positive pressure up for two bottom traces, down for two top traces, sweep speed 1 ms/cm left to right.)

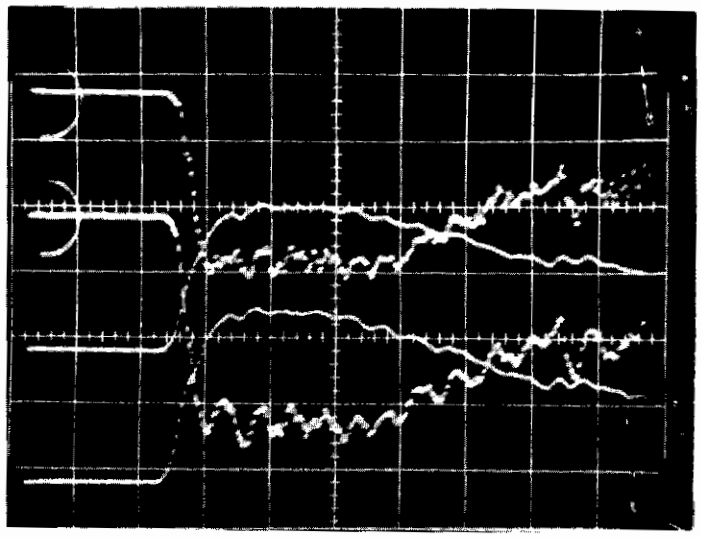

Fig. 23 - Output of Four Transducers Mounted on 1/32" Rubber Washer. (Positive pressure up for two bottom traces, down for two top traces, sweep speed 1 ms/cm left to right.)

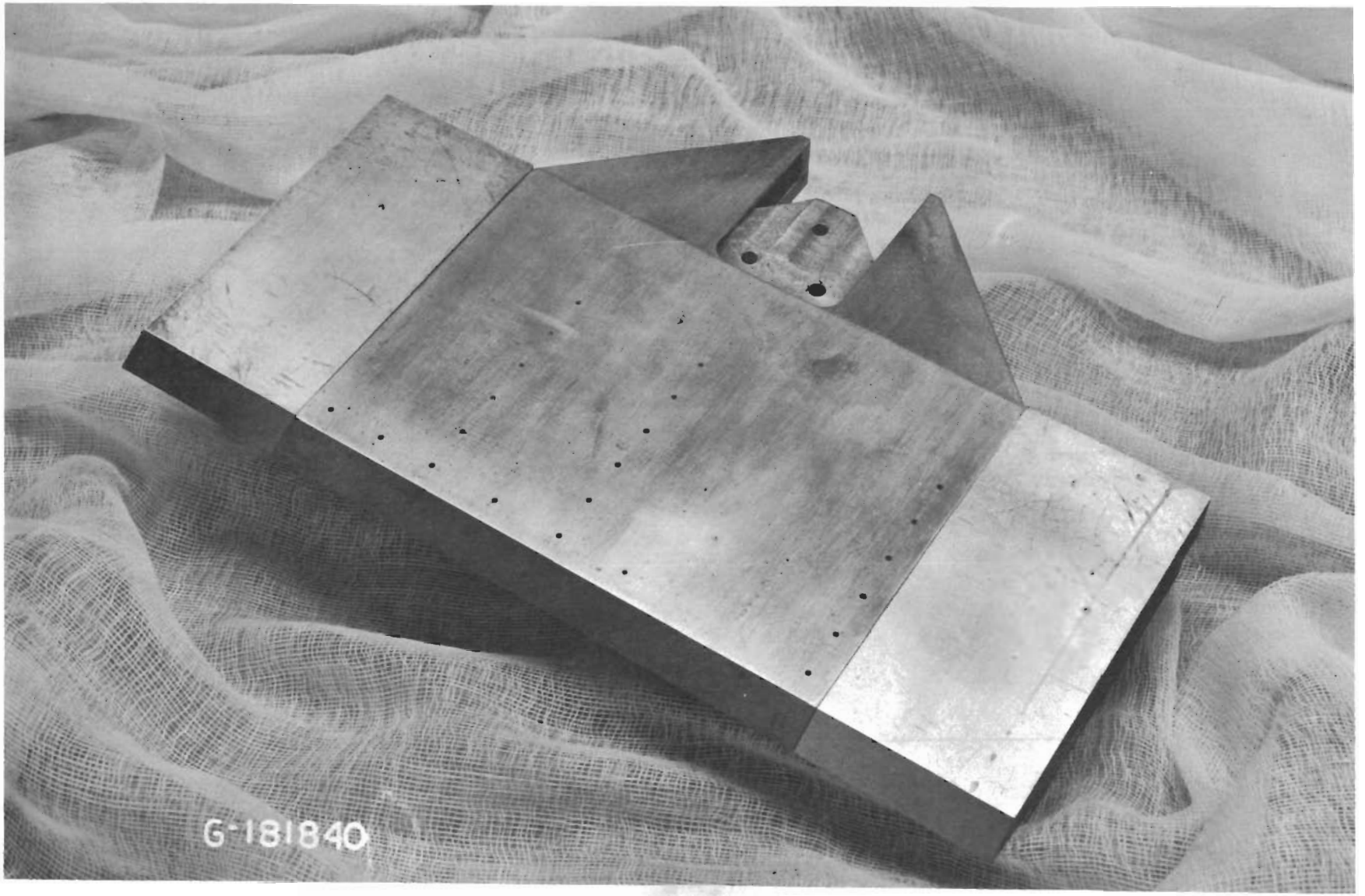

Fig. 24 - Photograph of Flat Rectangular Wing with Tip Extensions

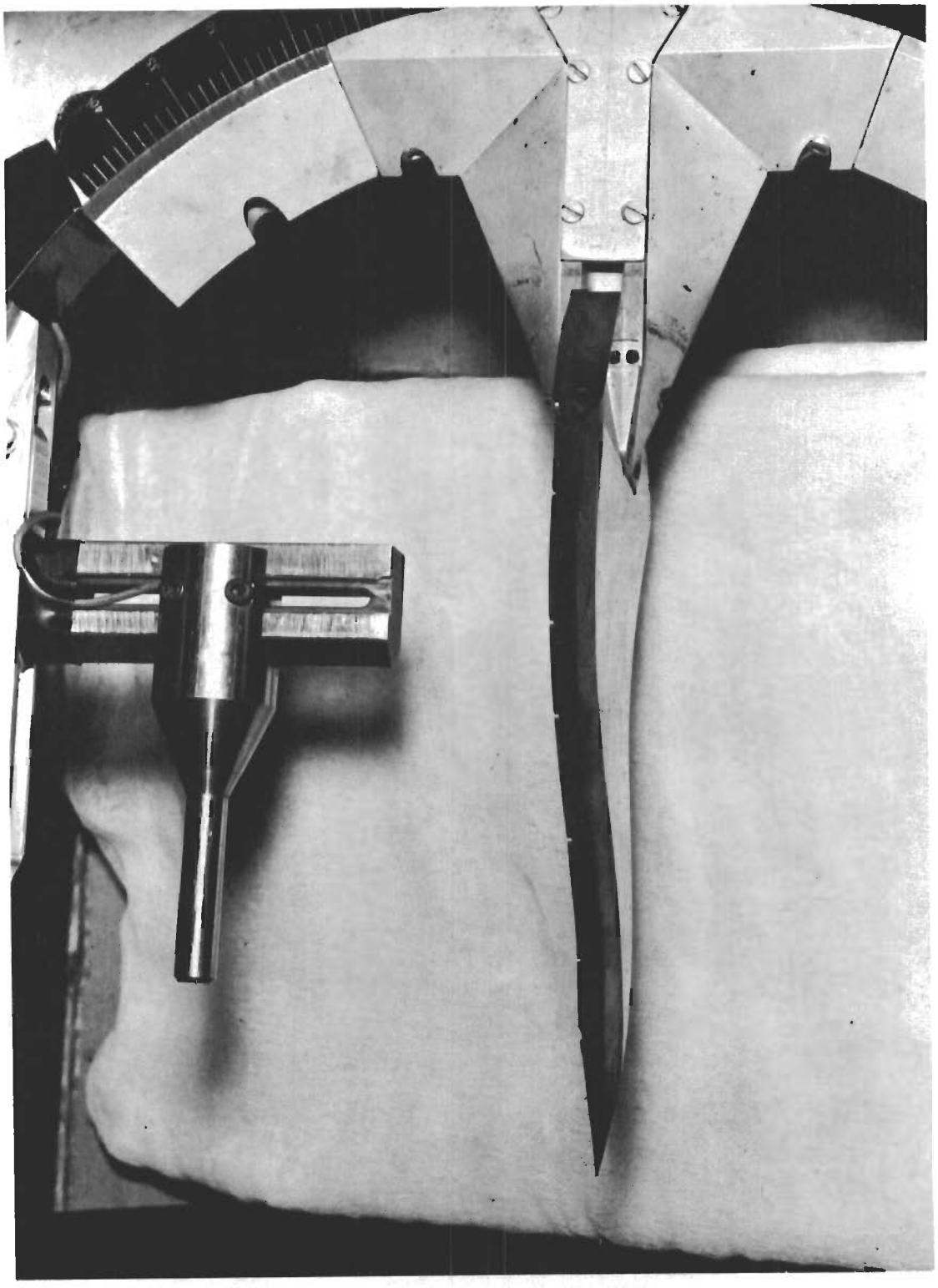

Fig. 25 - 70° Delta Wing with Sine-Wave Camber Mounted in Test Section

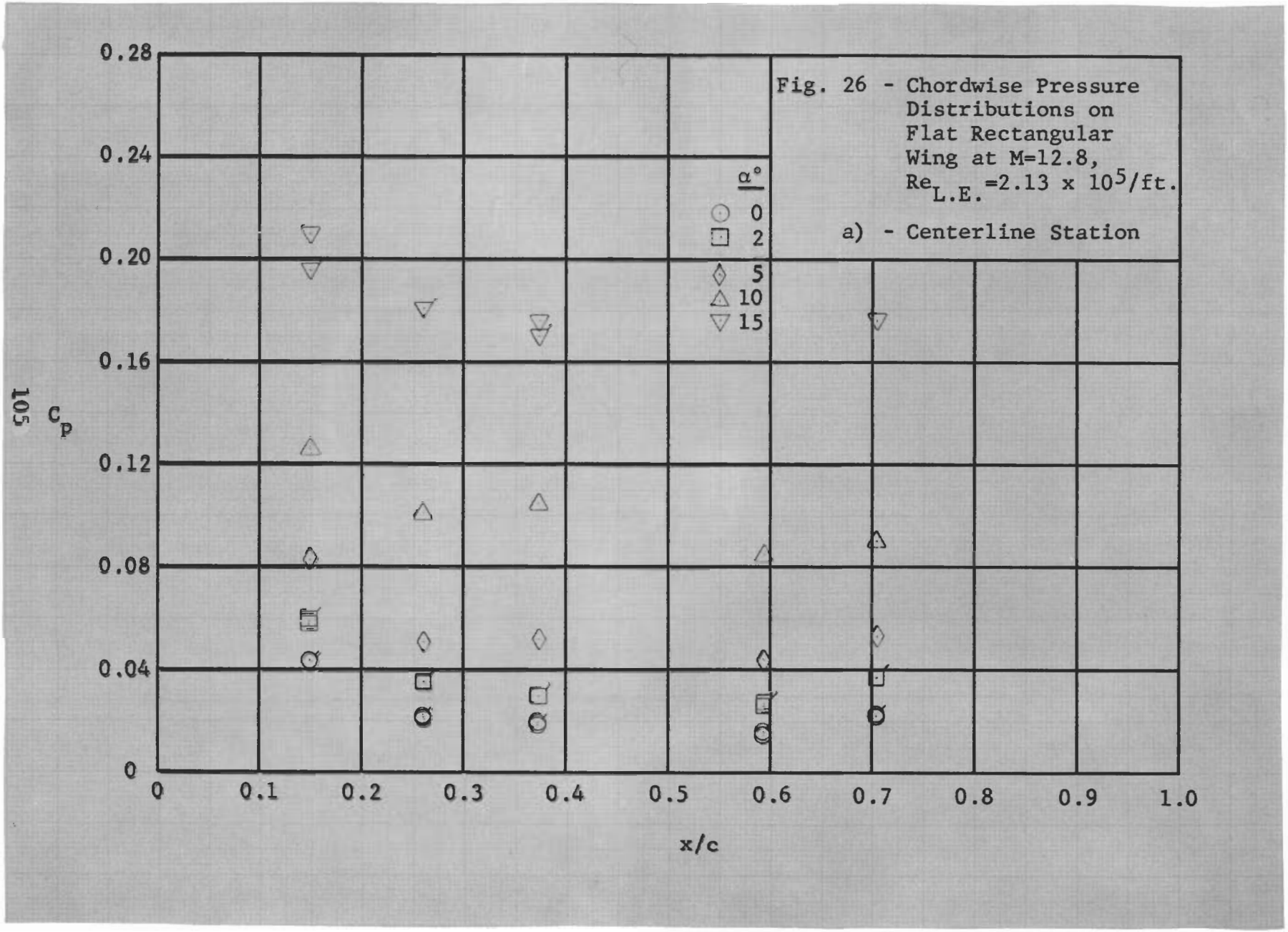

Fig. 26 - Chordwise Pressure Distributions on Flat Rectangular Wing at M=12.8, $Re_{L.E.}$ =2.13 x 10^5/ft.

a) - Centerline Station

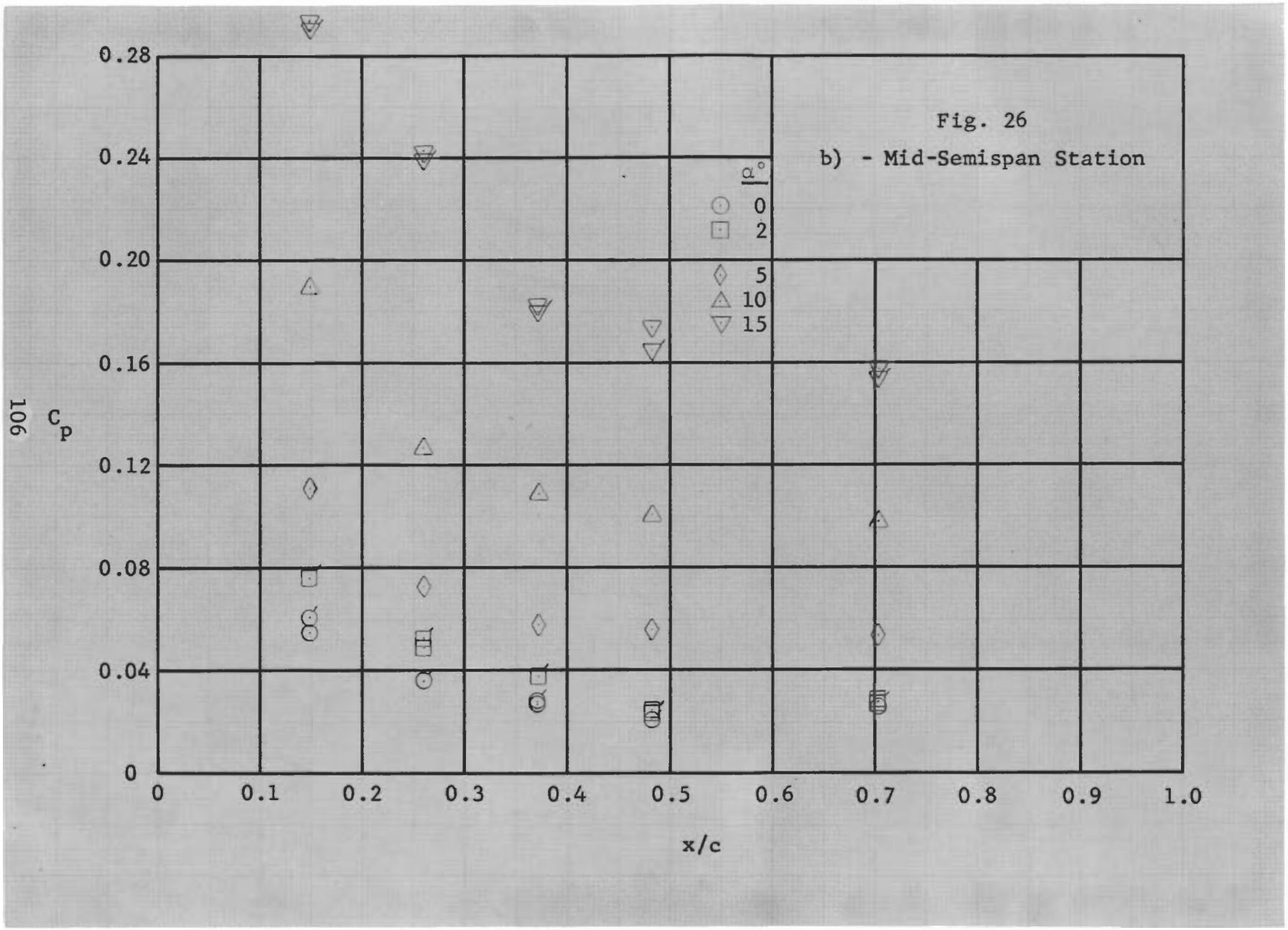

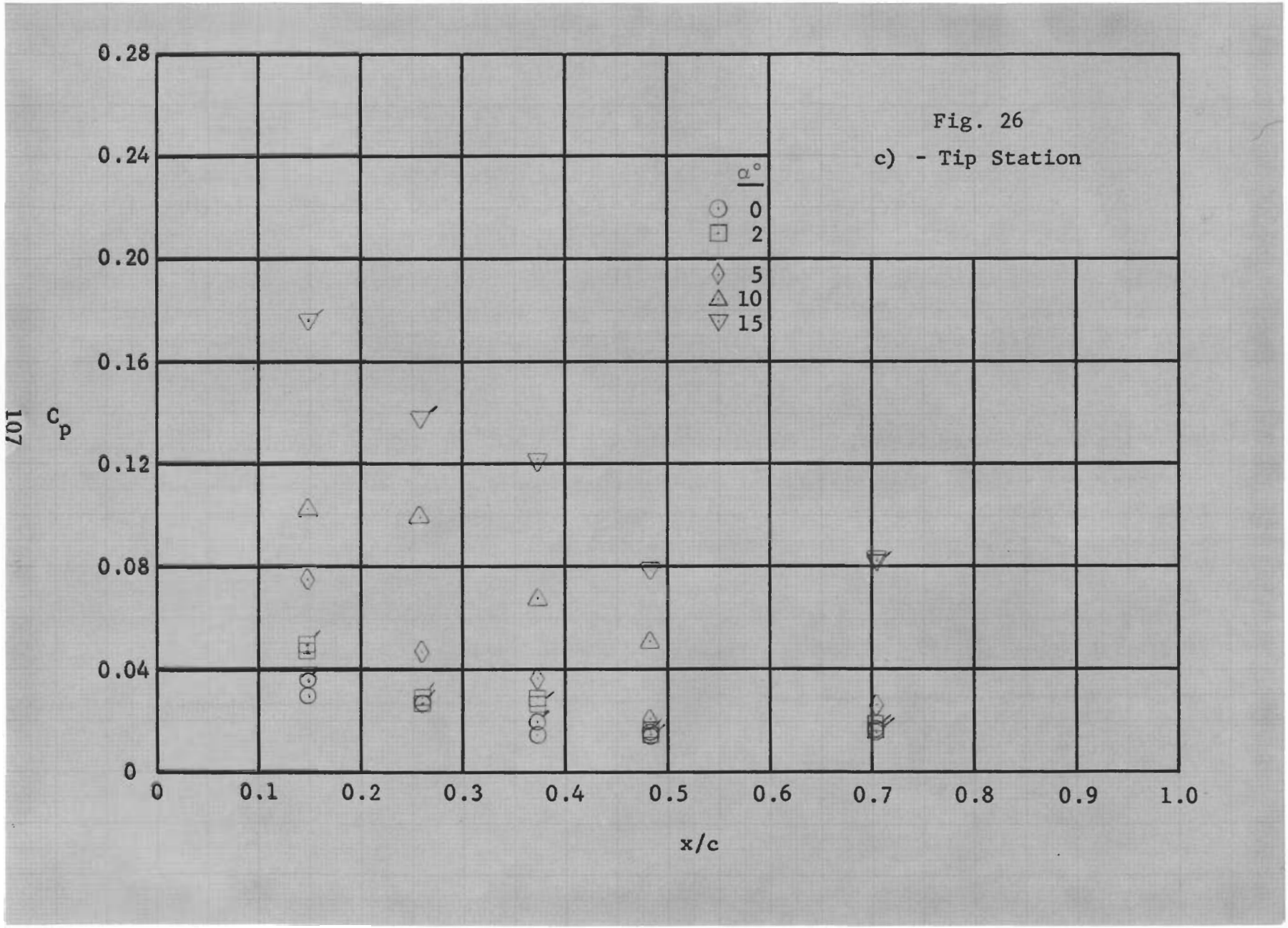

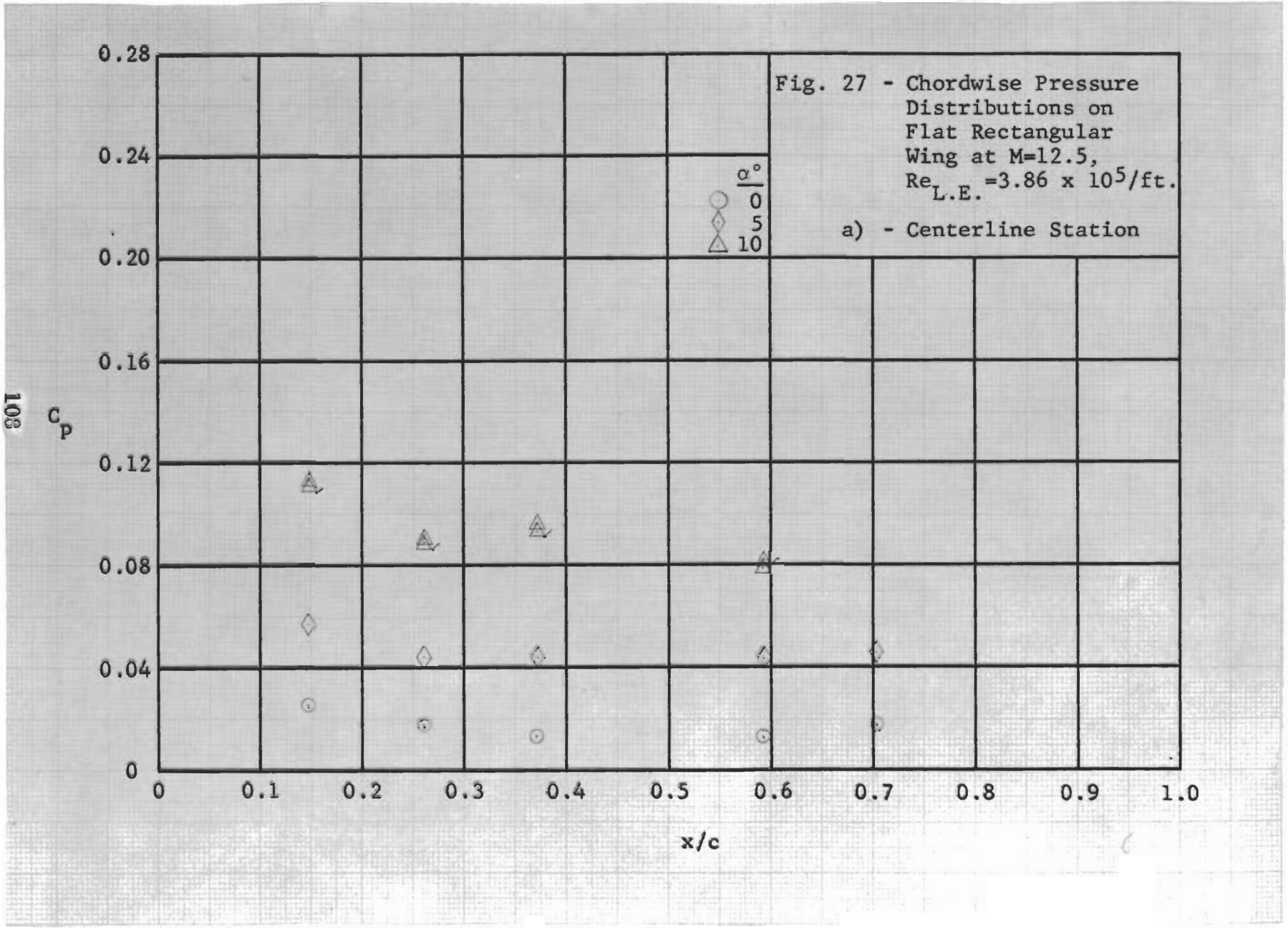

Fig. 27 - Chordwise Pressure Distributions on Flat Rectangular Wing at M=12.5, $Re_{L.E.}$ =3.86 x 10^5/ft.

a) - Centerline Station

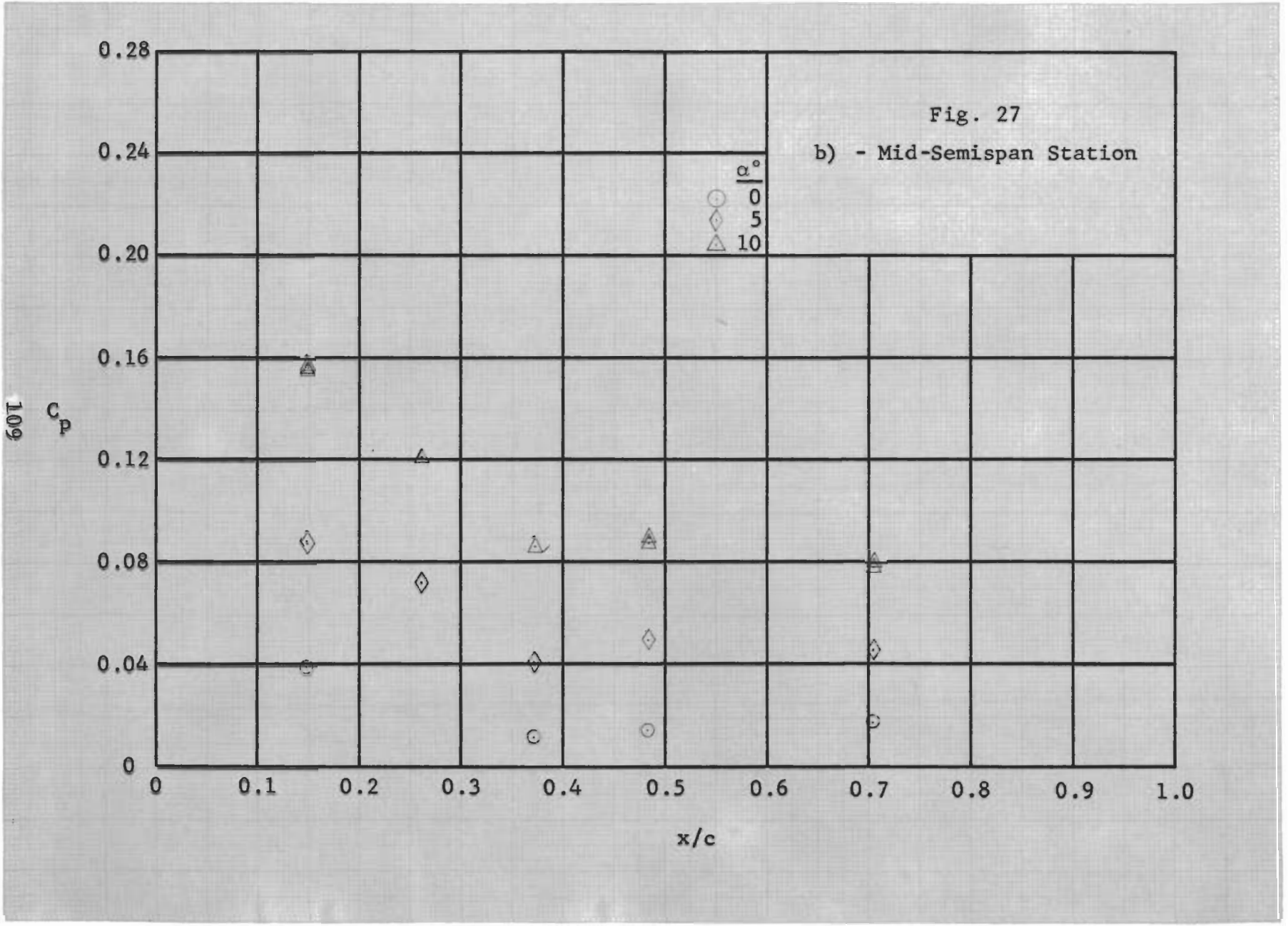

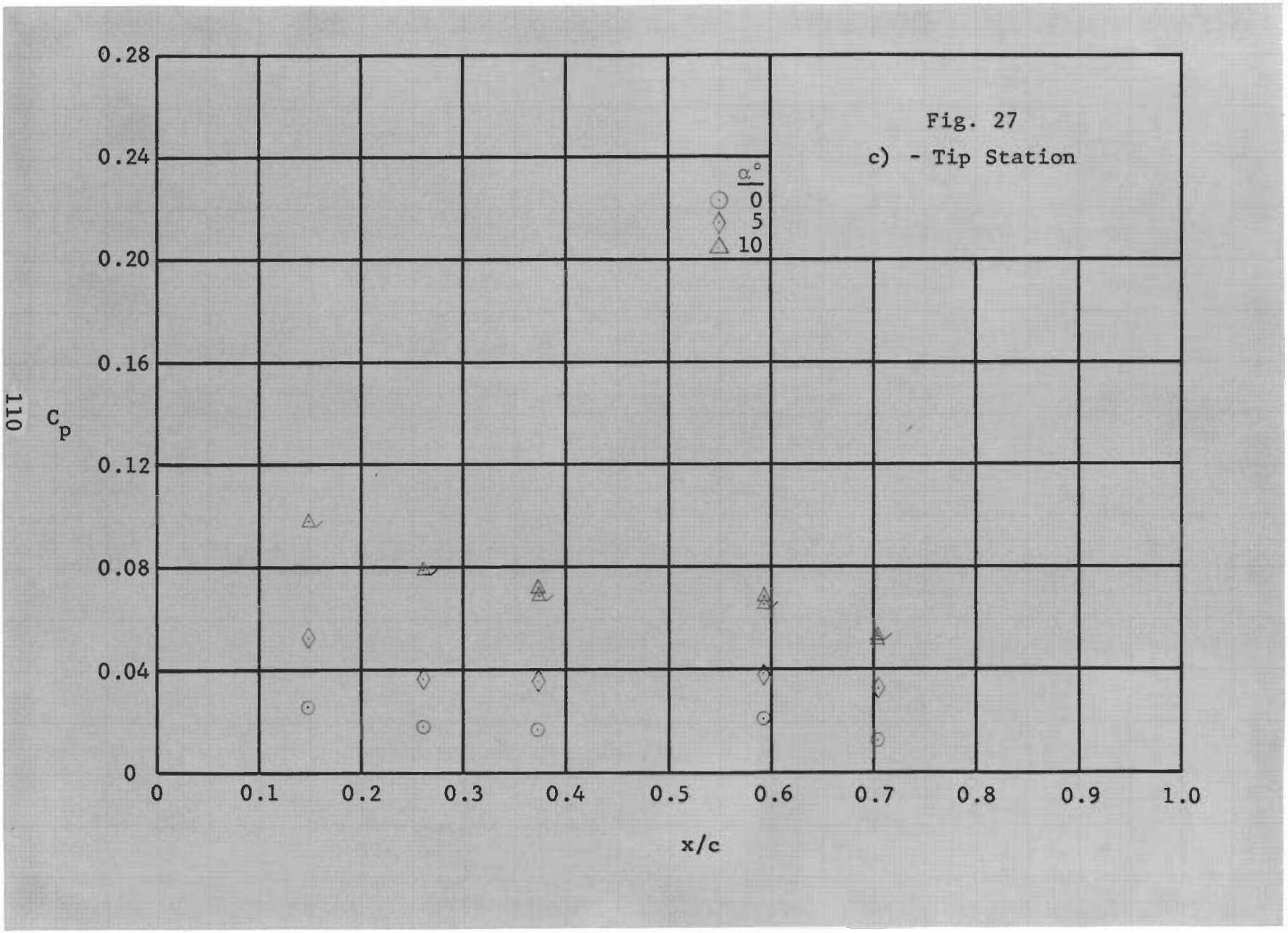

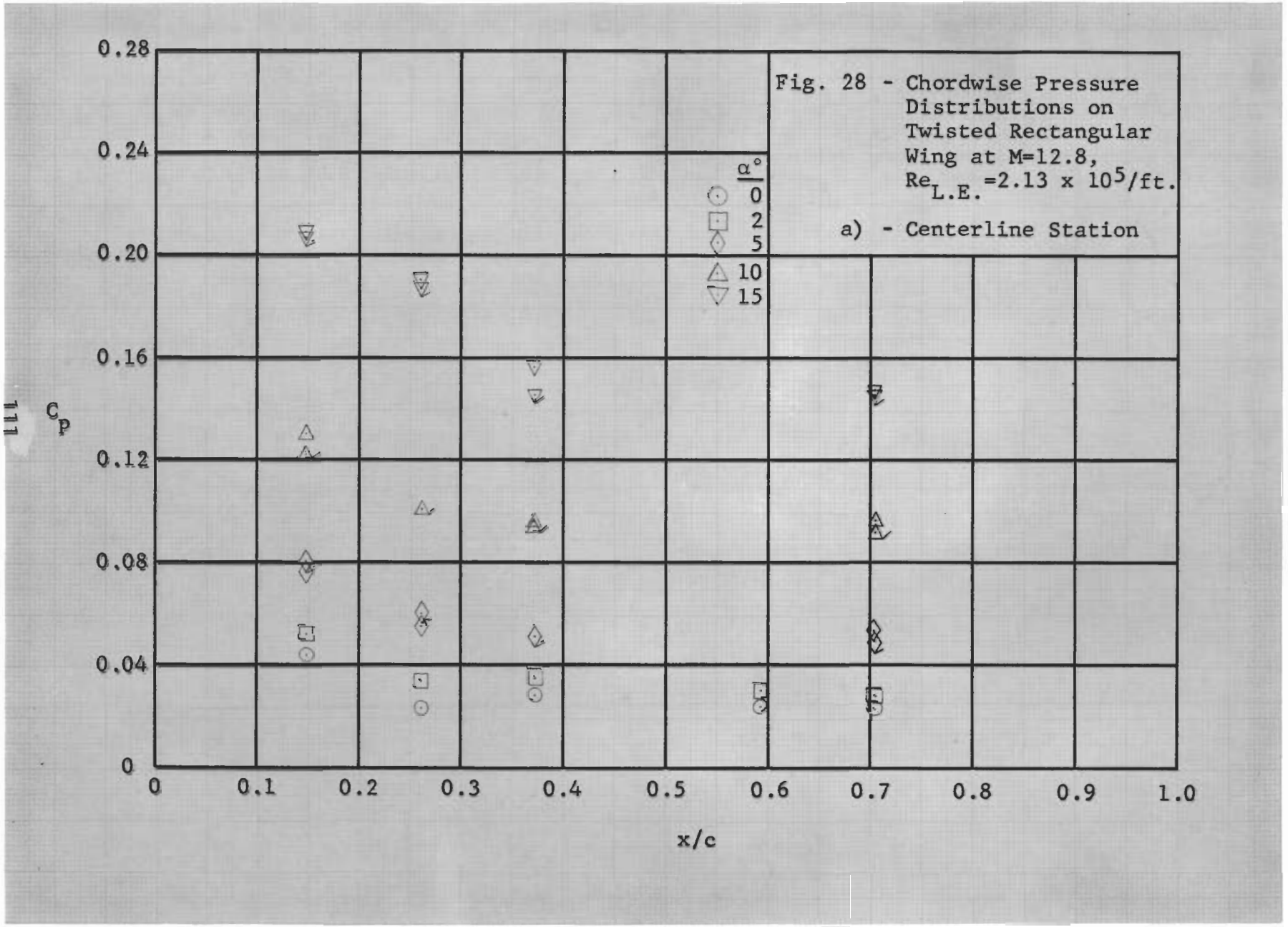

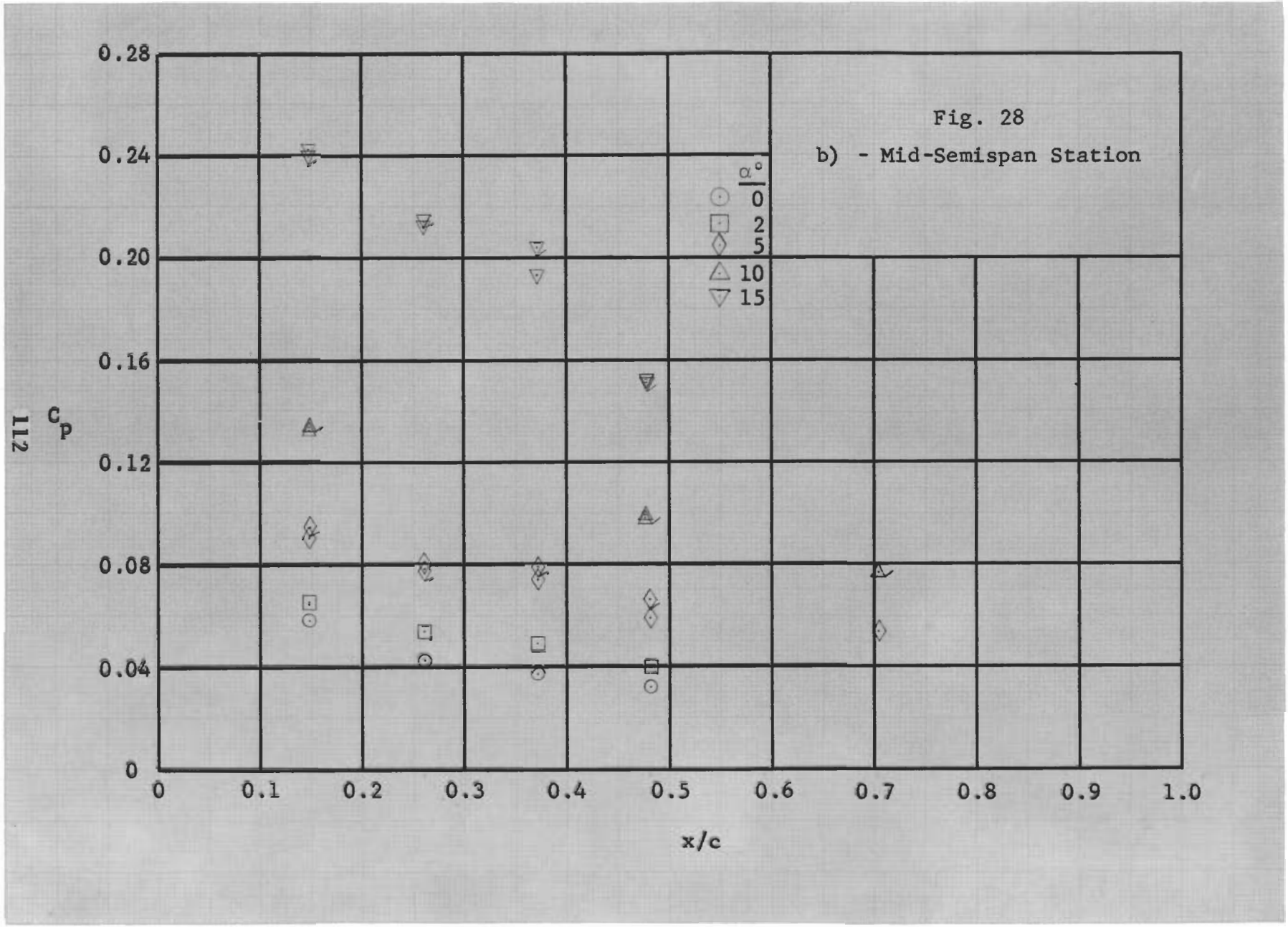

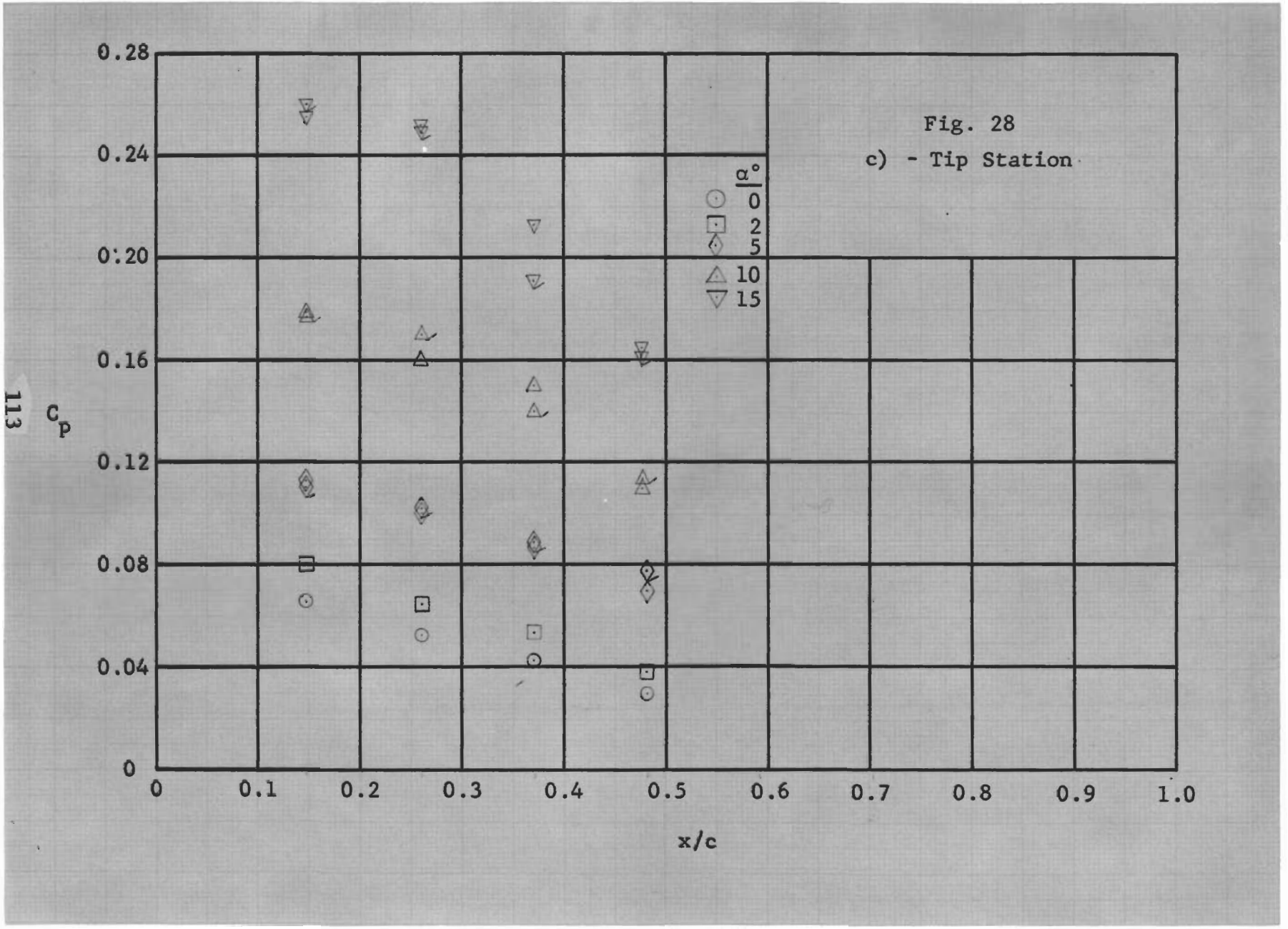

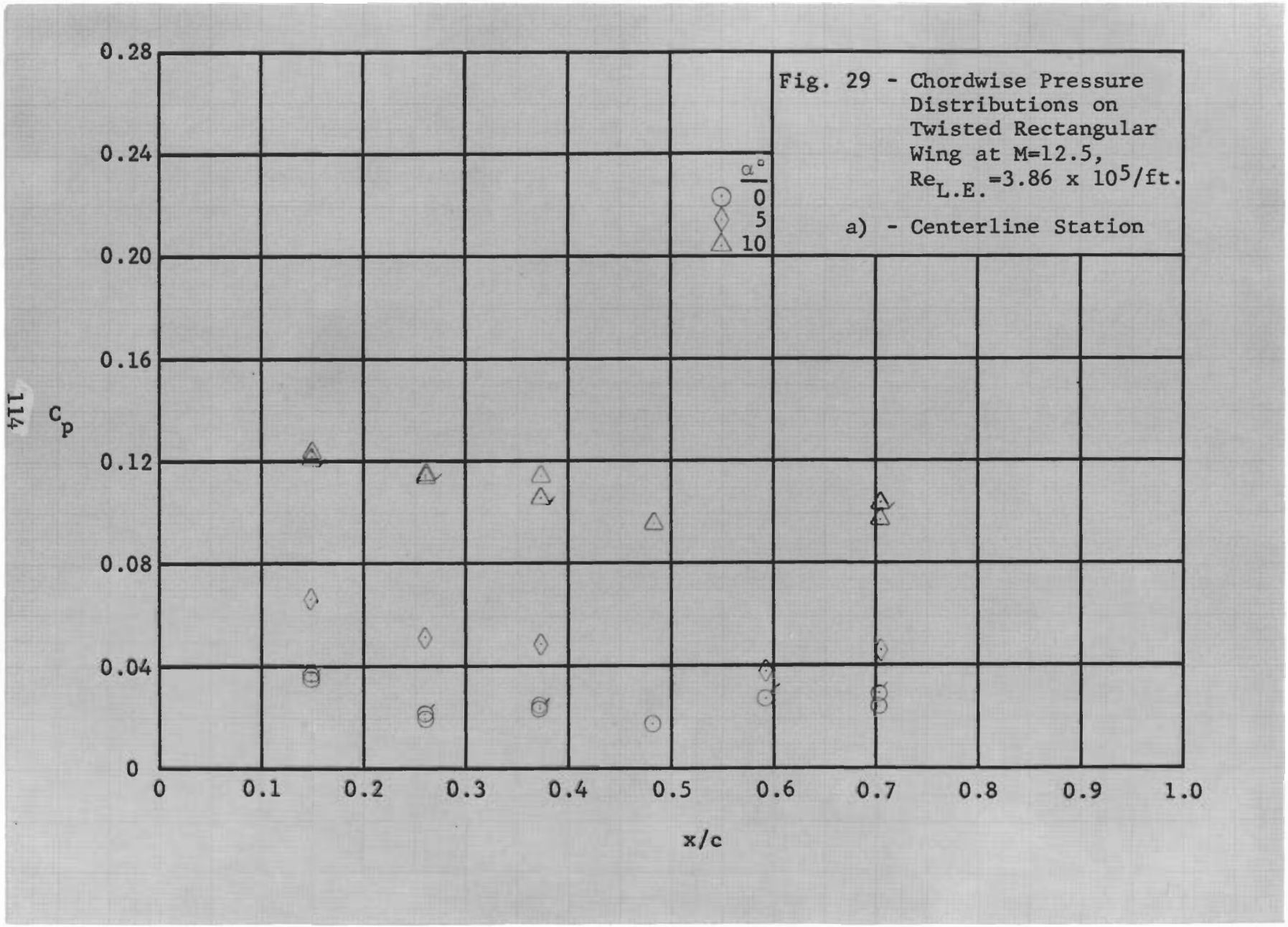

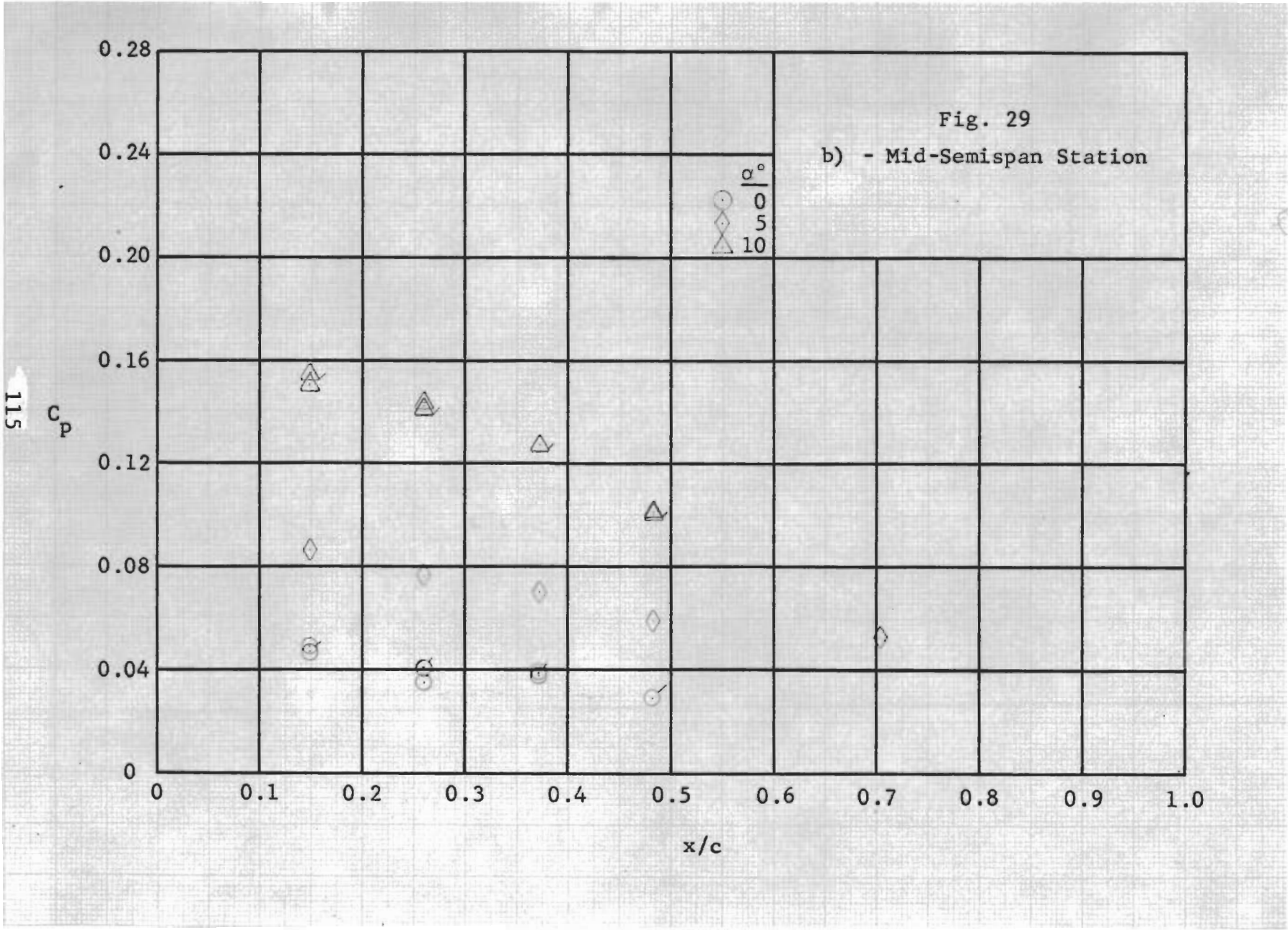

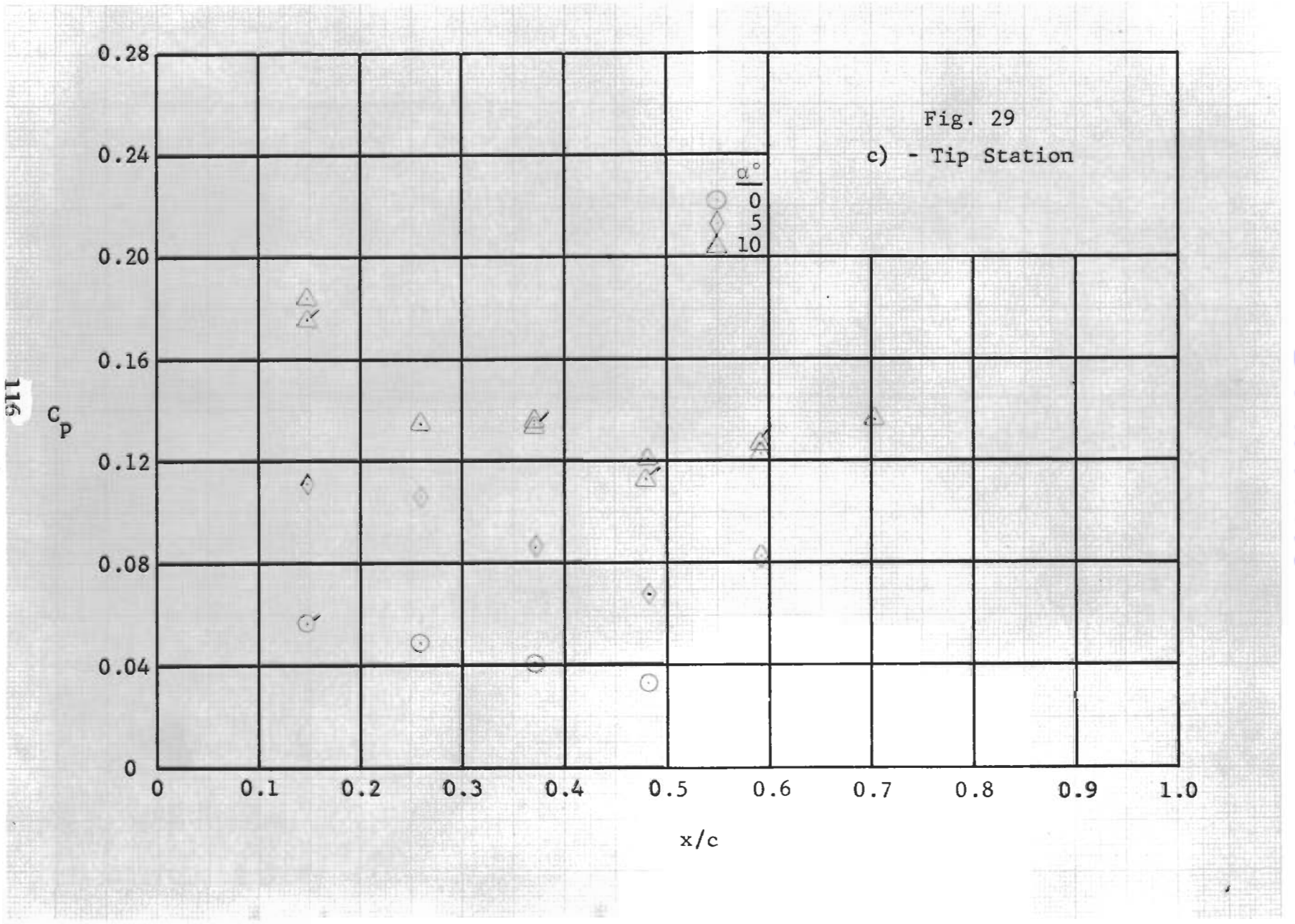

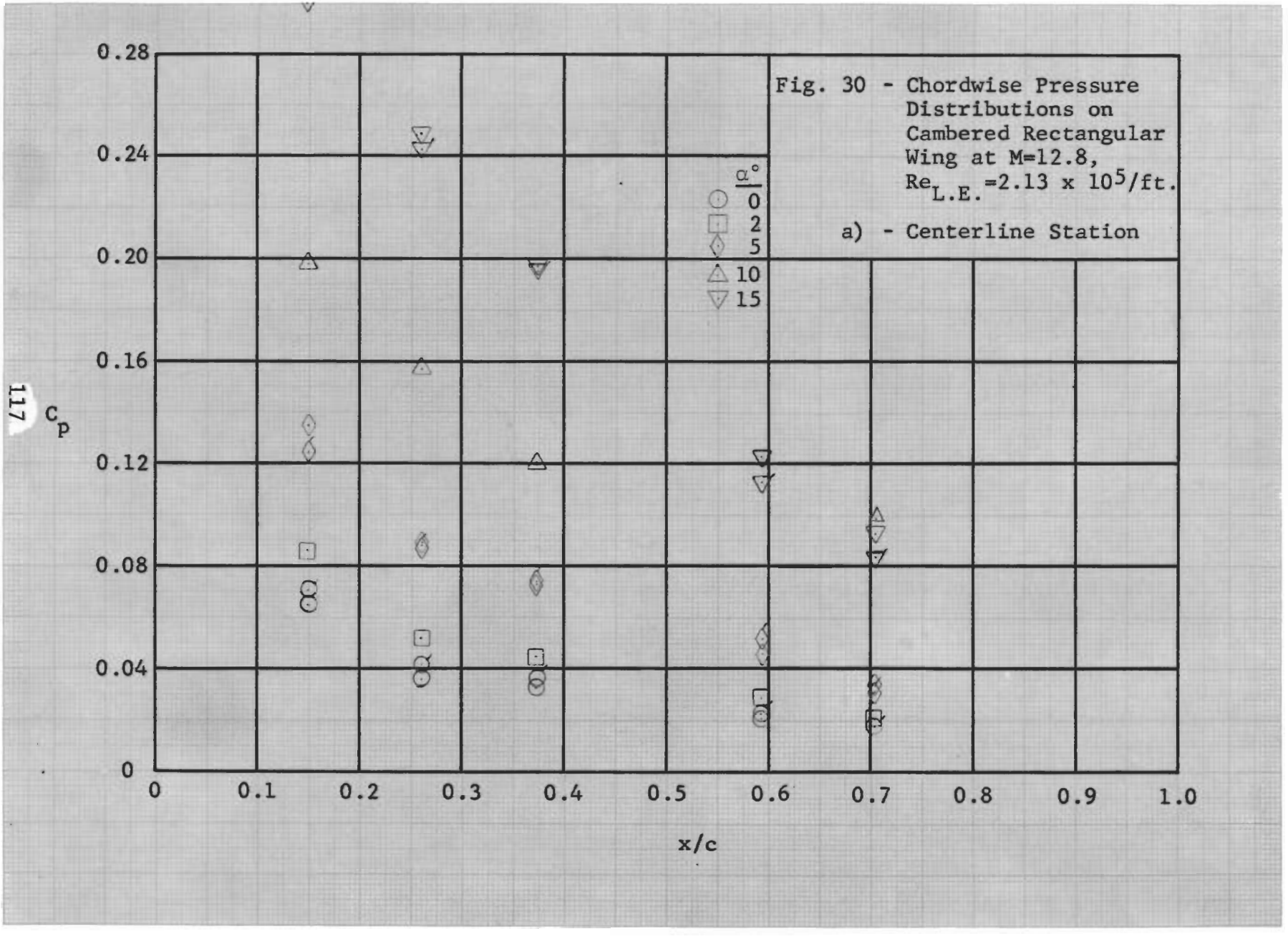

Fig. 30 - Chordwise Pressure Distributions on Cambered Rectangular Wing at M=12.8, $Re_{L.E.}$ =2.13 x 10^5/ft.

a) - Centerline Station

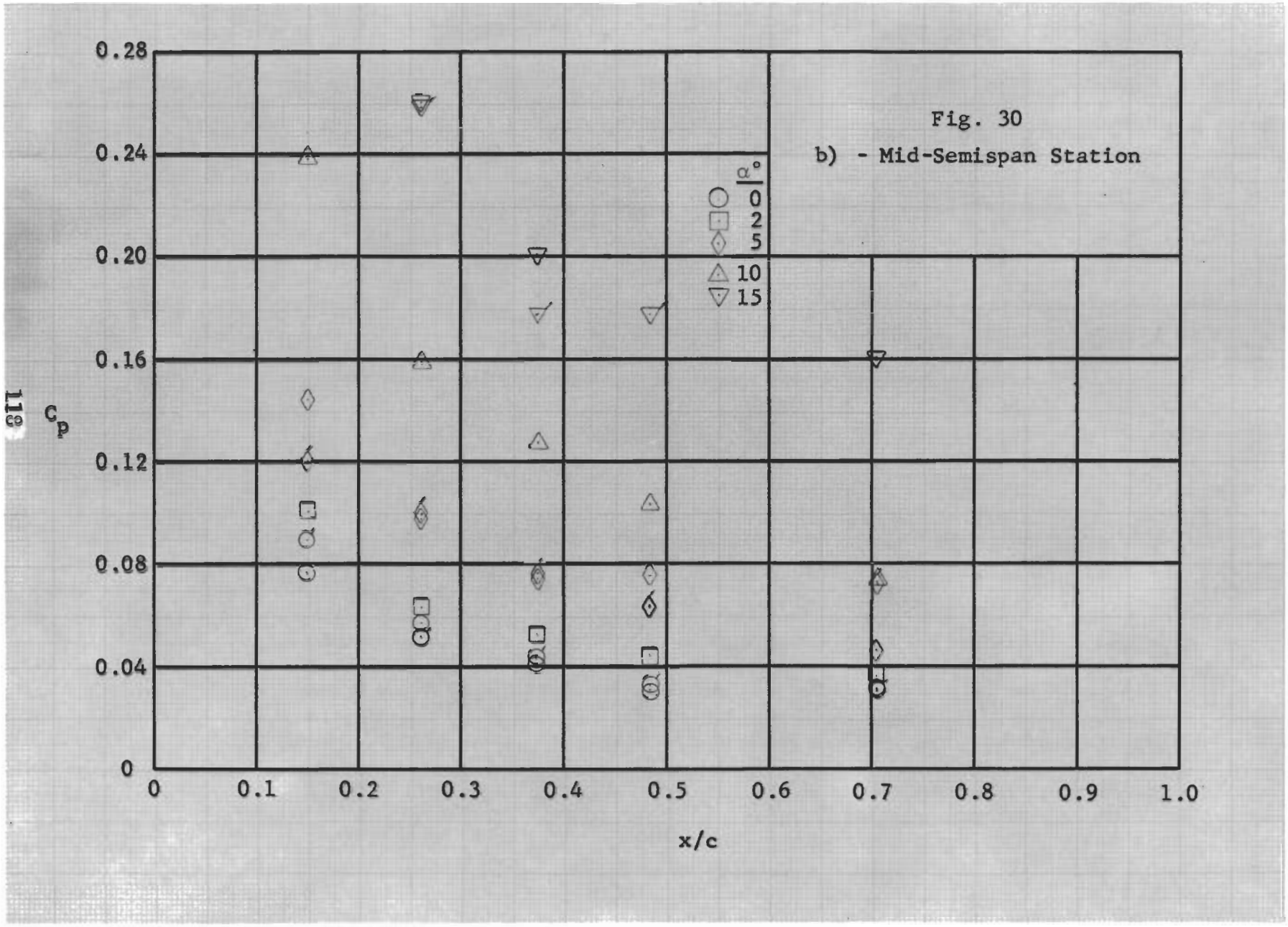

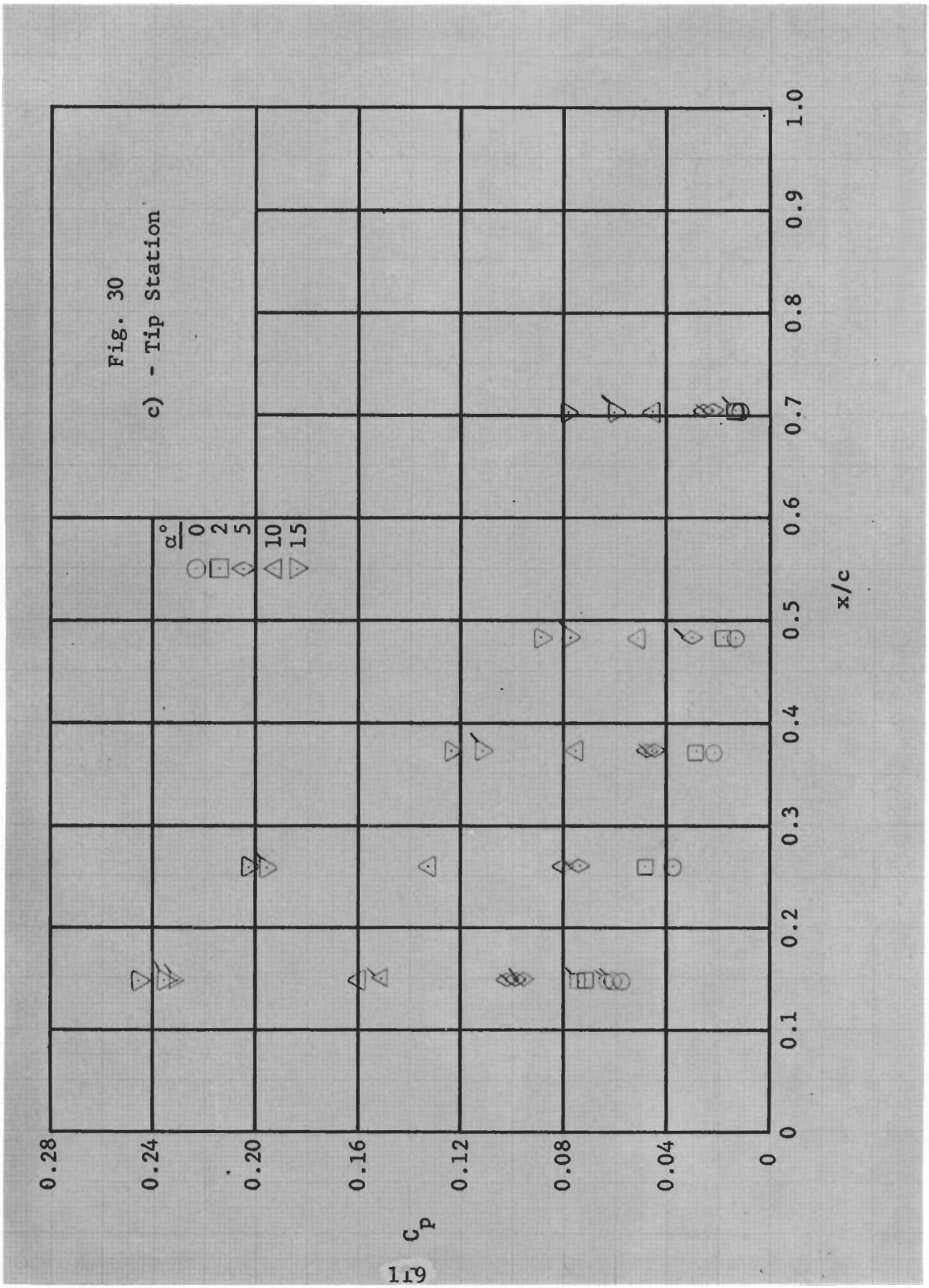

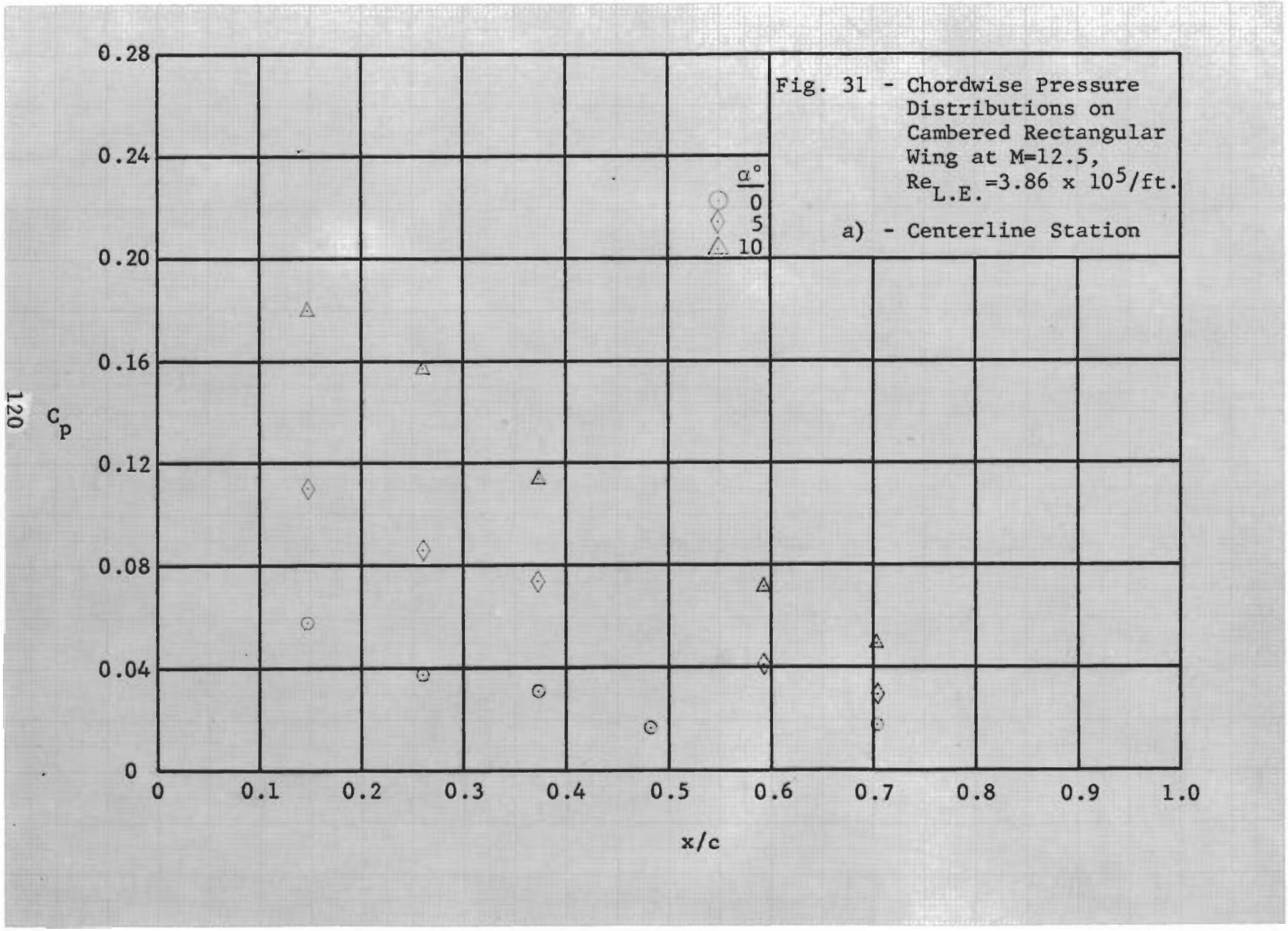

Fig. 31 - Chordwise Pressure Distributions on Cambered Rectangular Wing at M=12.5, $Re_{L.E.}$ =3.86 x 10^5/ft.

a) - Centerline Station

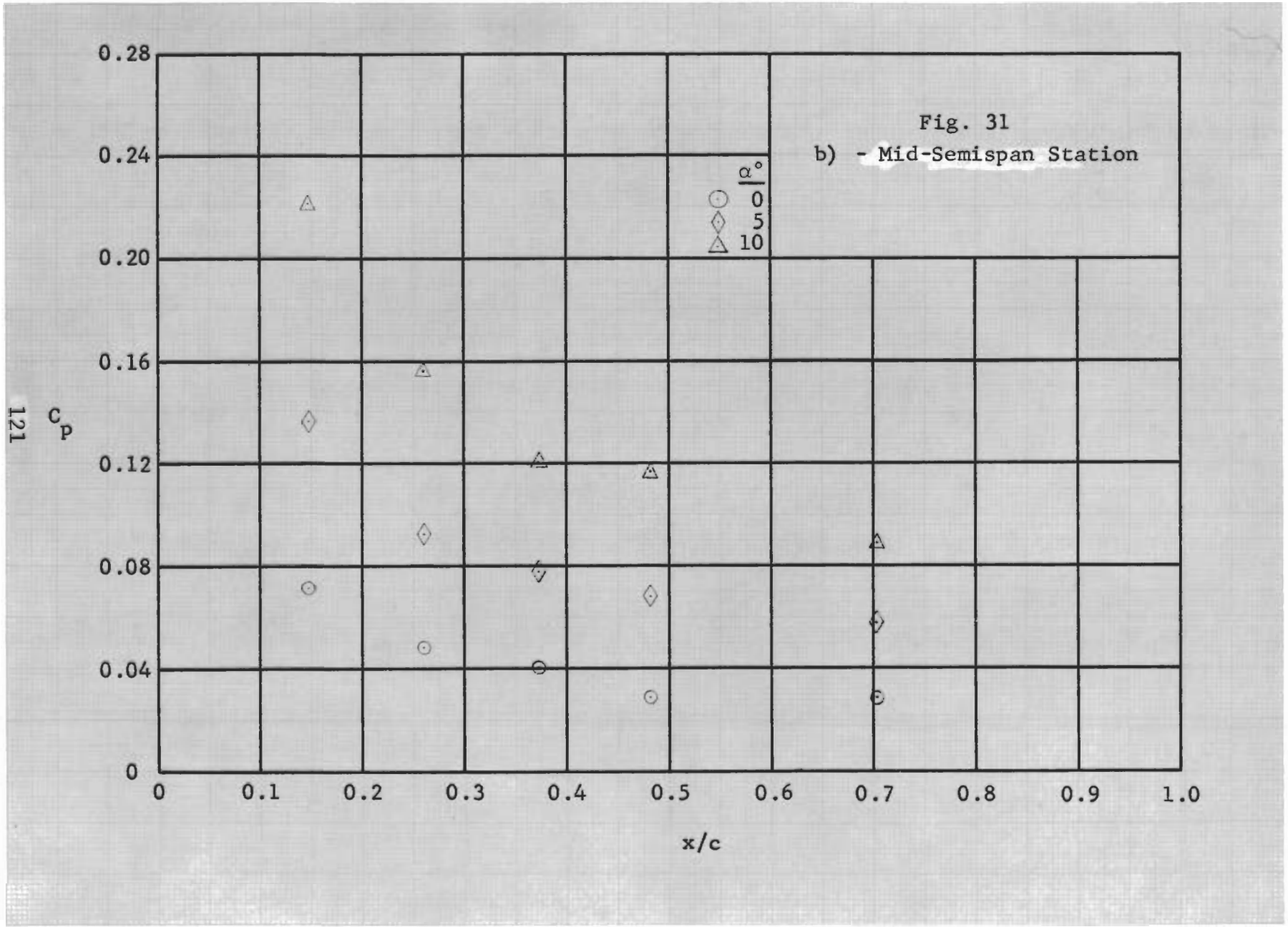

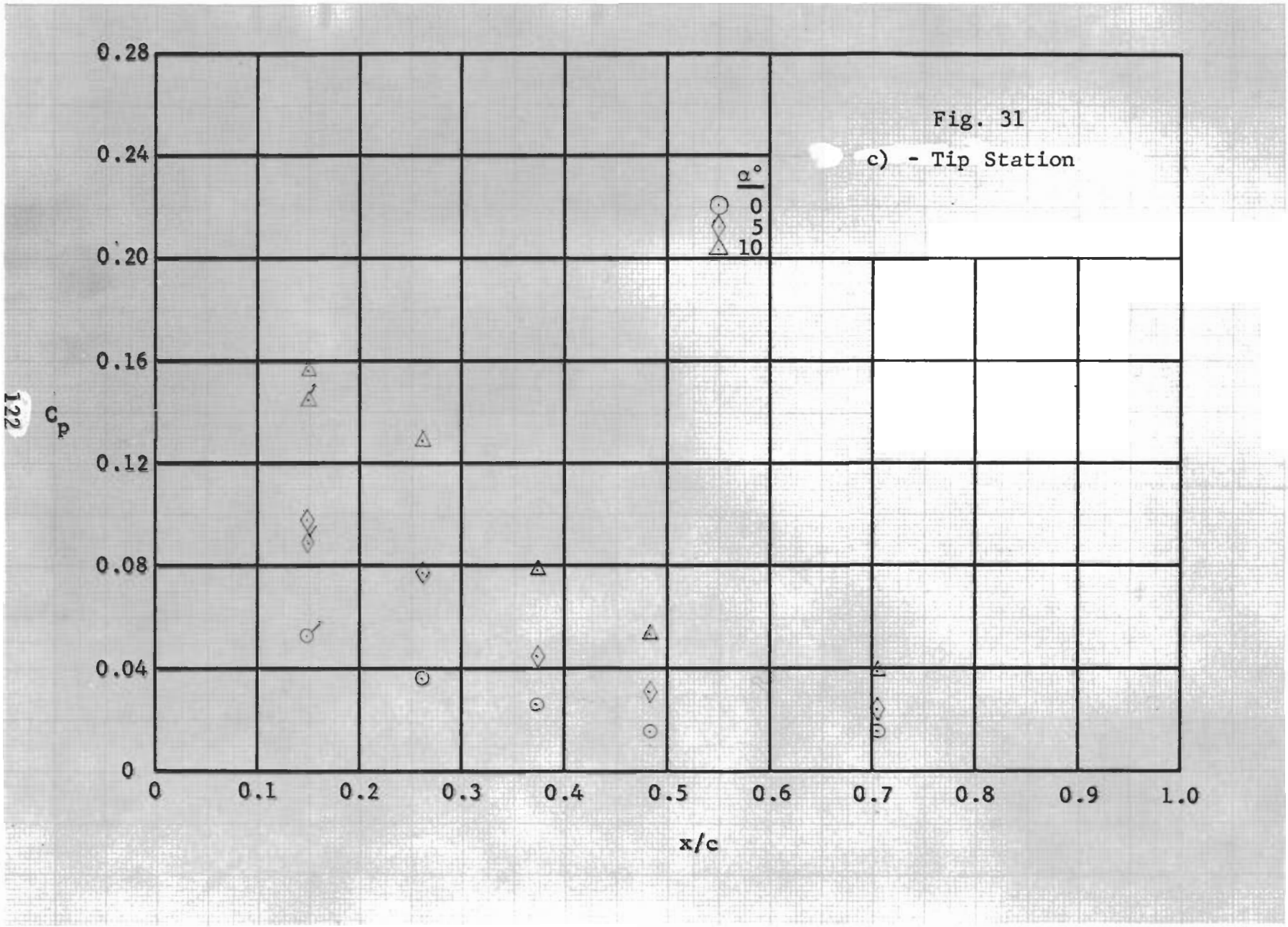

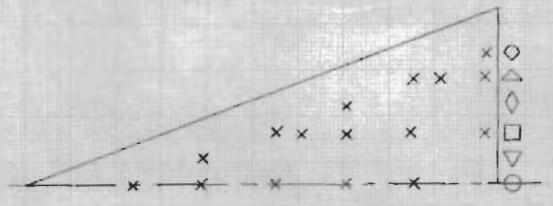

Fig. 32 - Chordwise Pressure Distribution on Flat 70° Delta Wing at M_{apex}=12.6, Re/ft = 2.13 x 10^5

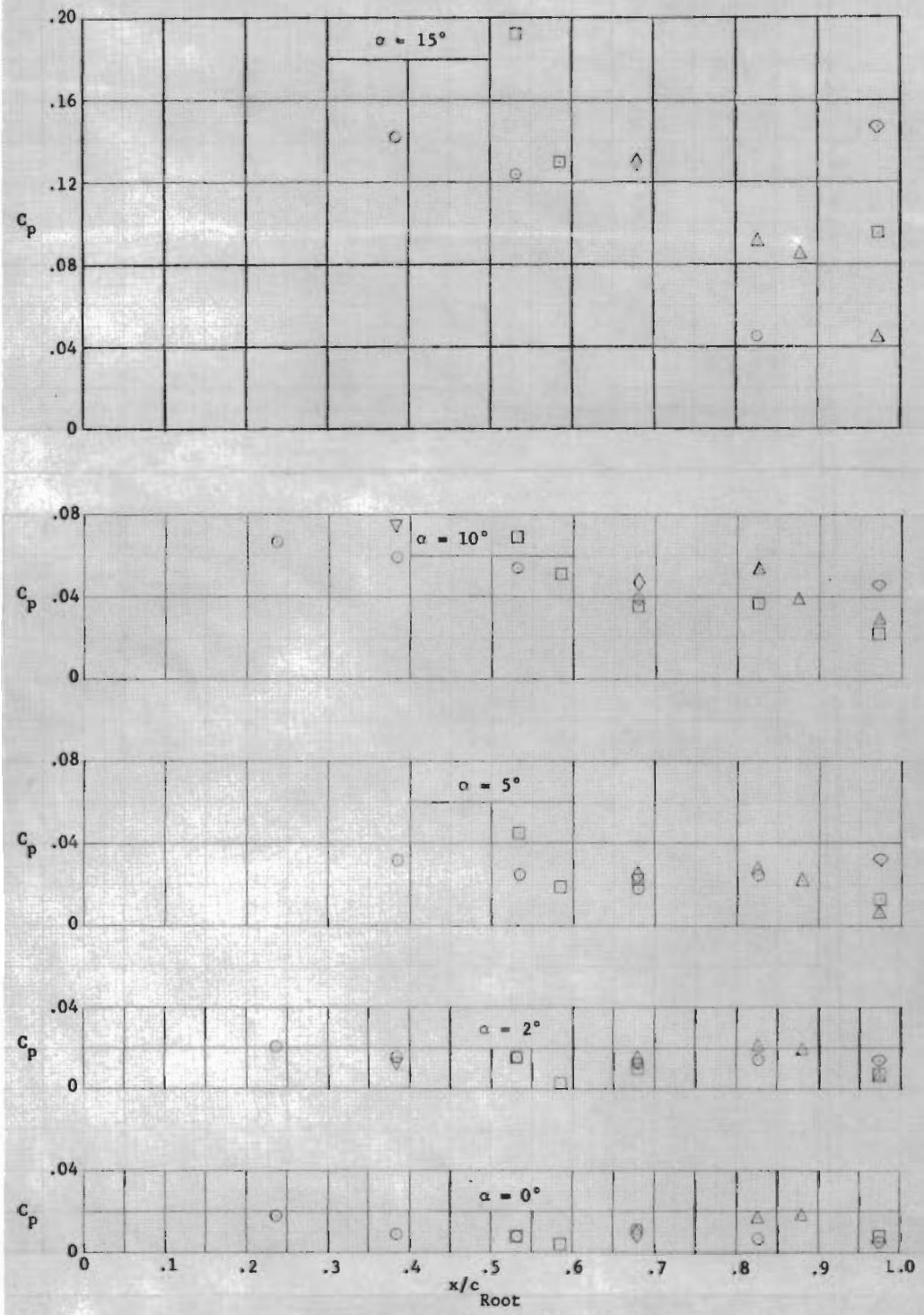

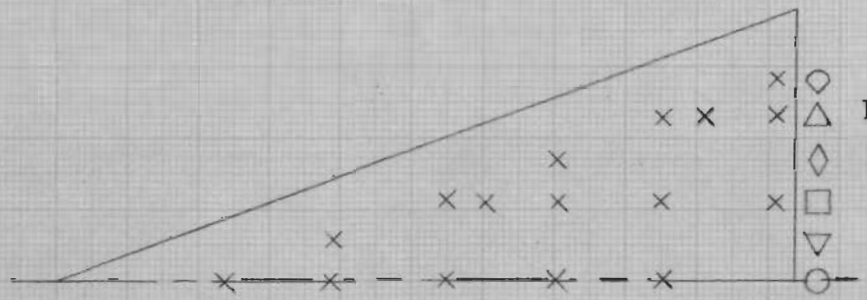

Fig. 33 - Chordwise Pressure Distribution on Flat 70° Delta Wing at M_{apex}=12.3, Re/ft = 3.86 x 10^5

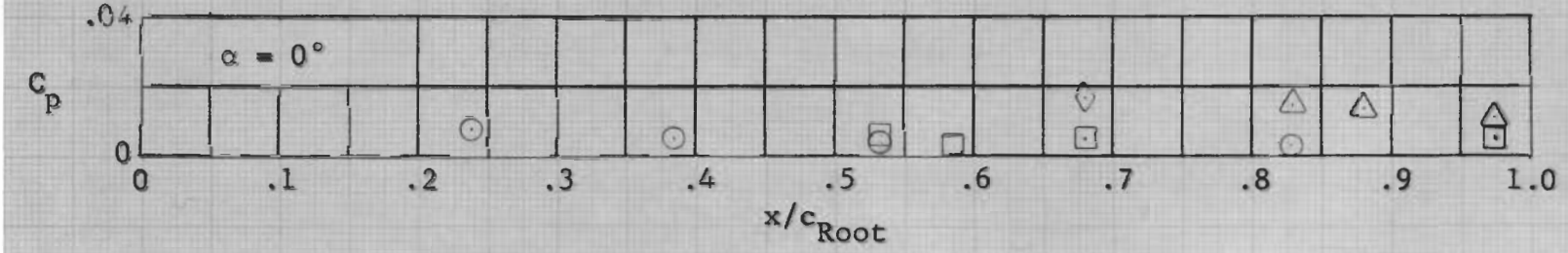

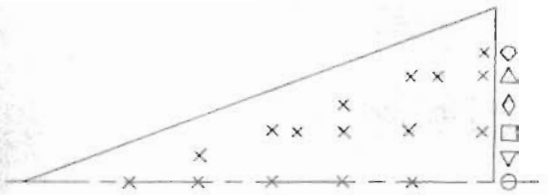

Fig. 34 - Chordwise Pressure Distribution on 70° Delta Wing with Circular-Arc Camber at M_{apex}=12.6, Re/ft = 2.13 x 10^5

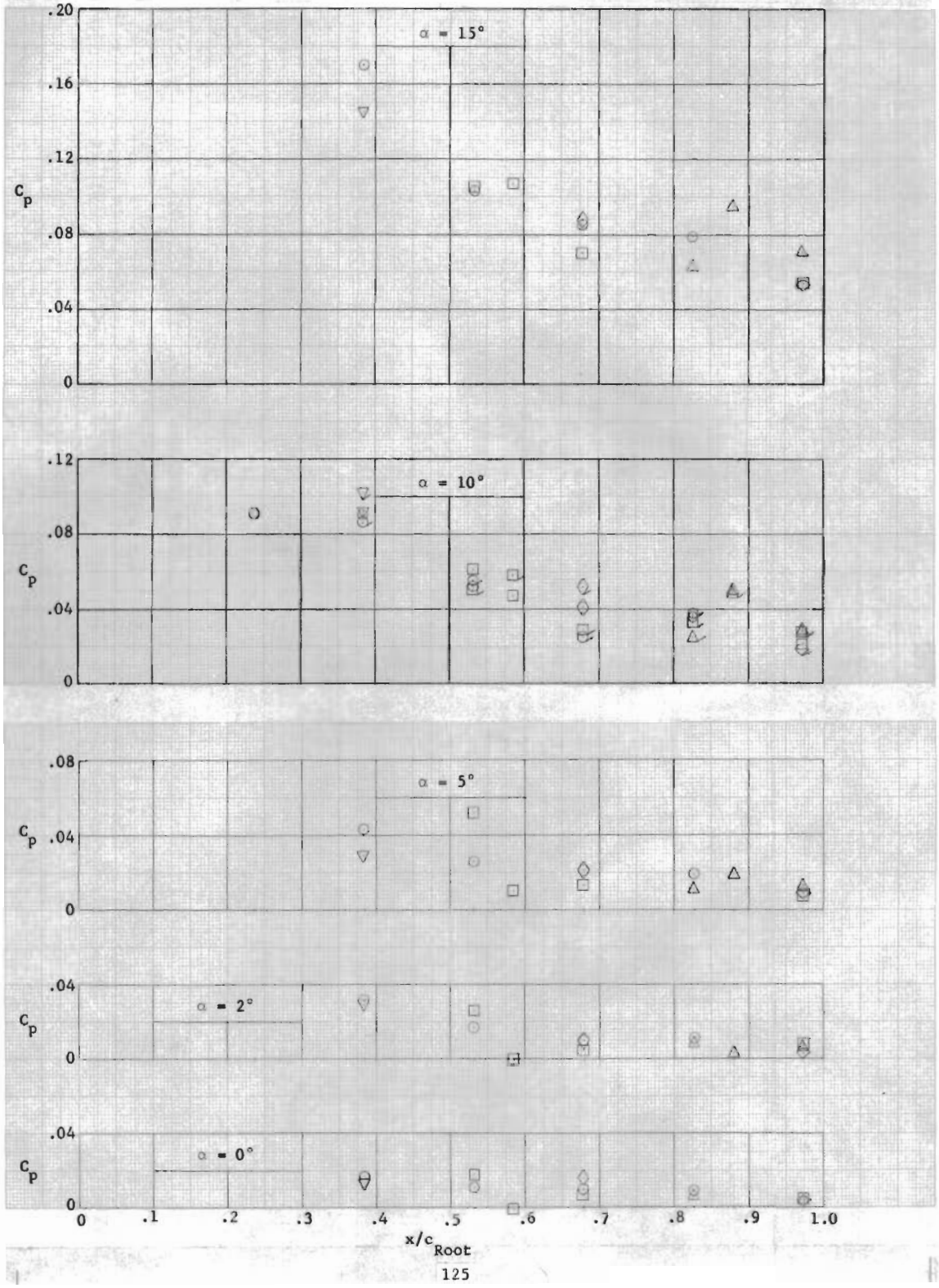

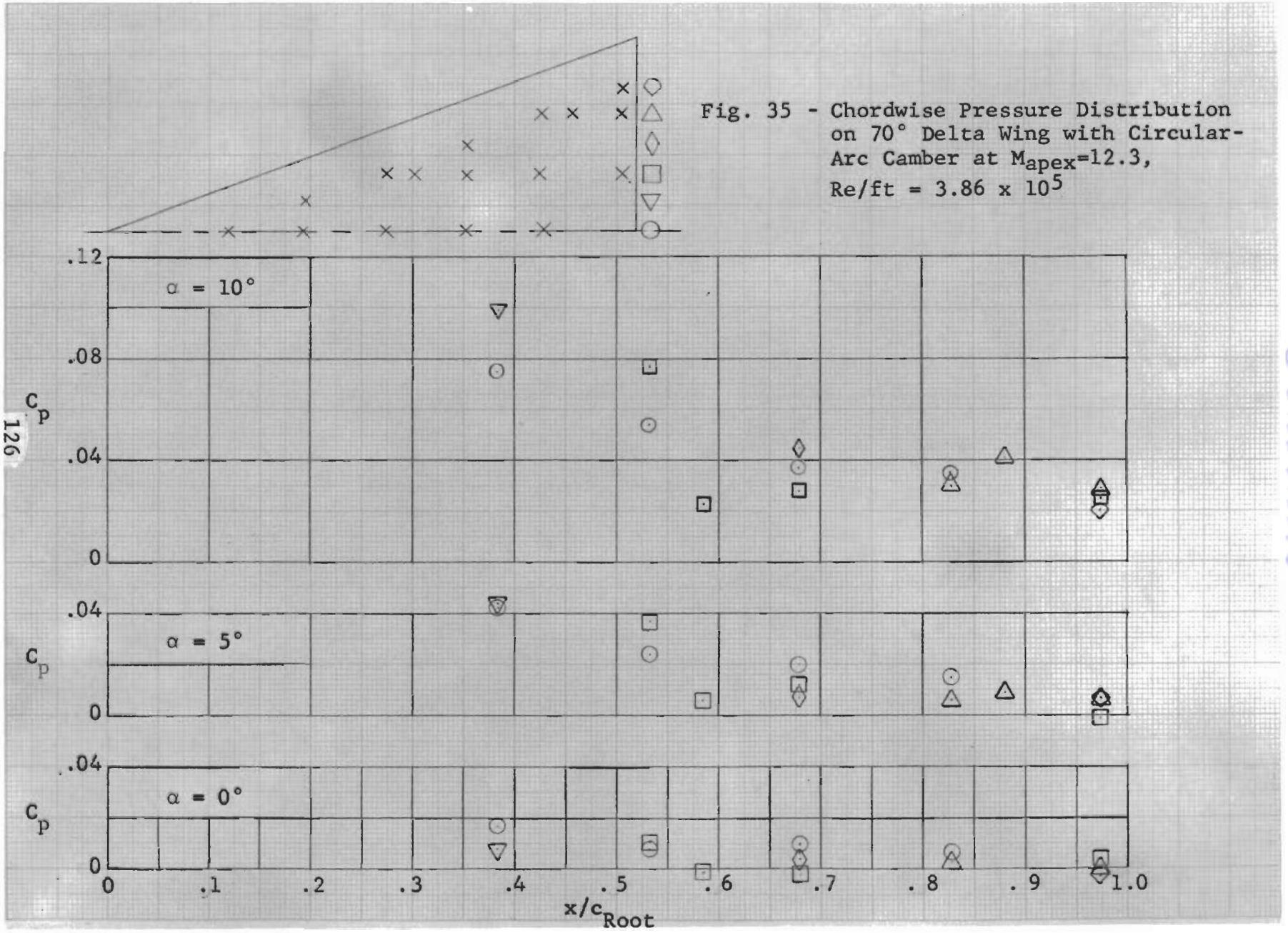

Fig. 35 - Chordwise Pressure Distribution on 70° Delta Wing with Circular-Arc Camber at M_{apex}=12.3, Re/ft = 3.86×10^5

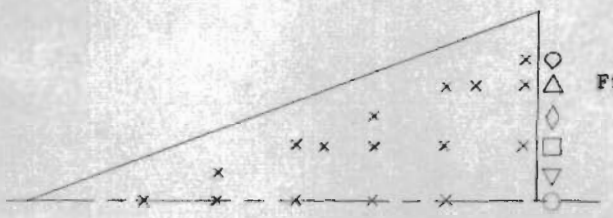

Fig. 36 - Chordwise Pressure Distribution on 70° Delta Wing with Sine-Wave Camber M_{apex}=12.6, Re/ft = 2.13 x 10^5

a) - α = 15°

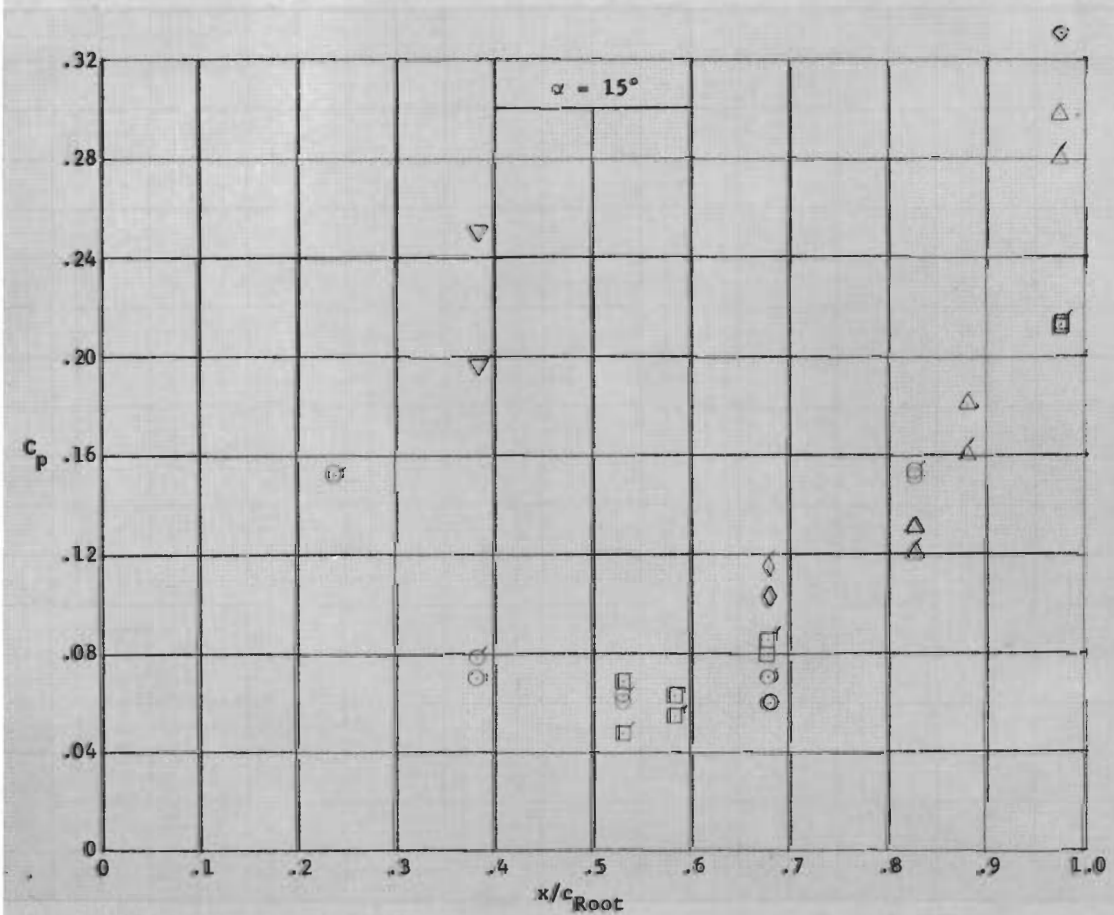

Fig. 36b - α = 0,2,5,10°

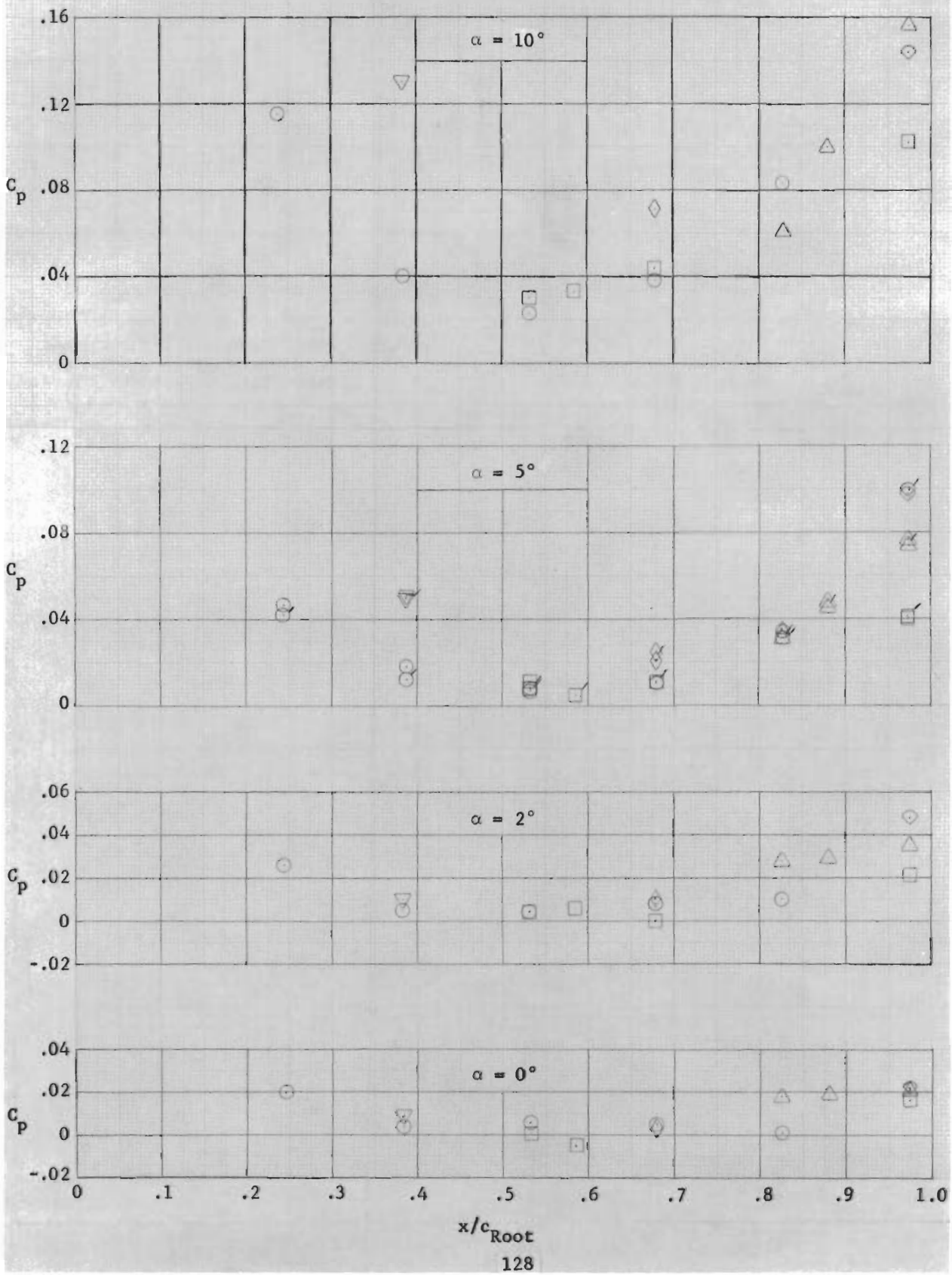

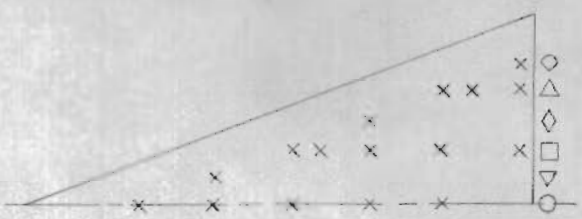

Fig. 37 - Chordwise Pressure Distribution on 70° Delta Wing with Sine-Wave Camber M_{apex}=12.3, Re/ft = 3.86 x 10^5

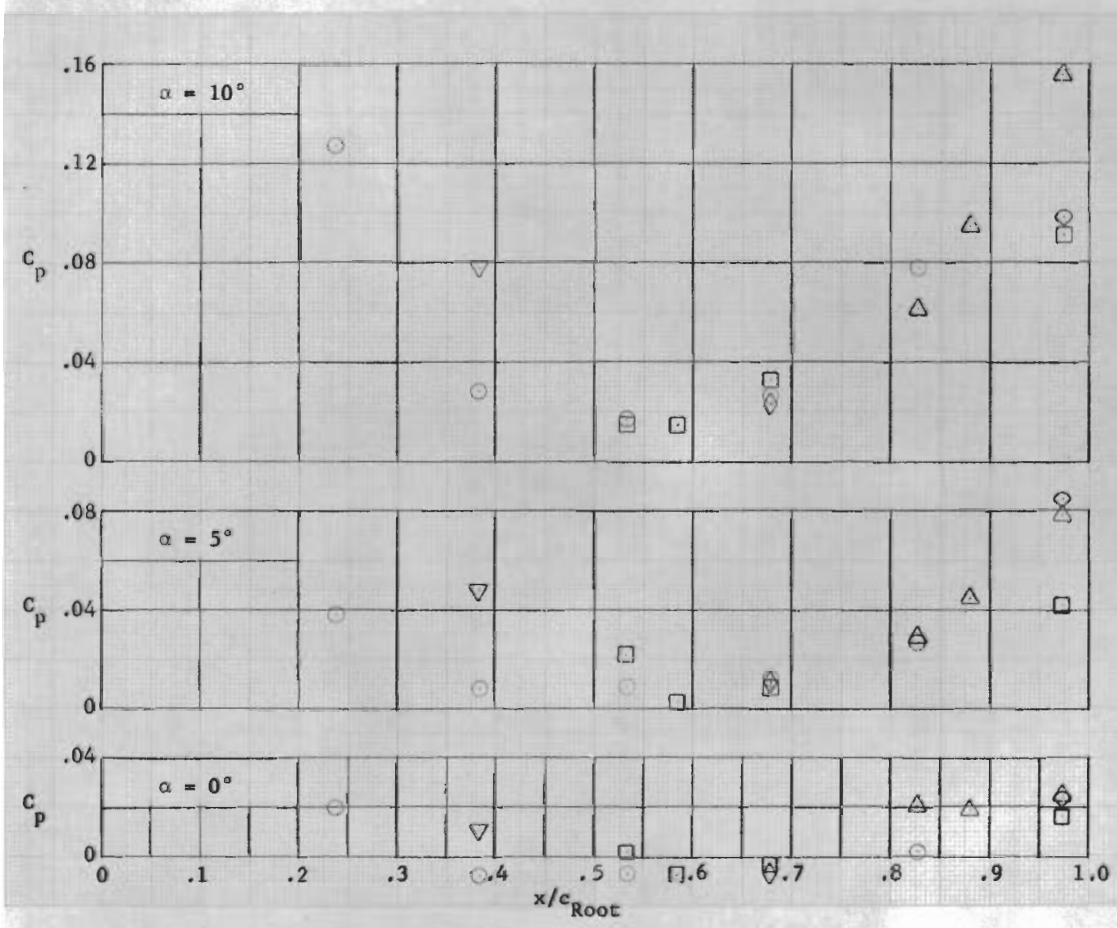

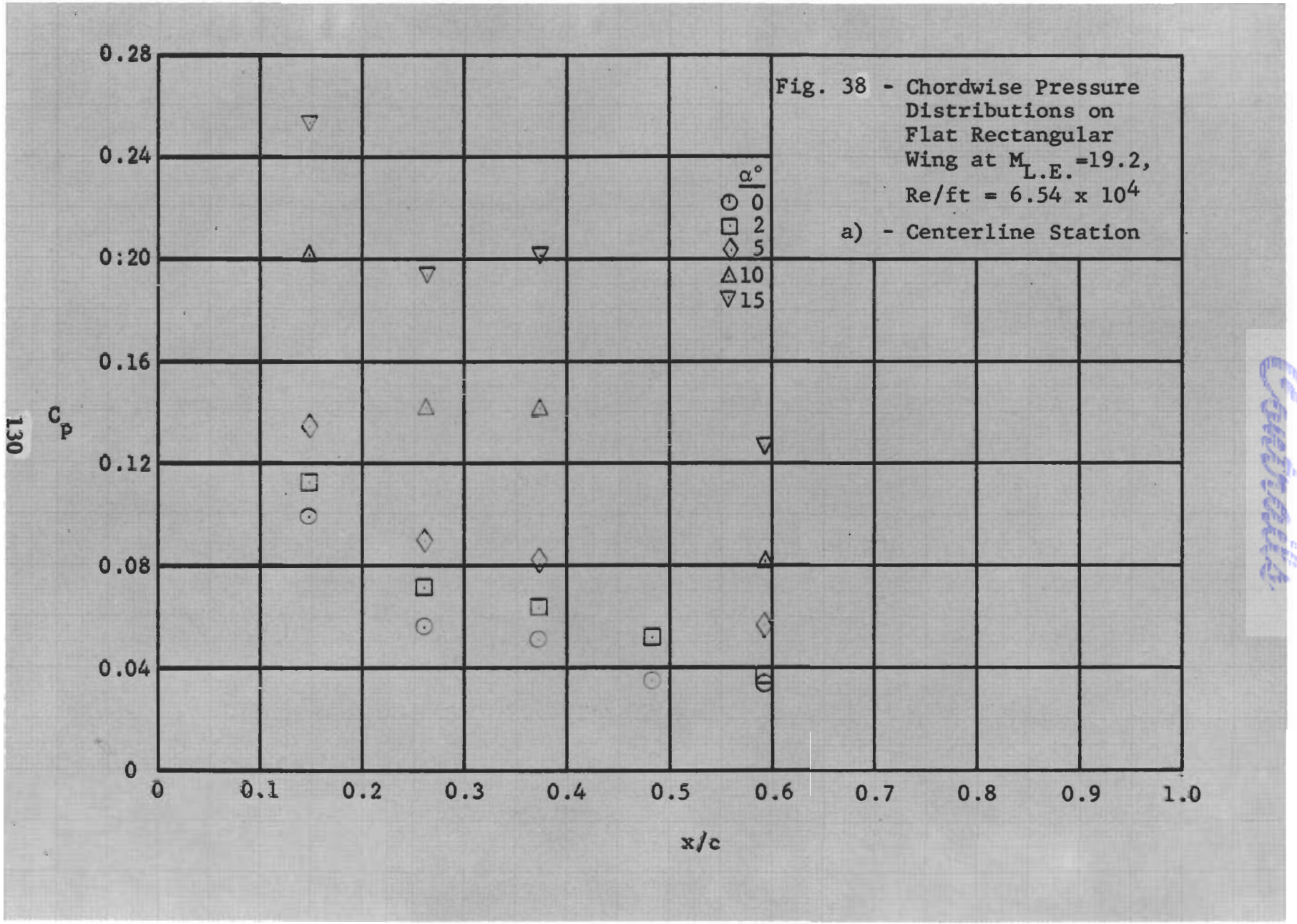

Fig. 38 - Chordwise Pressure Distributions on Flat Rectangular Wing at $M_{L.E.}$ =19.2, Re/ft = 6.54 x 10^4

a) - Centerline Station

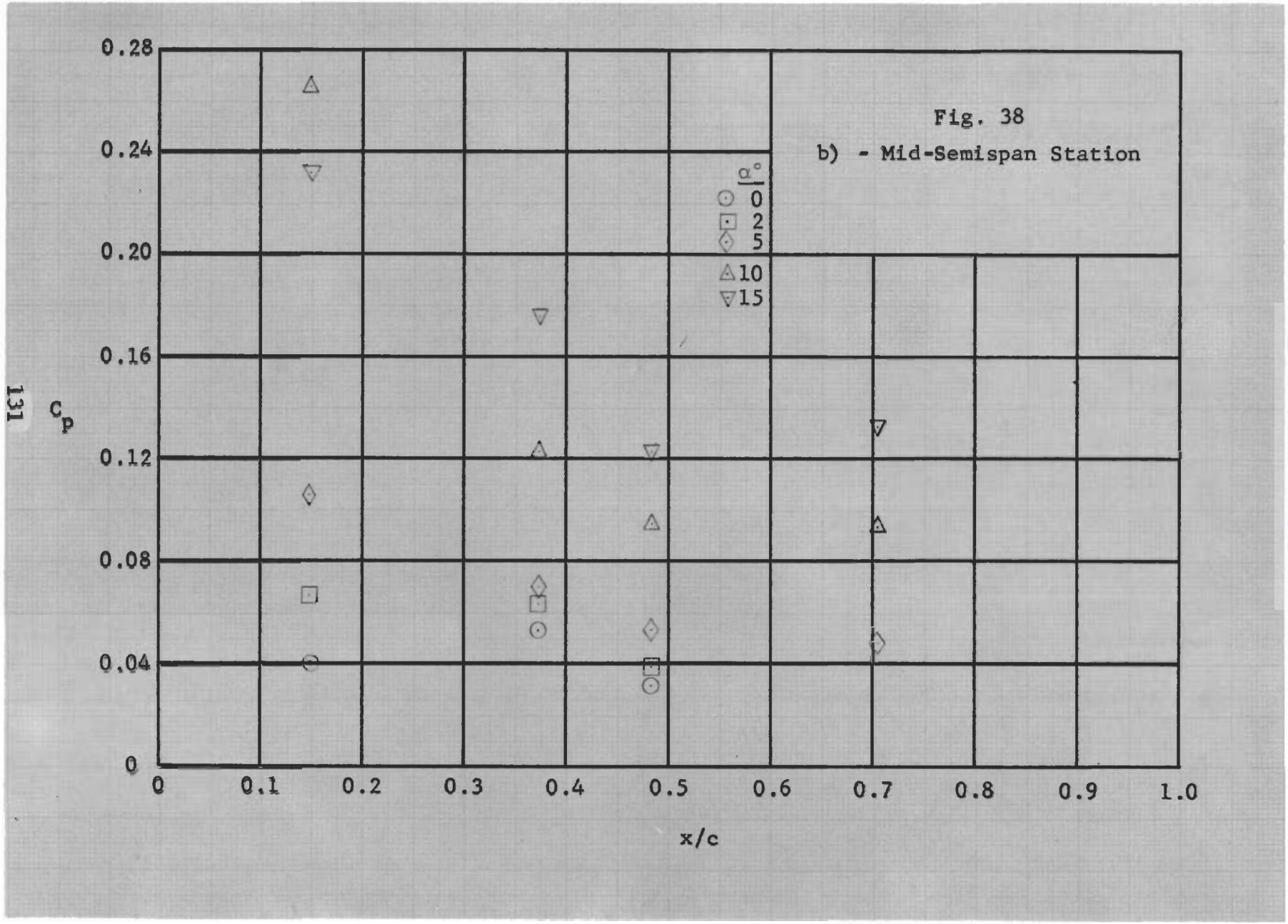

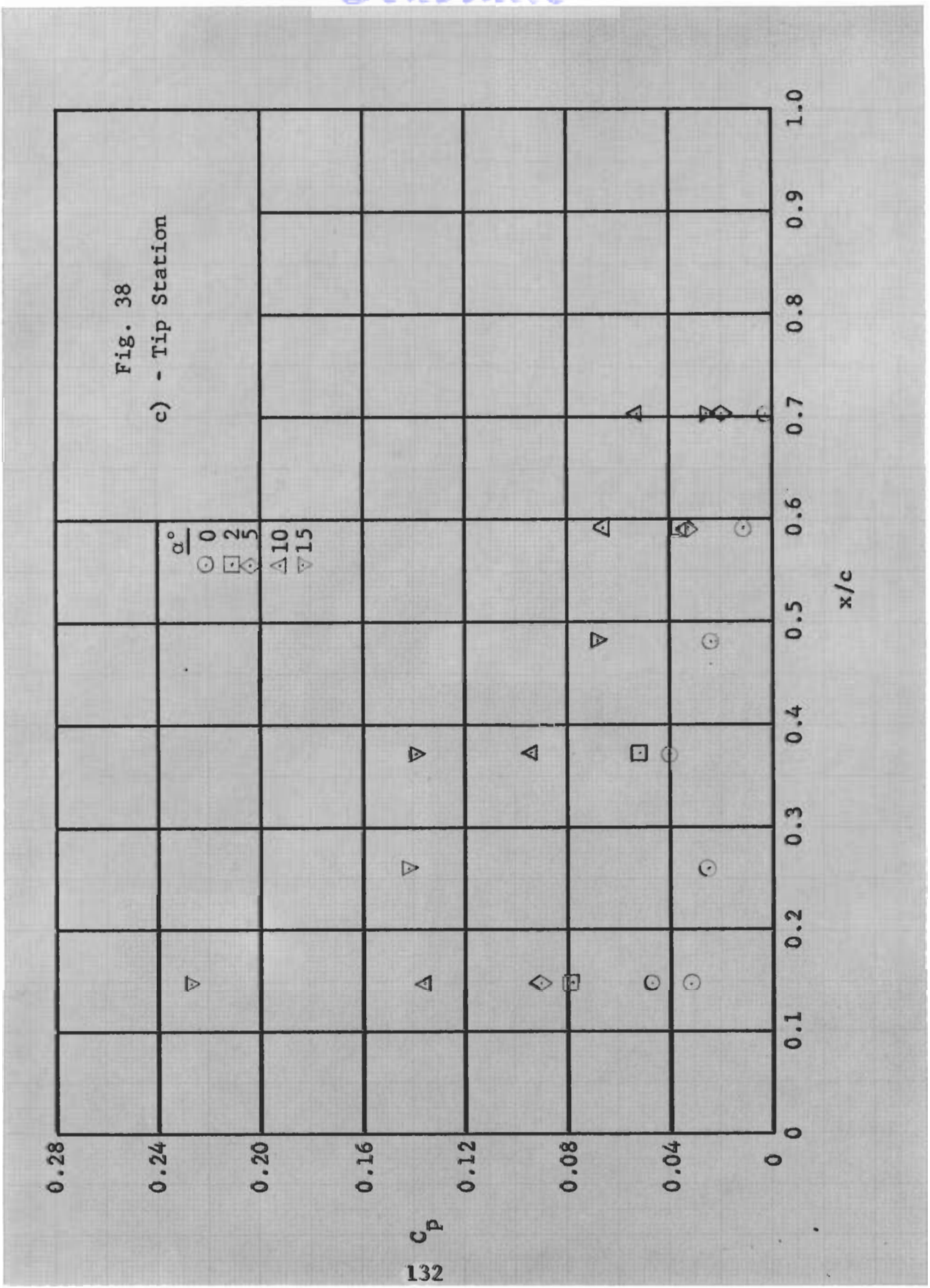

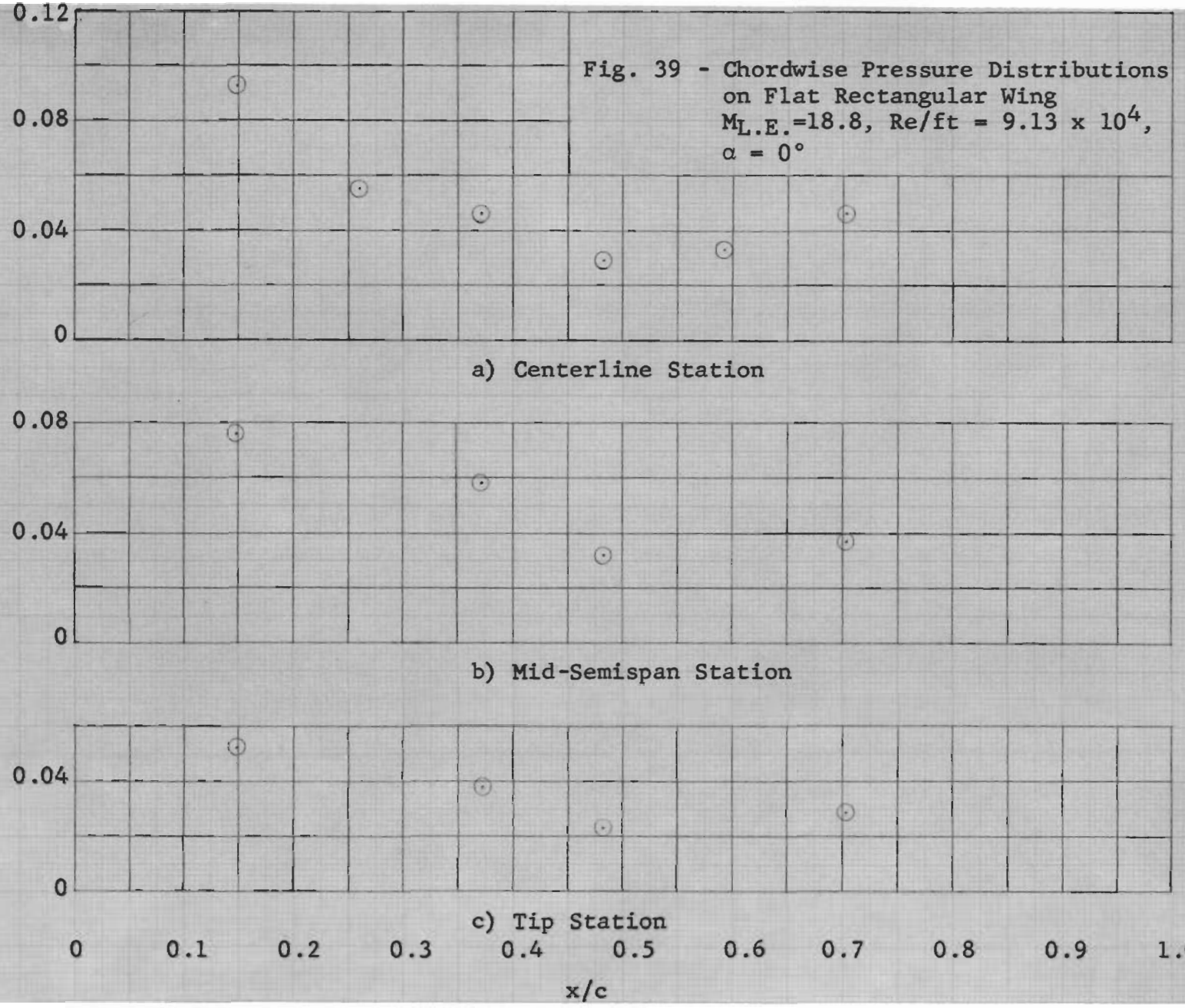

Fig. 39 - Chordwise Pressure Distributions on Flat Rectangular Wing $M_{L.E.}$=18.8, Re/ft = 9.13 x 10^4, $\alpha = 0°$

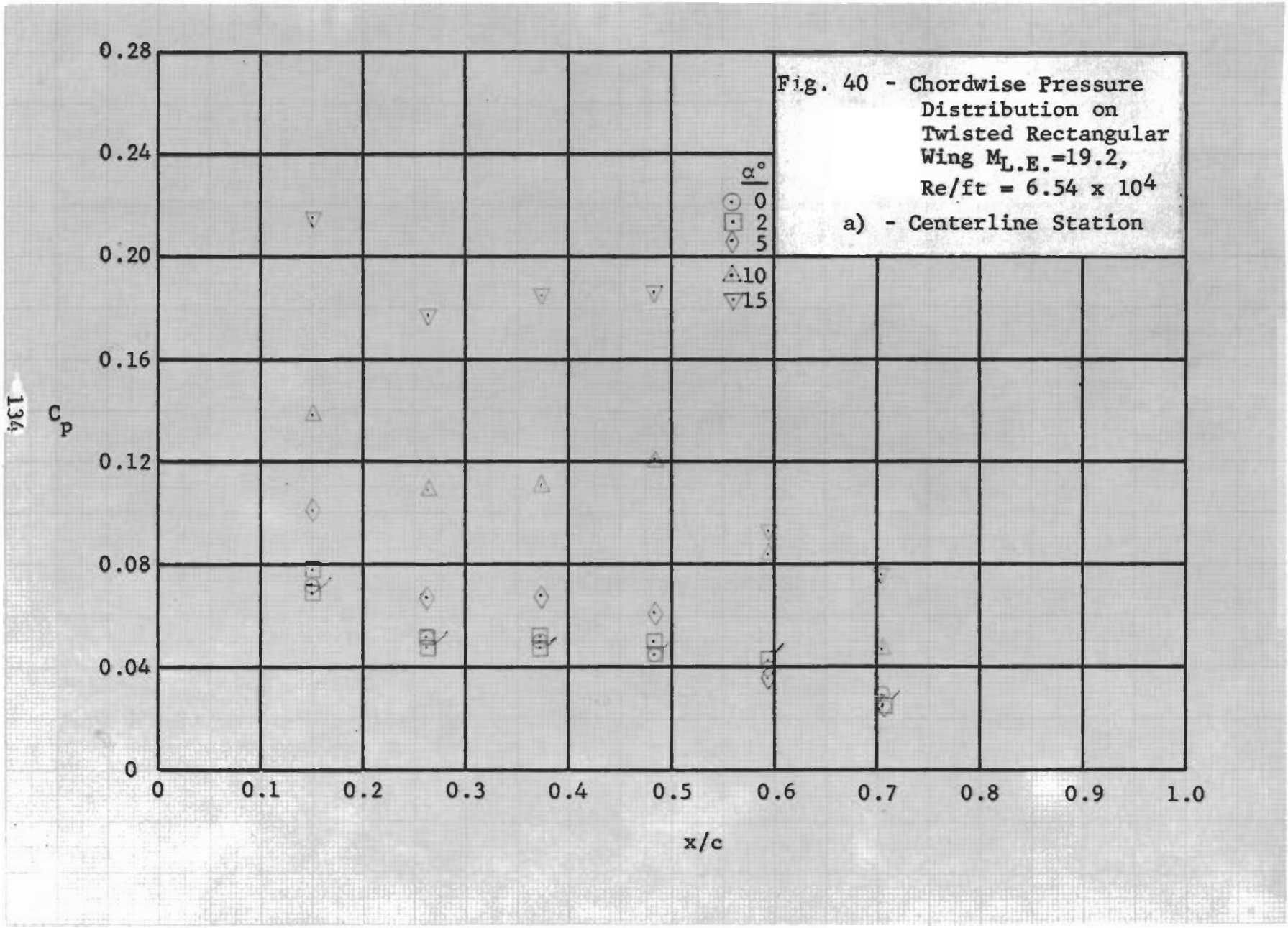

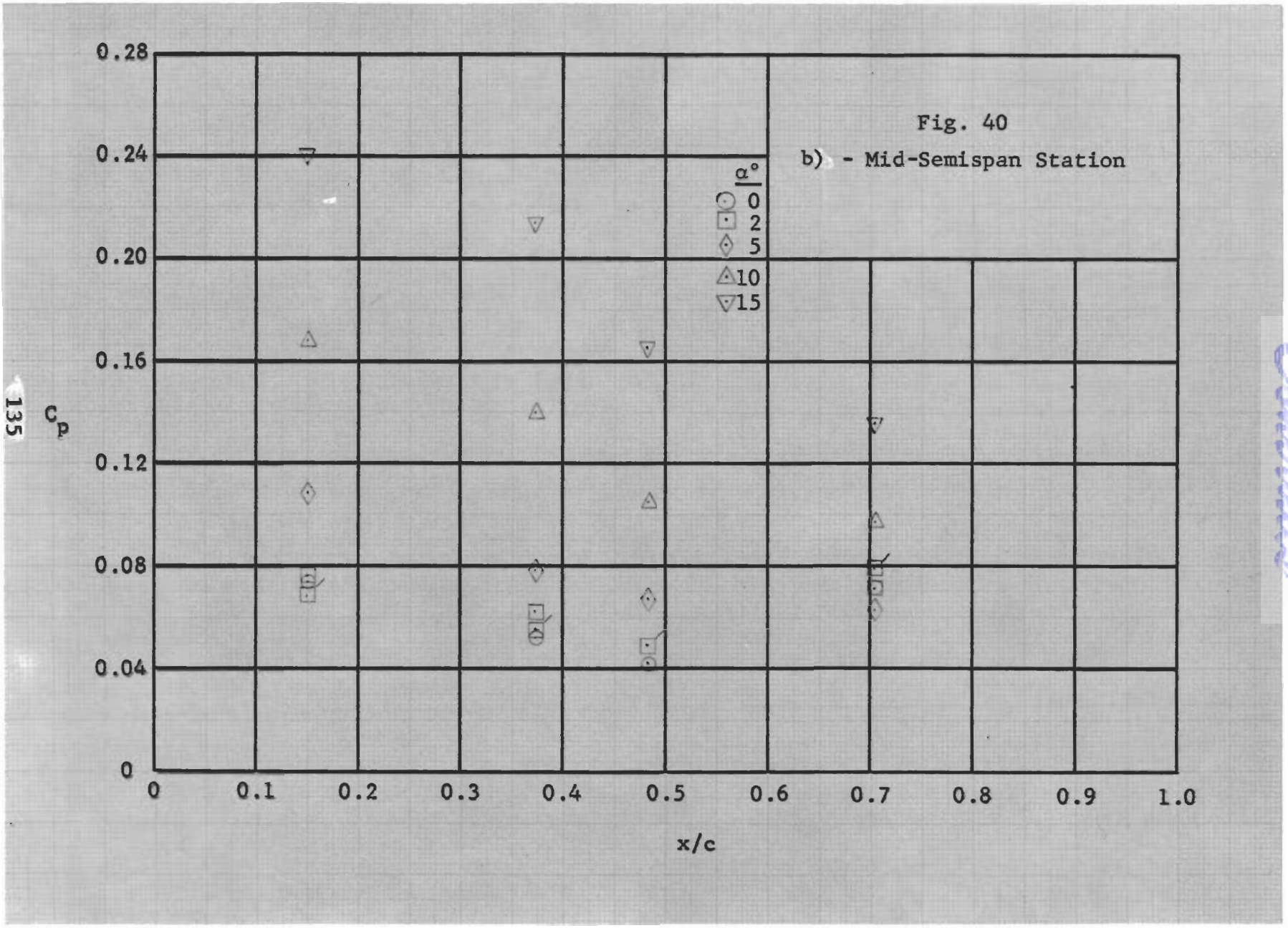

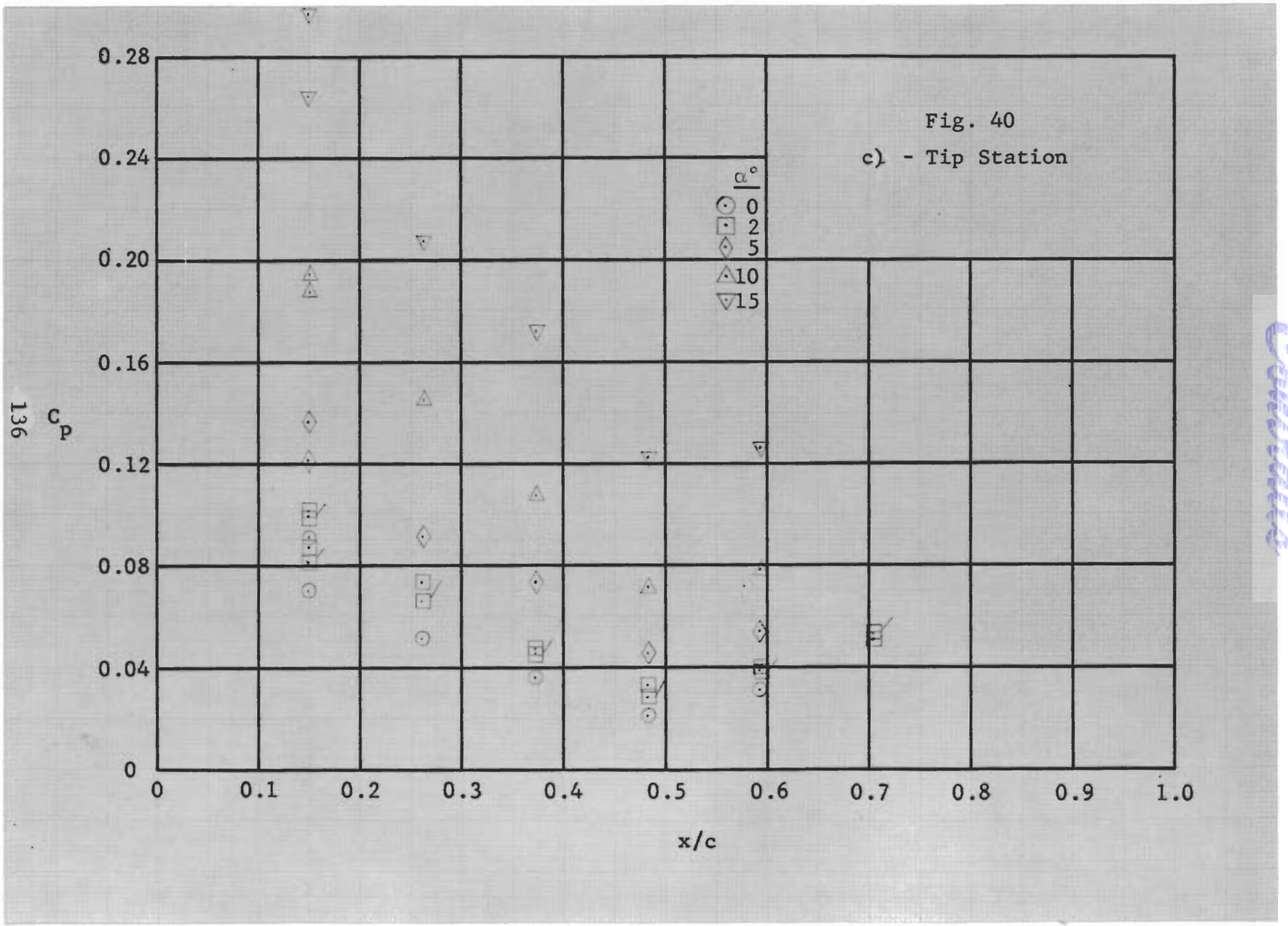

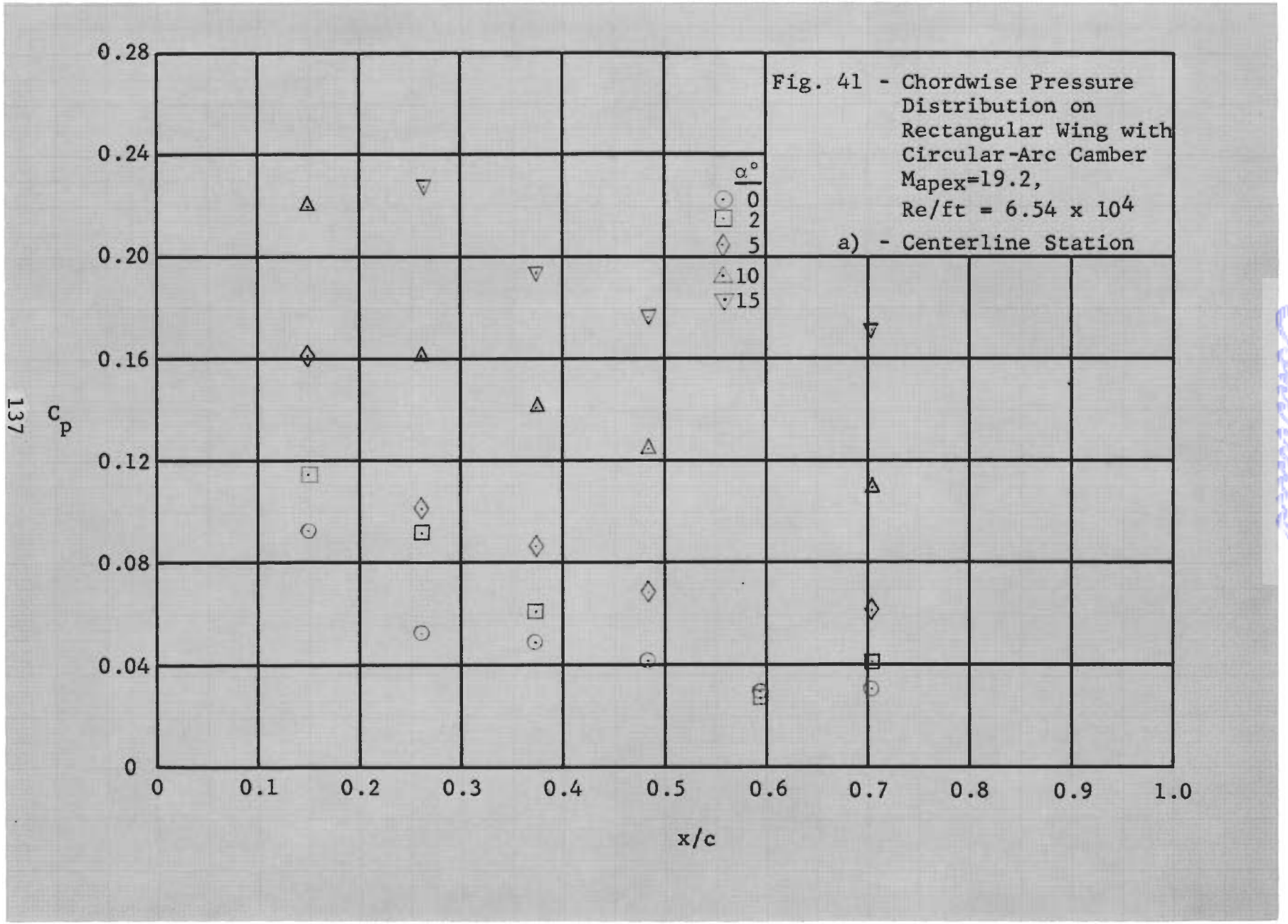

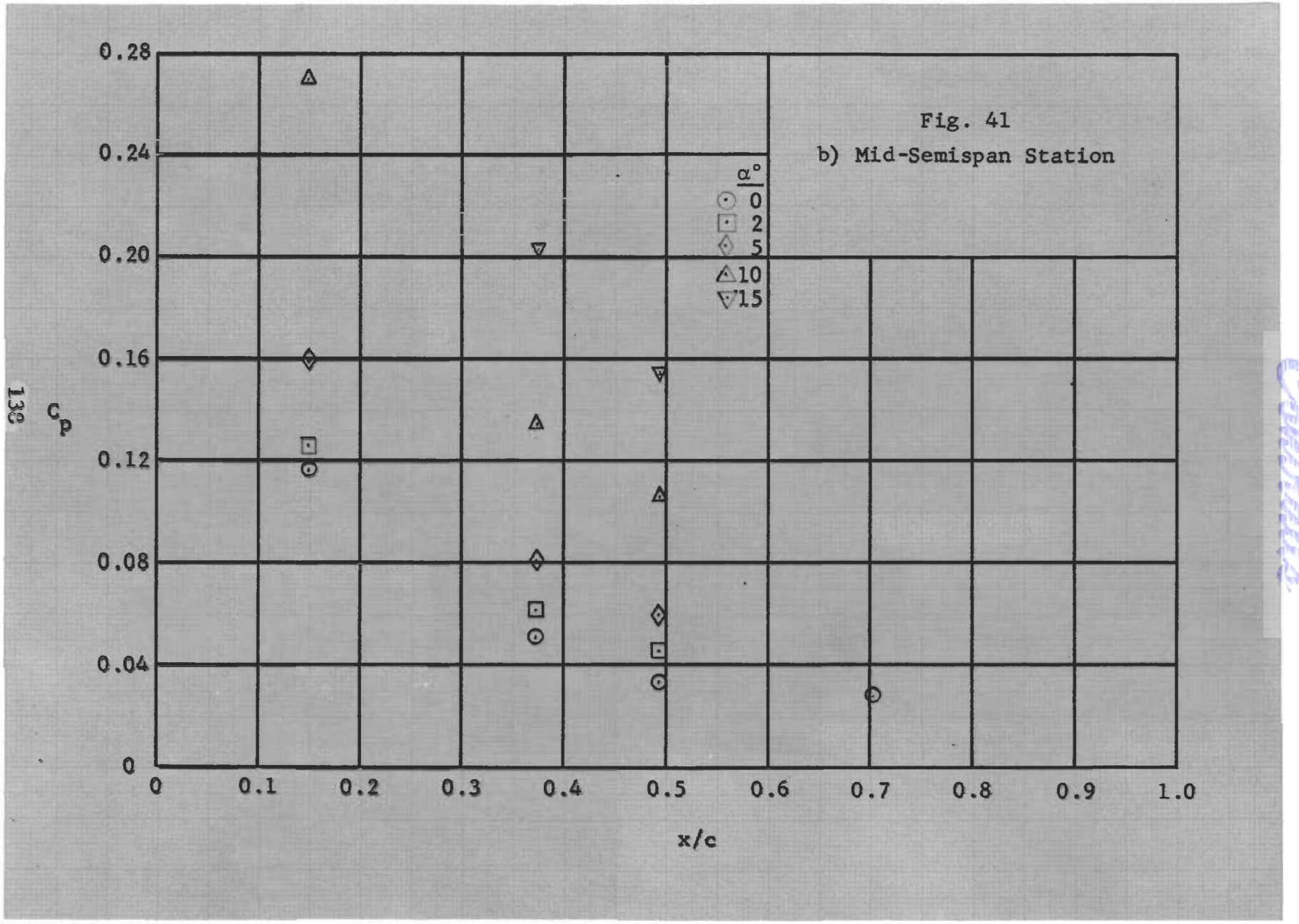

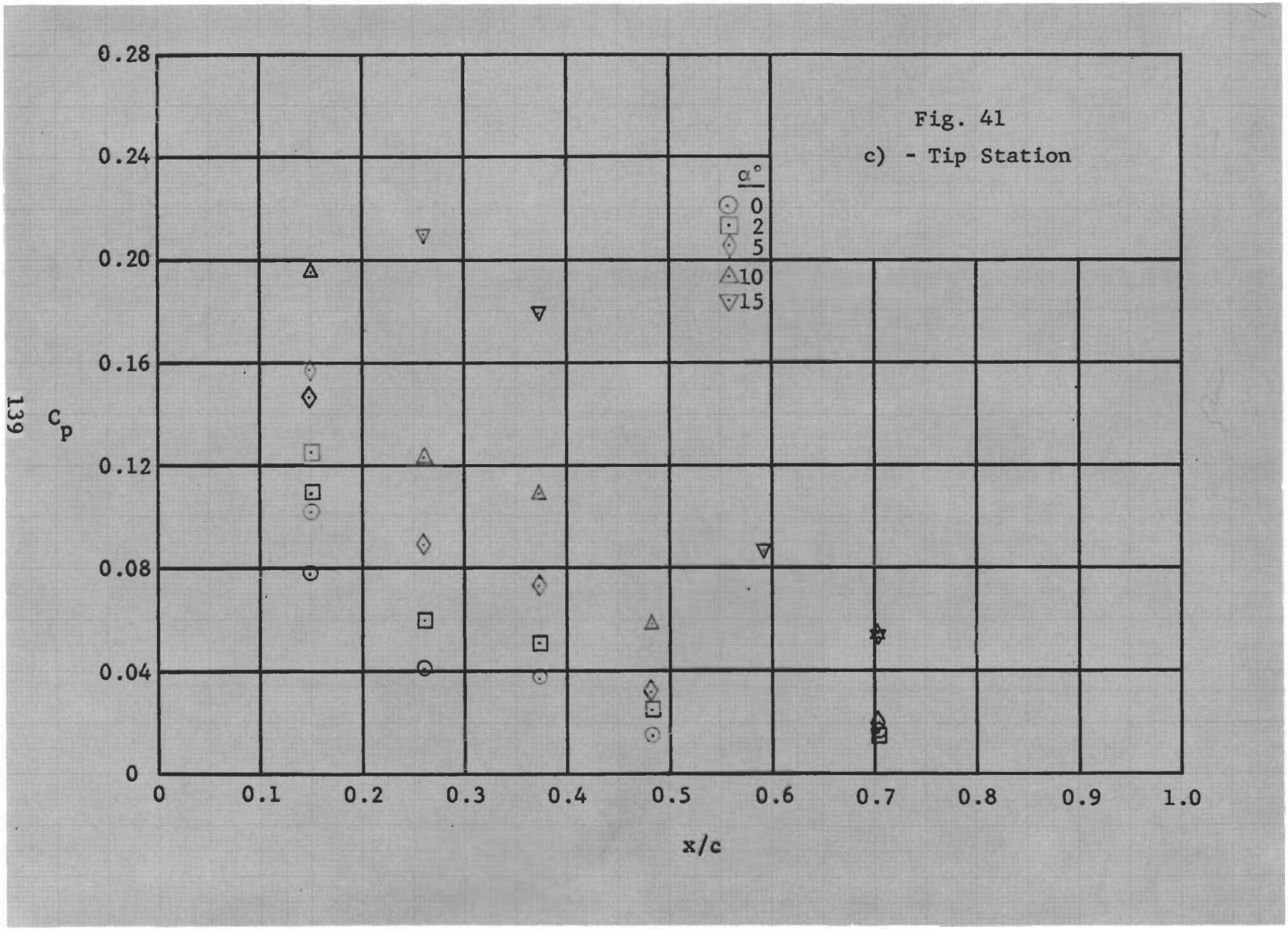

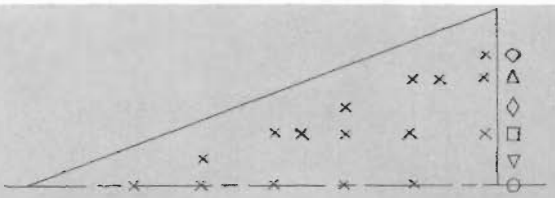

Fig. 42 - Chordwise Pressure Distribution on Flat 70° Delta Wing at M_{apex}=18.9, Re/ft = 6.54 x 10^4

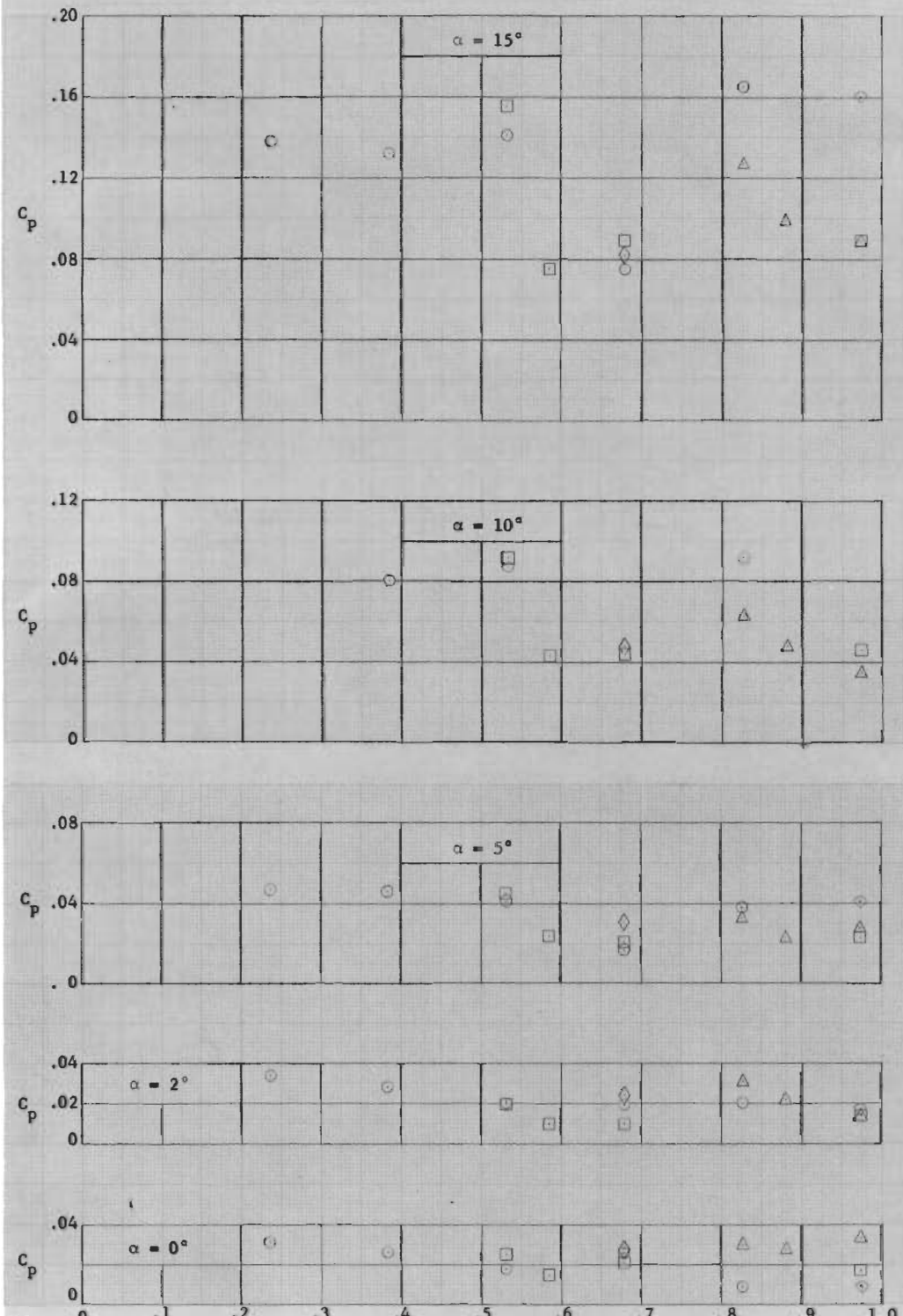

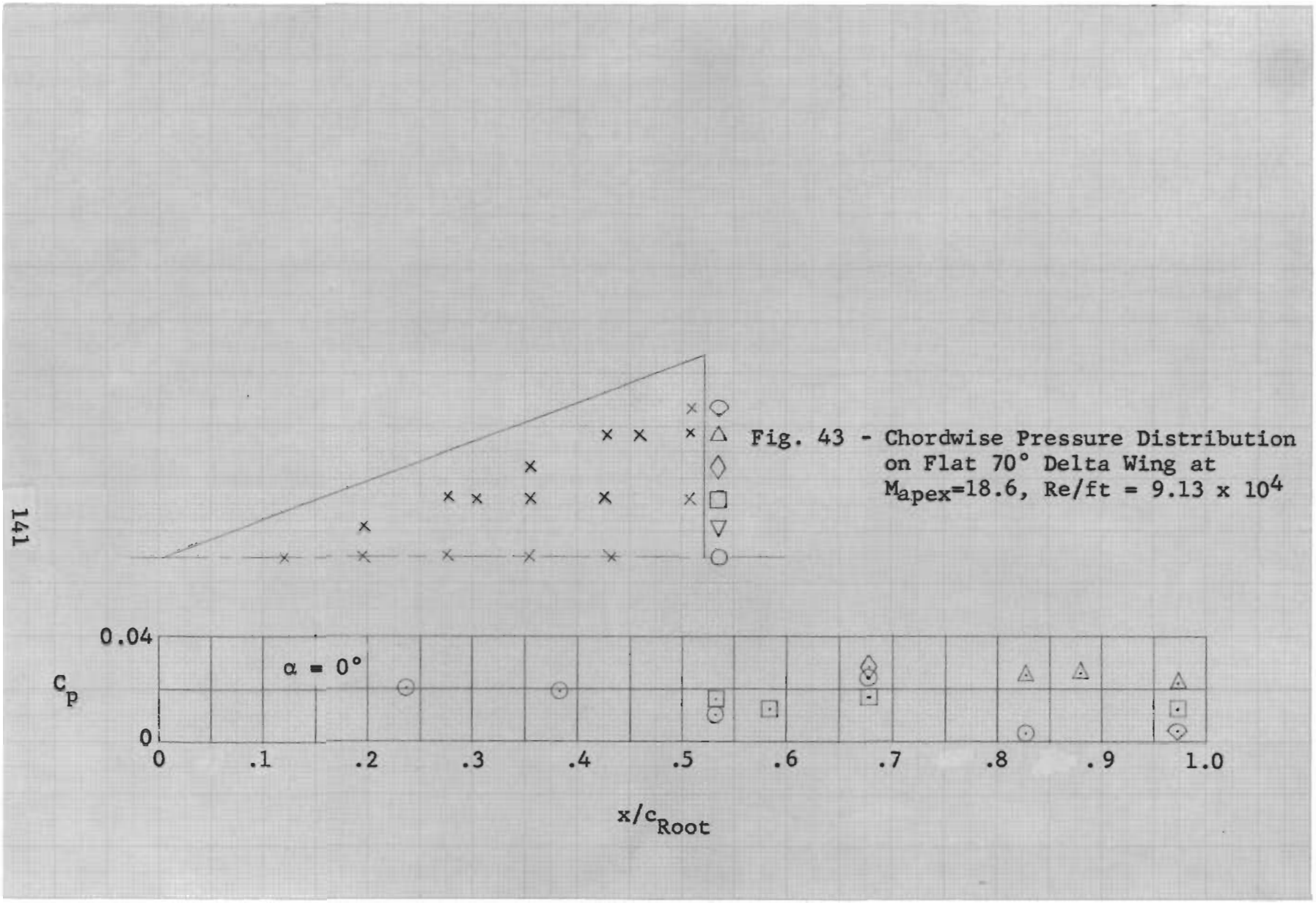

Fig. 43 - Chordwise Pressure Distribution on Flat 70° Delta Wing at M_{apex}=18.6, Re/ft = 9.13×10^4

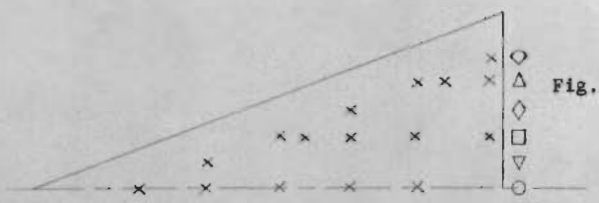

Fig. 44 - Chordwise Pressure Distribution on 70° Delta Wing with Circular-Arc Camber M_{apex} = 18.9, Re/ft = 6.54 x 10^4

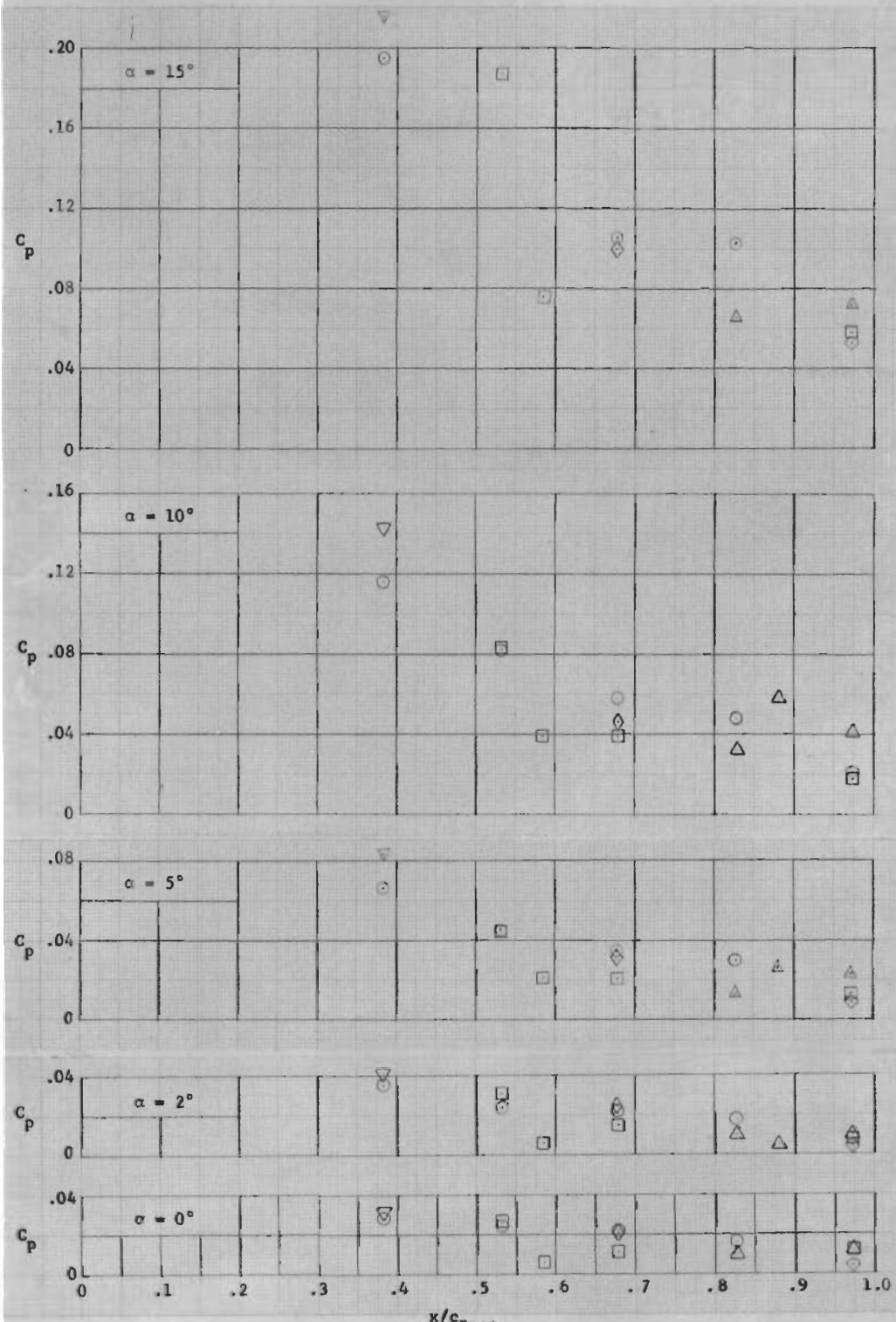

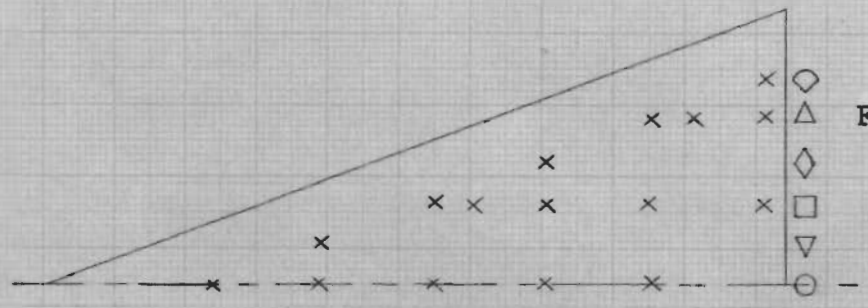

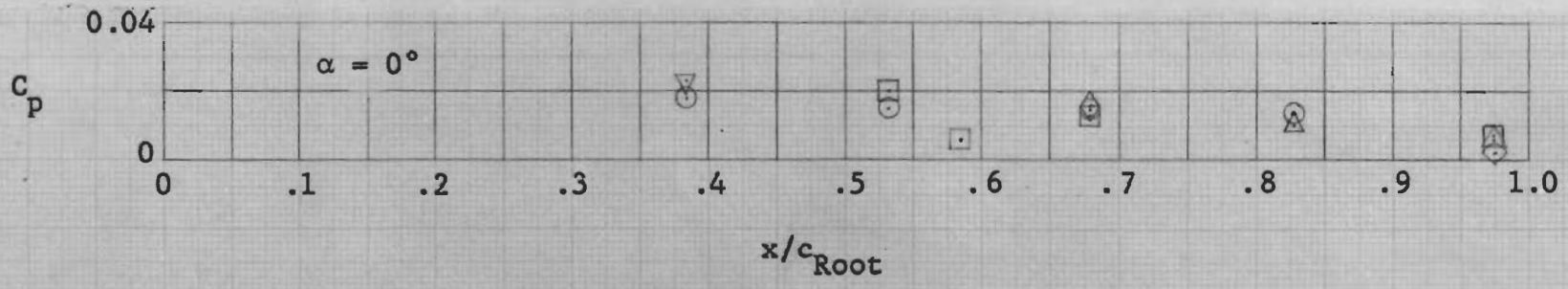

Fig. 45 - Chordwise Pressure Distribution on 70° Delta Wing with Circular-Arc Camber at M_{apex}= 18.6, Re/ft = 9.13×10^4

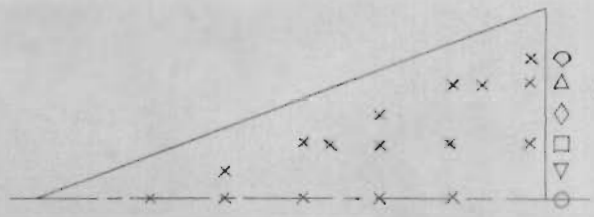

Fig. 46 - Chordwise Pressure Distribution on 70° Delta Wing with Sine-Wave Camber M_{apex}=18.9, Re/ft = 6.54 x 10^4

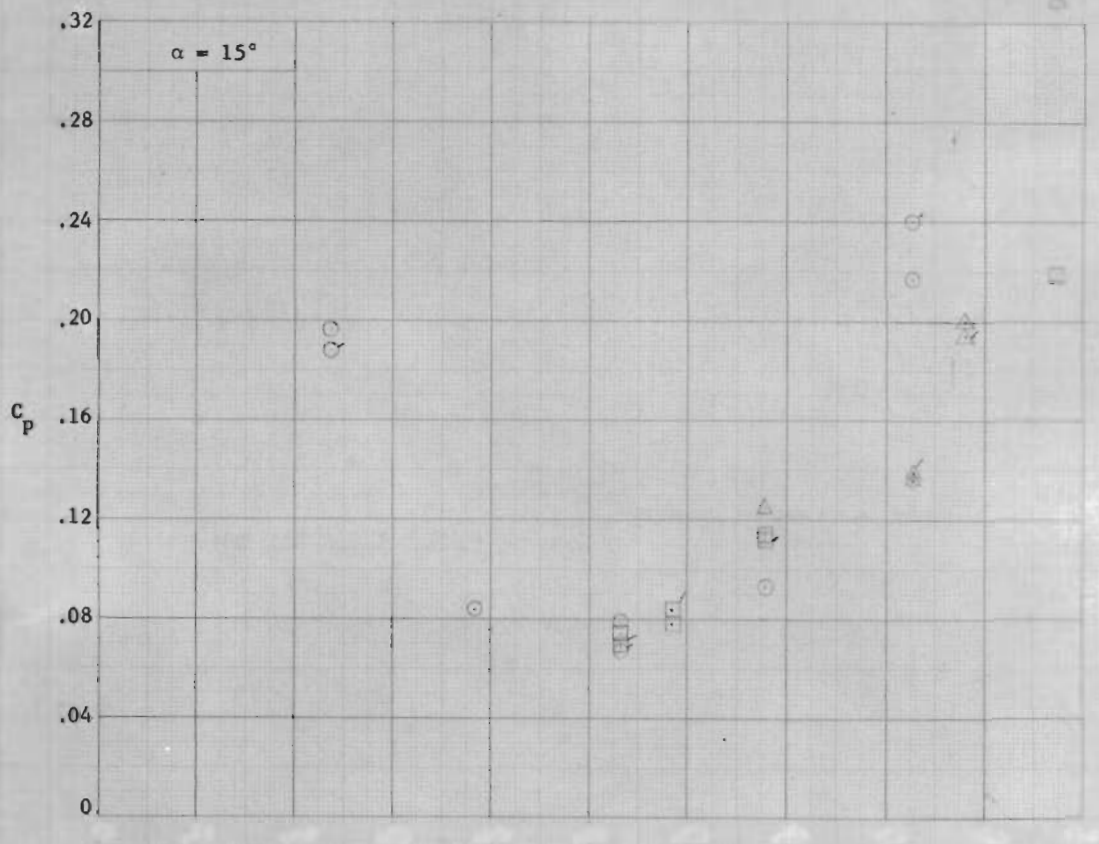

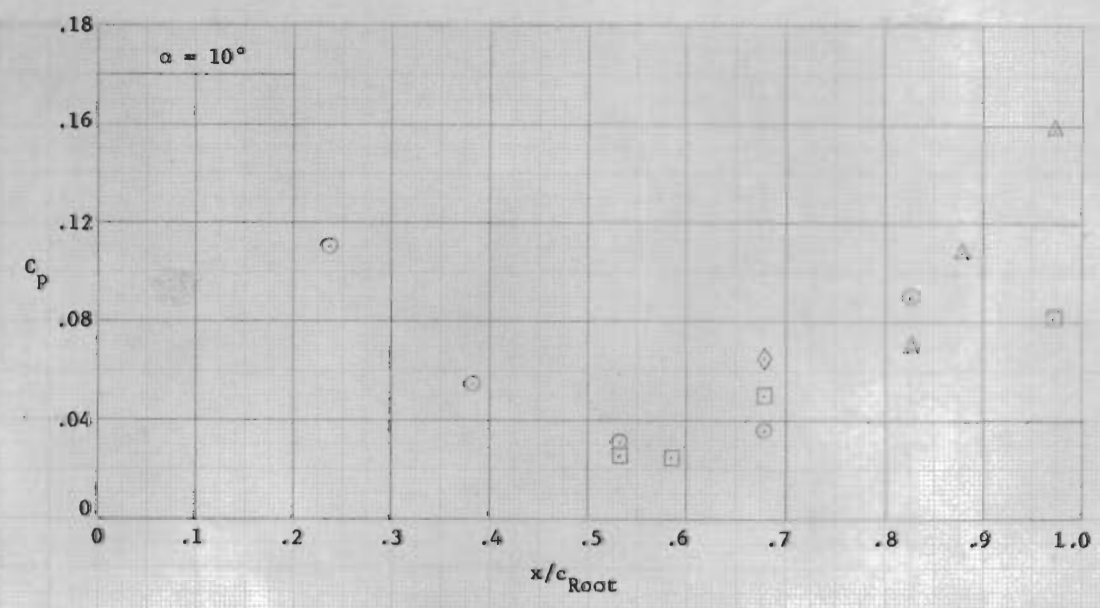

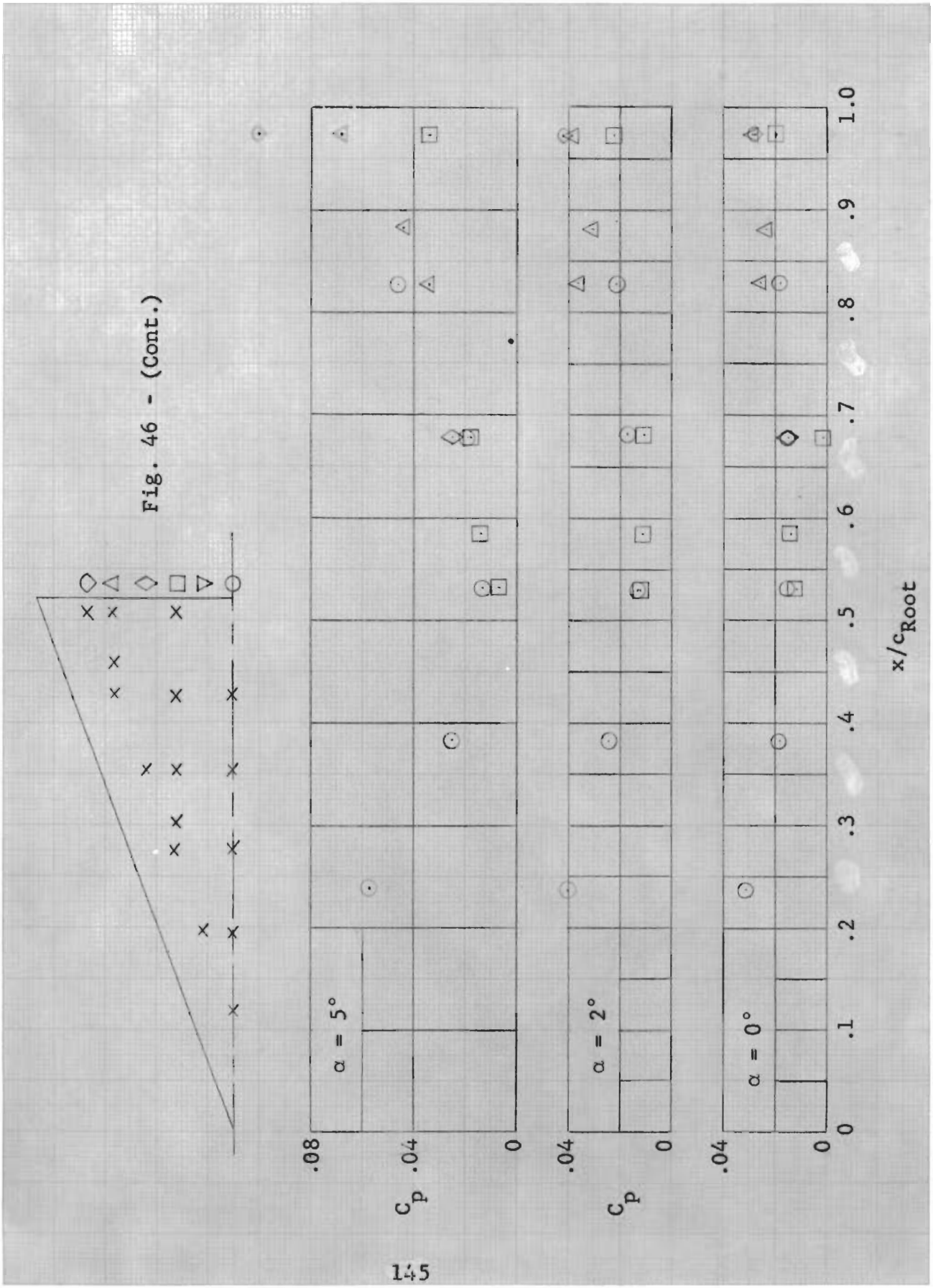

Fig. 46 - (Cont.)

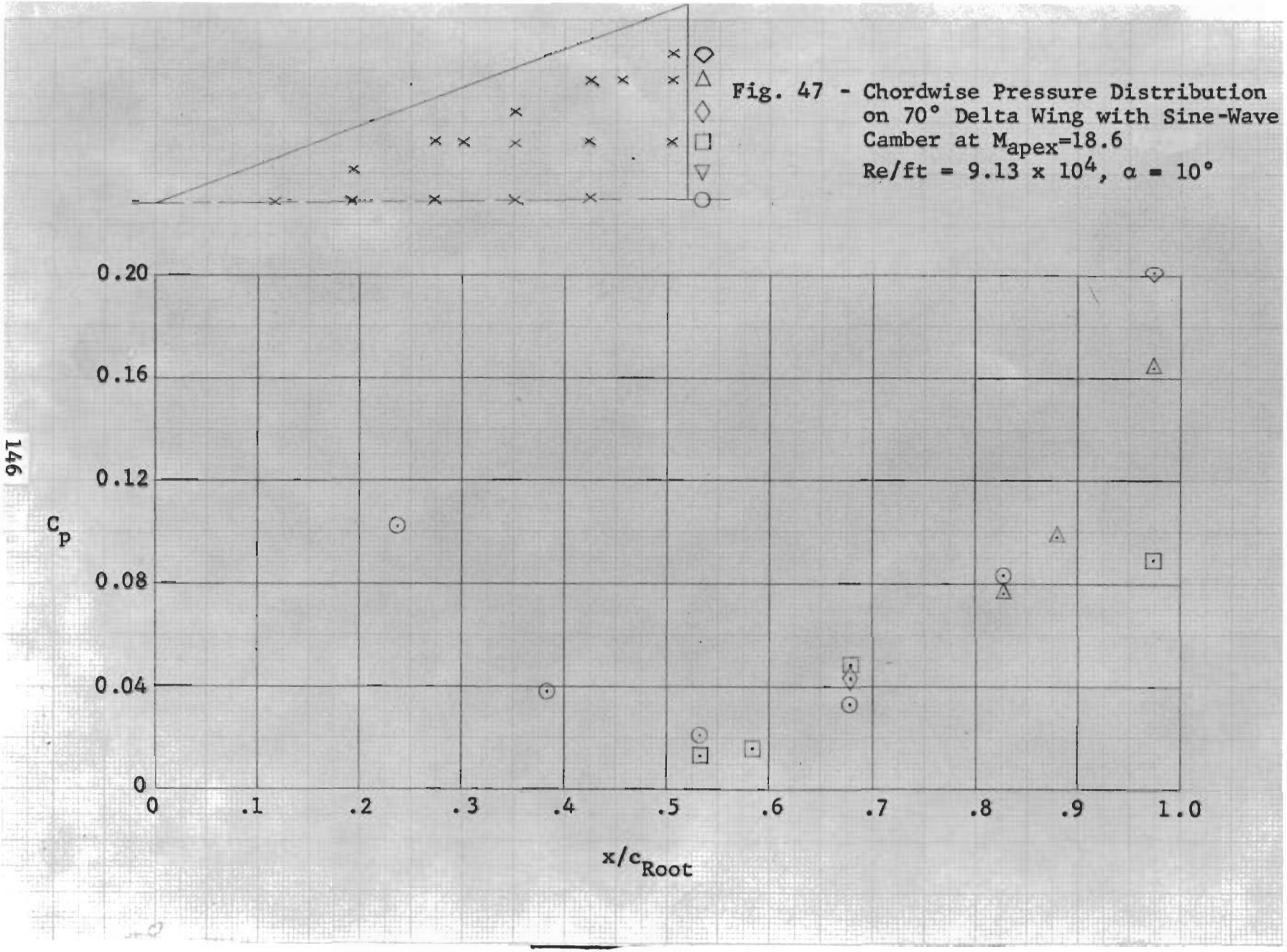

Fig. 47 - Chordwise Pressure Distribution on 70° Delta Wing with Sine-Wave Camber at $M_{apex}=18.6$
$Re/ft = 9.13 \times 10^4$, $\alpha = 10°$

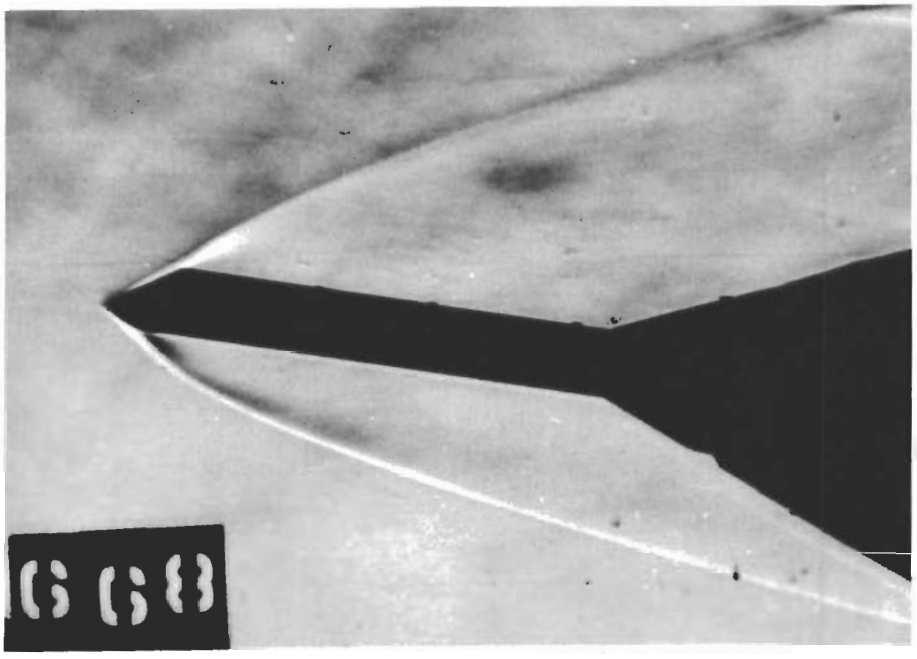

Fig. 48 - Schlieren Photograph of Flat Rectangular Wing, $\alpha = 10°$, Nominal $M_\infty = 12$, Nominal $Re_\infty = 2.1 \times 10^5/ft$

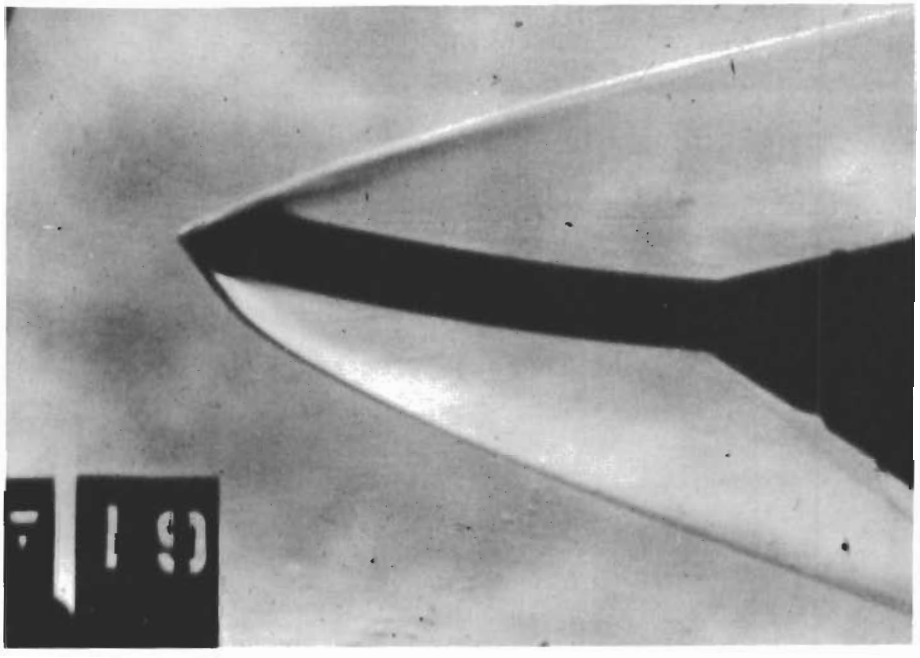

Fig. 49 - Schlieren Photograph of Rectangular Wing with Circular-Arc Camber, $\alpha = 10°$, Nominal $M_\infty = 12$, Nominal $Re_\infty = 3.9 \times 10^5/ft$

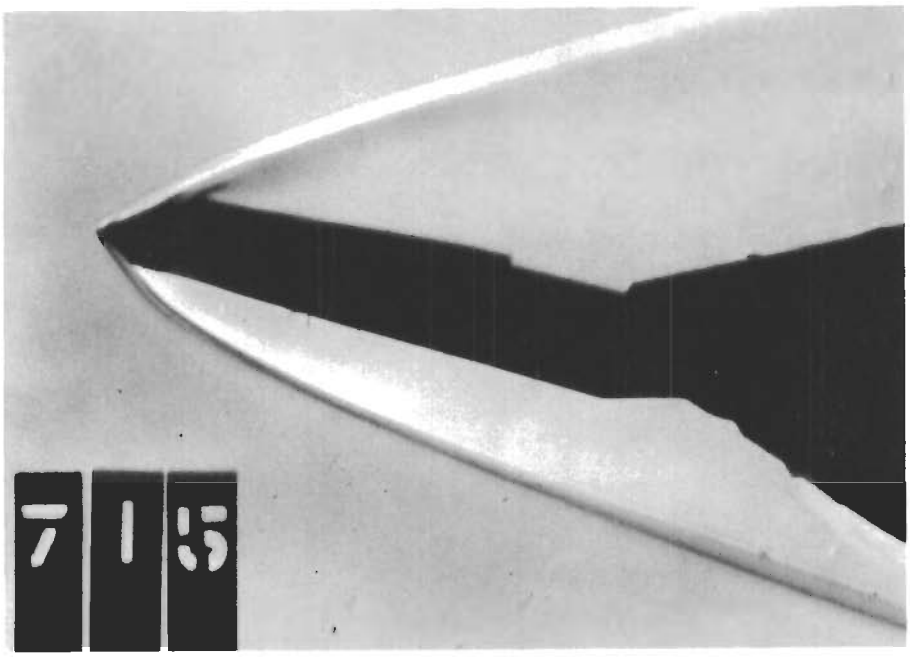

Fig. 50 - Schlieren Photograph of Twisted Rectangular Wing, $\alpha = 10°$, Nominal $M_\infty = 12$, Nominal $Re_\infty = 3.9 \times 10^5/ft$

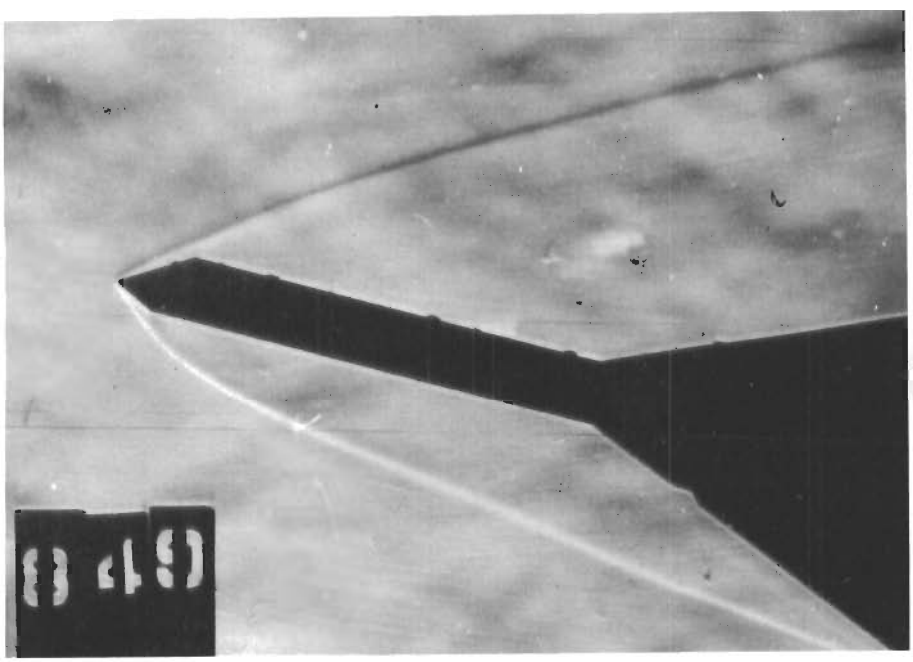

Fig. 51 - Schlieren Photograph of Flat Rectangular Wing, $\alpha = 15°$, Nominal $M_\infty = 19$, Nominal $Re_\infty = .65 \times 10^5/ft$

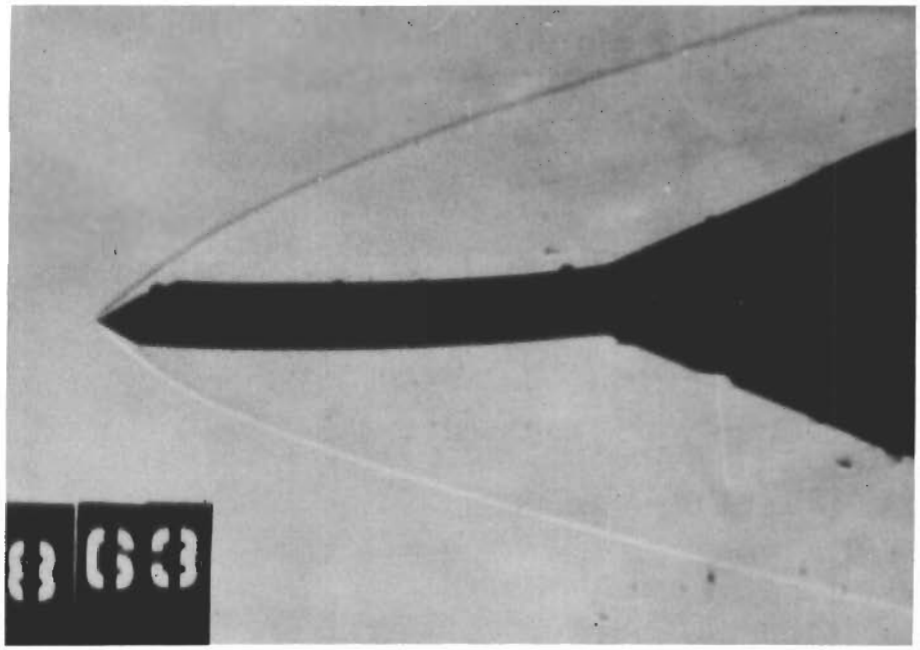

Fig. 52 - Schlieren Photograph of Rectangular Wing with Circular-Arc Camber, $\alpha = 0°$, Nominal $M_\infty = 19$, Nominal $Re_\infty = .65 \times 10^5/ft$

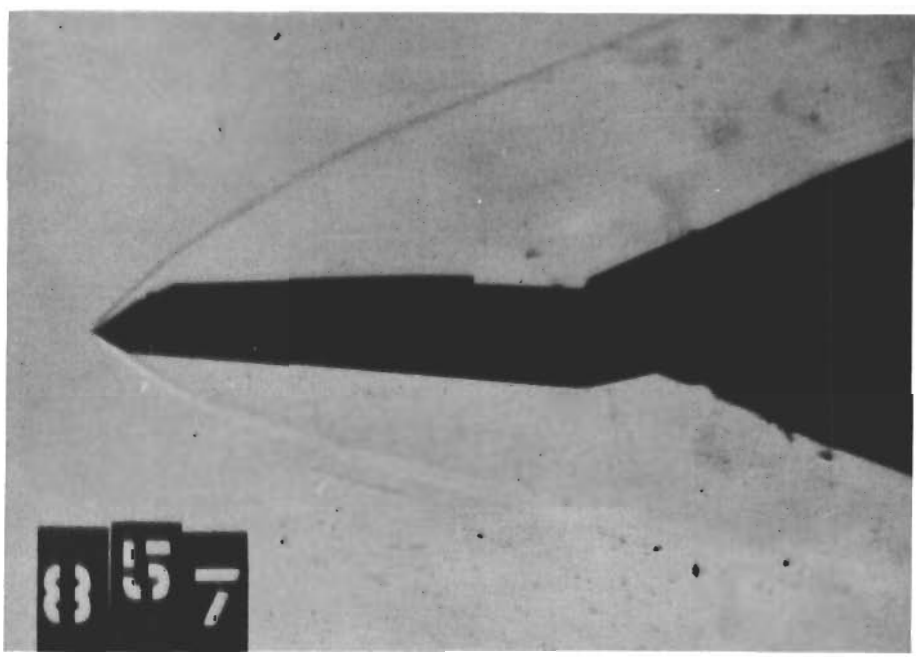

Fig. 53 - Schlieren Photograph of Twisted Rectangular Wing, $\alpha = 2°$, Nominal $M_\infty = 19$, Nominal $Re_\infty = .65 \times 10^5/ft$

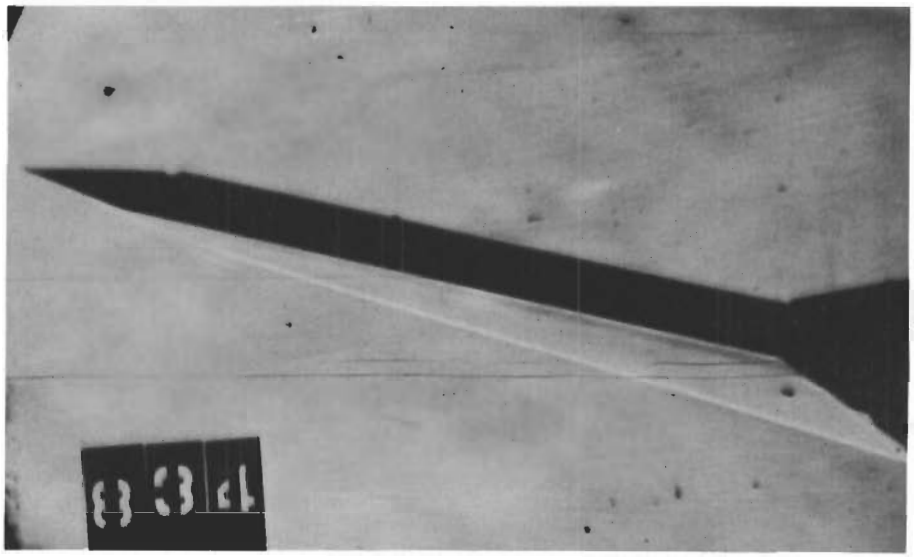

Fig. 54 - Schlieren Photograph of Flat 70° Delta Wing, α = 15°, Nominal M_∞ = 12, Nominal Re_∞ = 2.1 x 10^5/ft

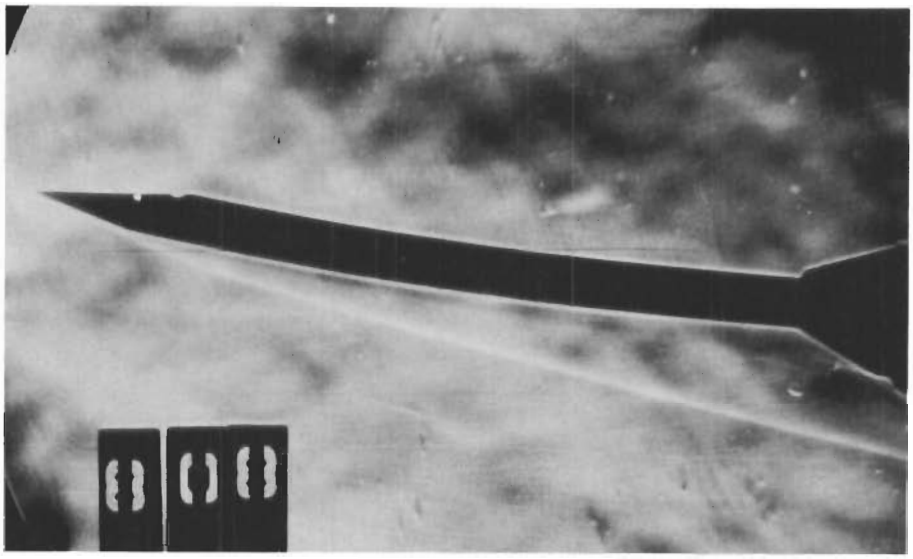

Fig. 55 - Schlieren Photograph of 70° Delta Wing with Circular-Arc Camber, α = 10°, Nominal M_∞ = 12, Re_∞ = 2.1 x 10^5/ft

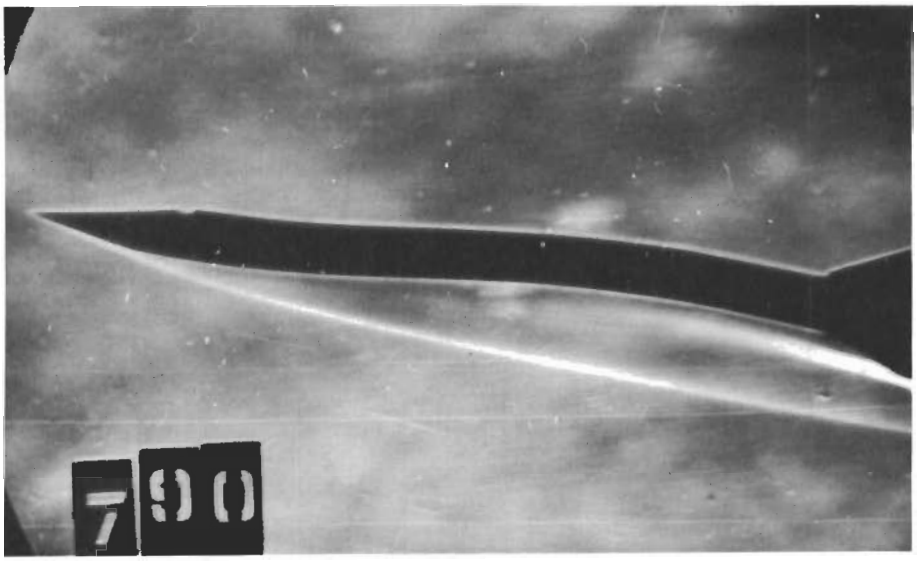

Fig. 56 - Schlieren Photograph of 70° Delta Wing with Sine-Wave Camber, α = 10°, Nominal M_∞ = 12, Nominal Re_∞ = 3.9 x 10^5/ft

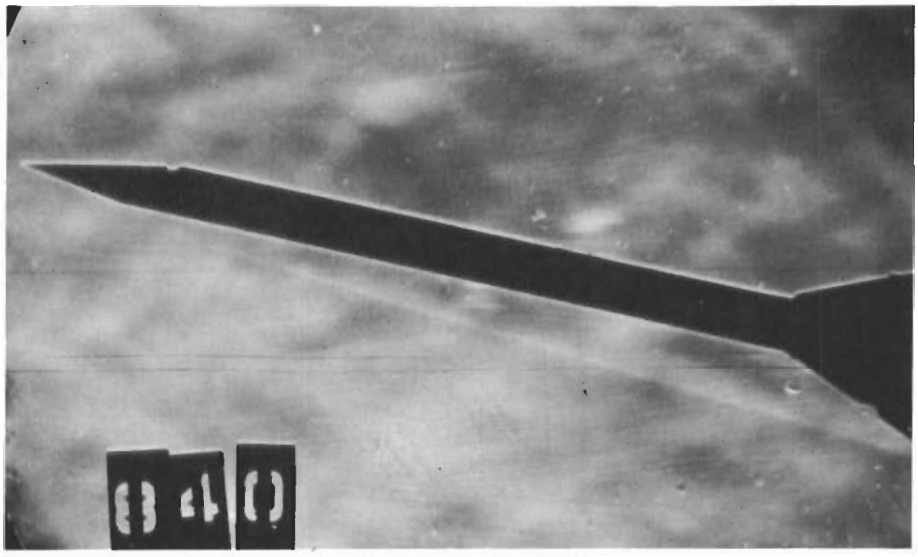

Fig. 57 - Schlieren Photograph of Flat 70° Delta Wing, α = 15°, Nominal M_∞ = 19, Nominal Re_∞ = .65 x 10^5/ft

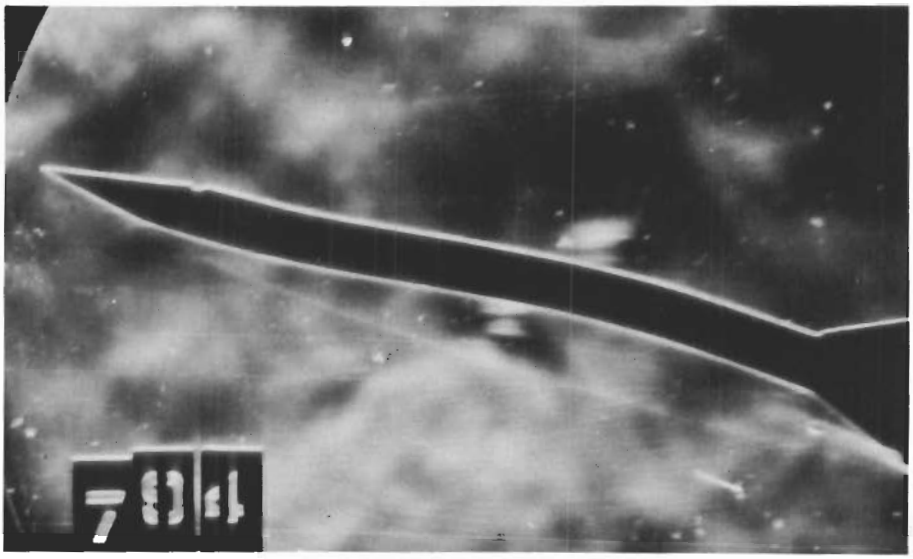

Fig. 58 - Schlieren Photograph of 70° Delta Wing with Sine-Wave Camber, α = 15°, Nominal M_∞ = 19, Nominal Re_∞ = .65 x 10^5/ft

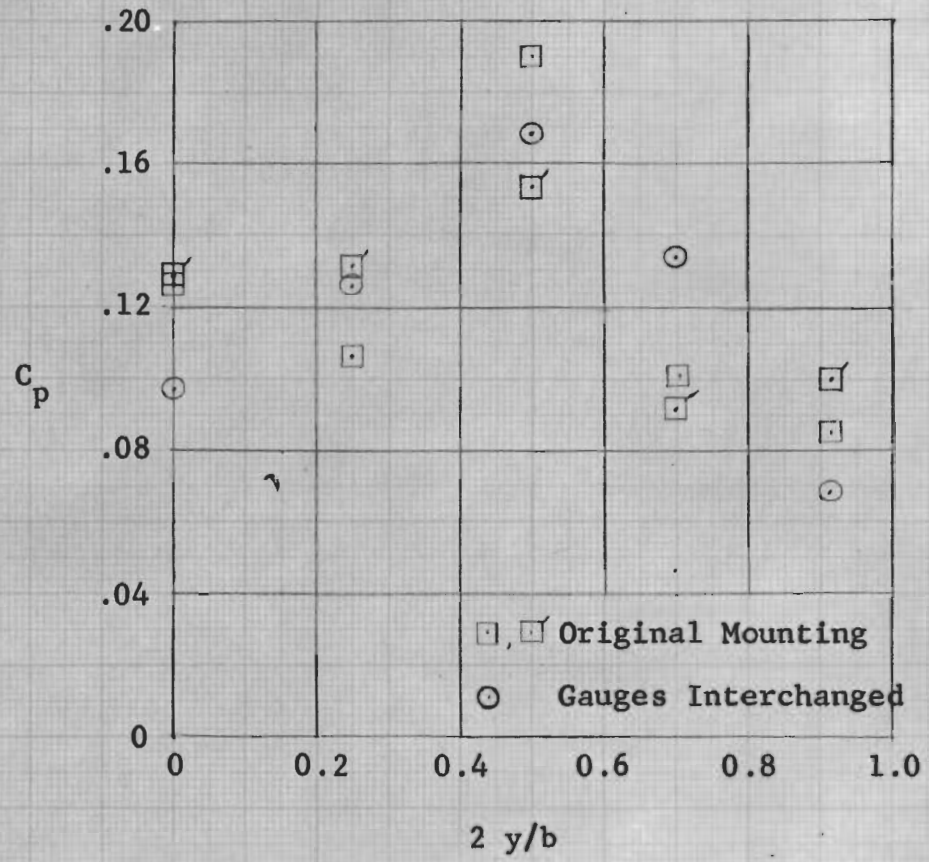

Fig. 59 - Comparison of Spanwise Pressure Distributions on Leading Edge of Flat Rectangular Wing at M=12 with Gauges Interchanged, $\alpha = 10°$

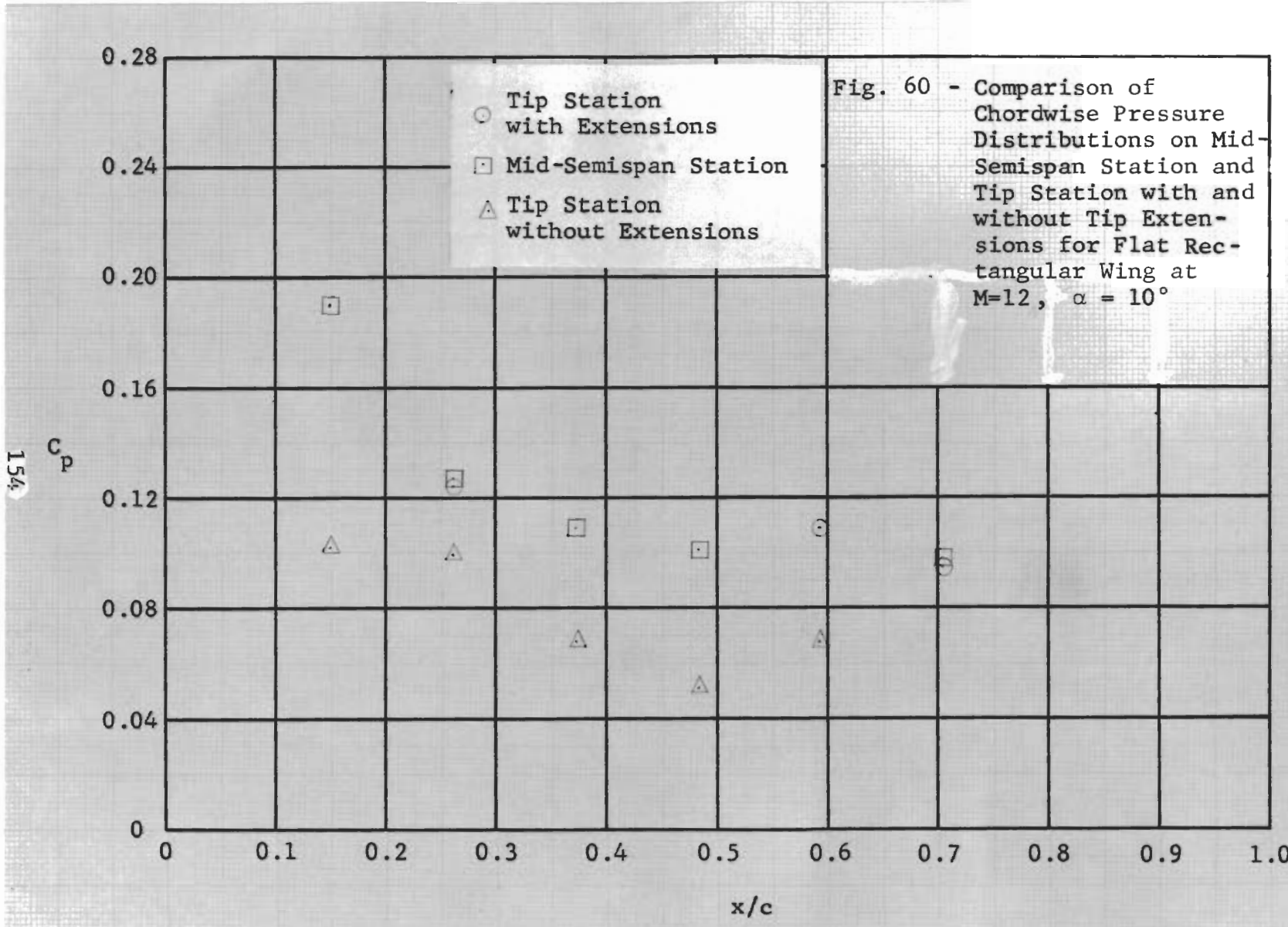

Fig. 60 - Comparison of Chordwise Pressure Distributions on Mid-Semispan Station and Tip Station with and without Tip Extensions for Flat Rectangular Wing at M=12, $\alpha = 10°$

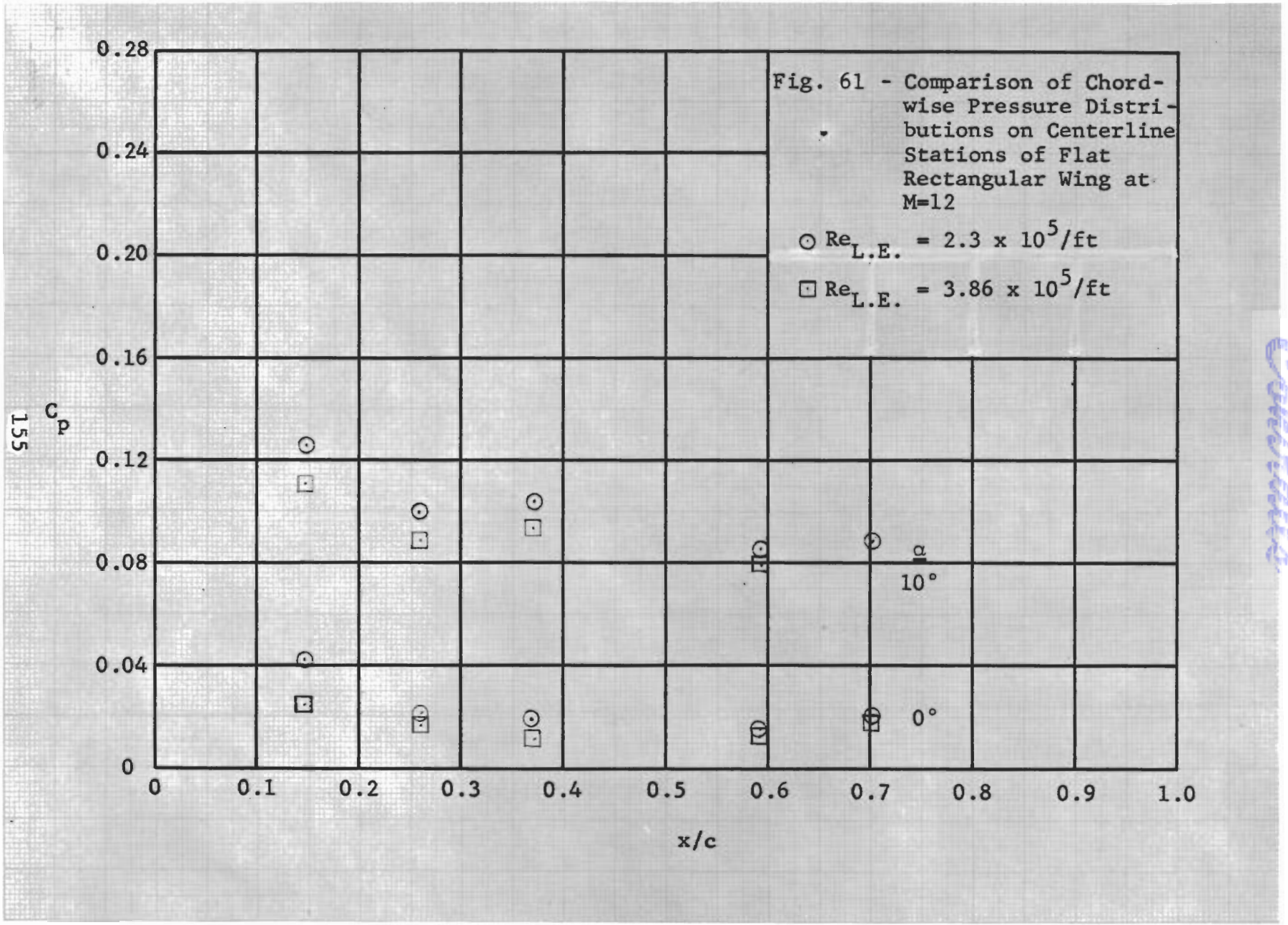

Fig. 61 - Comparison of Chordwise Pressure Distributions on Centerline Stations of Flat Rectangular Wing at M=12

⊙ $Re_{L.E.}$ = 2.3 x 10^5/ft

⊡ $Re_{L.E.}$ = 3.86 x 10^5/ft

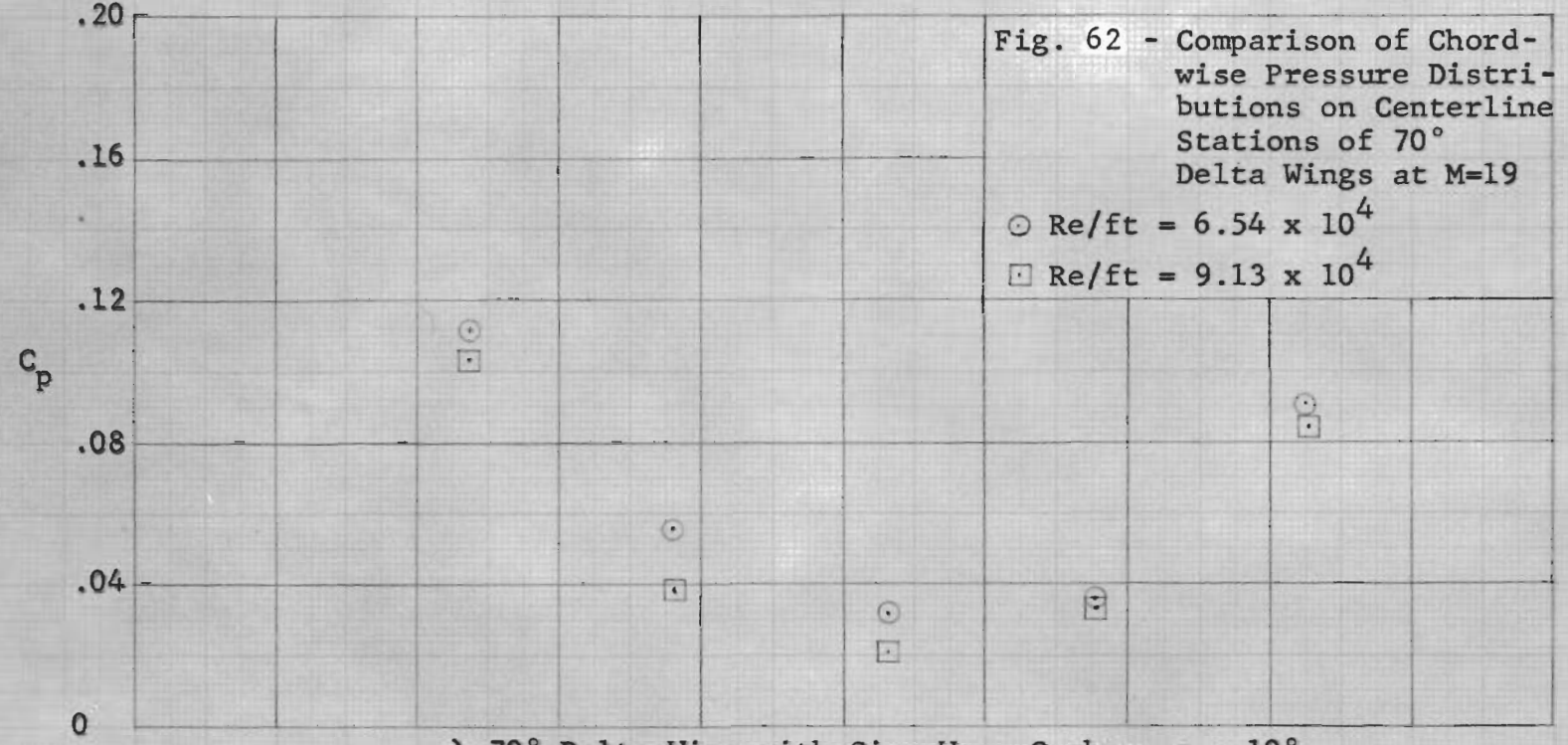

Fig. 62 - Comparison of Chordwise Pressure Distributions on Centerline Stations of 70° Delta Wings at M=19

⊙ Re/ft = 6.54×10^4

⊡ Re/ft = 9.13×10^4

a) 70° Delta Wing with Sine-Wave Camber, $\alpha = 10°$

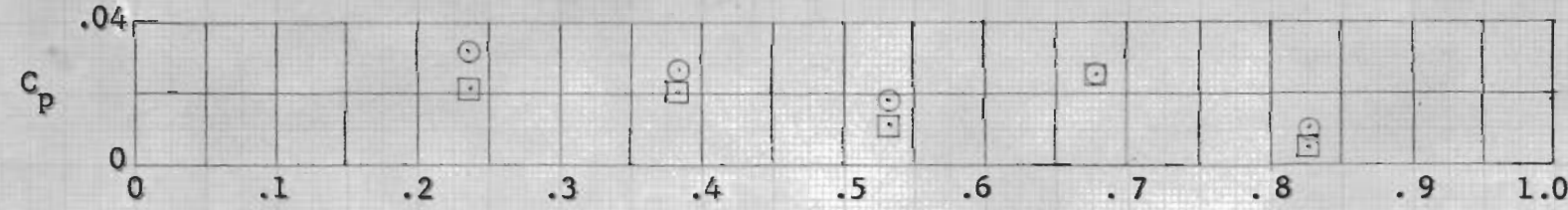

b) Flat 70° Delta Wing, $\alpha = 0°$

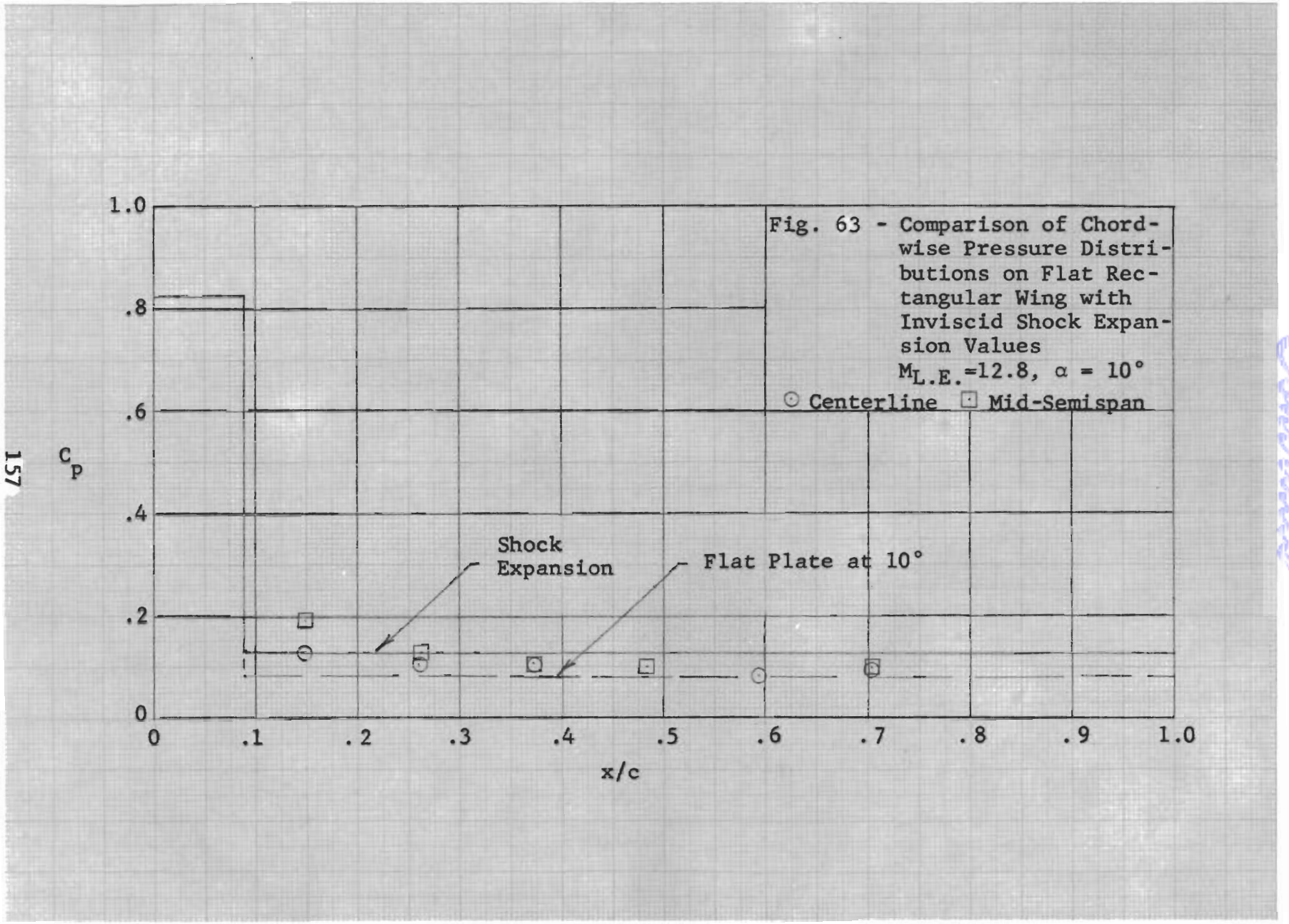

Fig. 63 - Comparison of Chordwise Pressure Distributions on Flat Rectangular Wing with Inviscid Shock Expansion Values $M_{L.E.}$=12.8, α = 10°

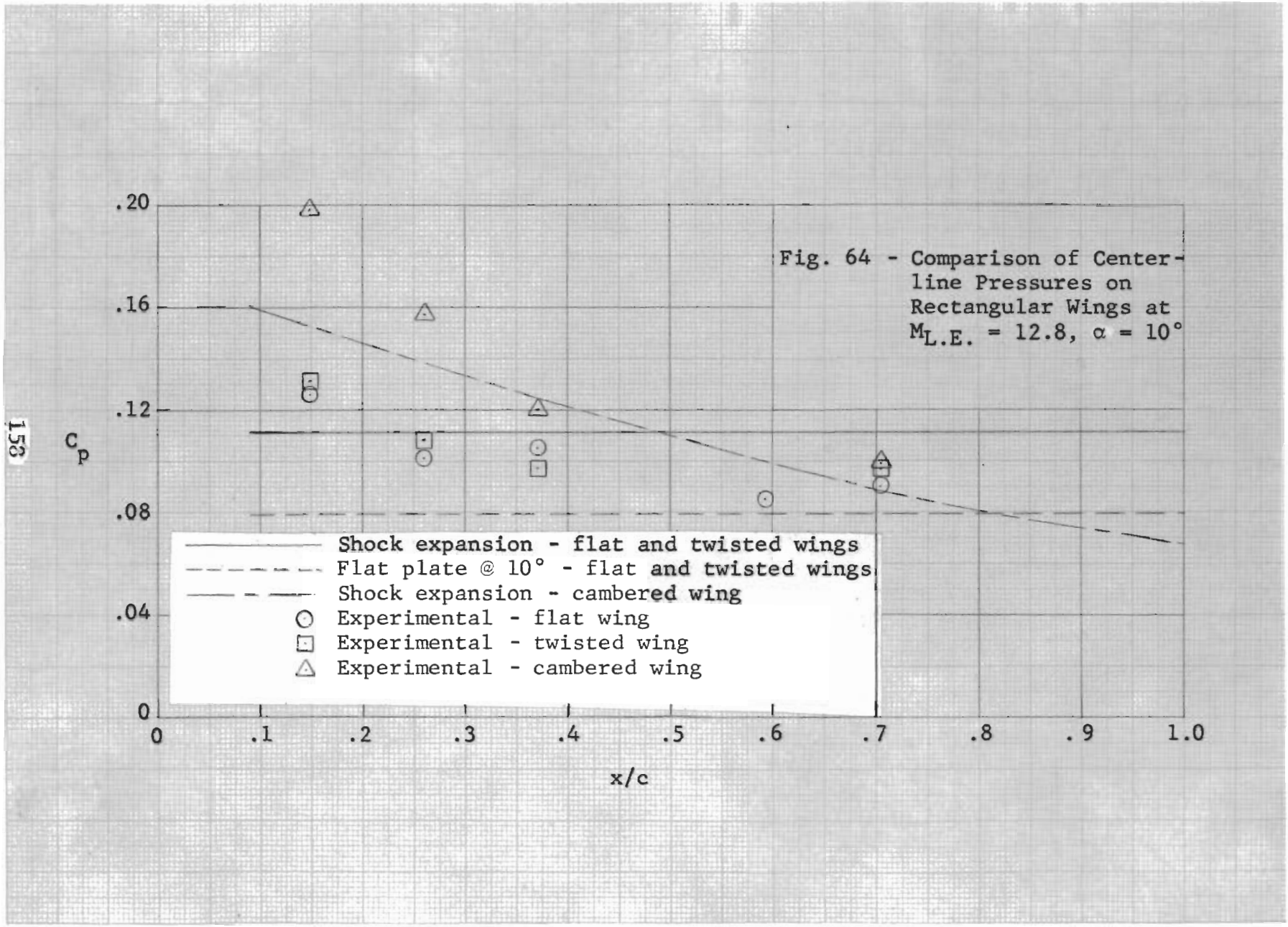

Fig. 64 - Comparison of Center-line Pressures on Rectangular Wings at $M_{L.E.} = 12.8$, $\alpha = 10°$

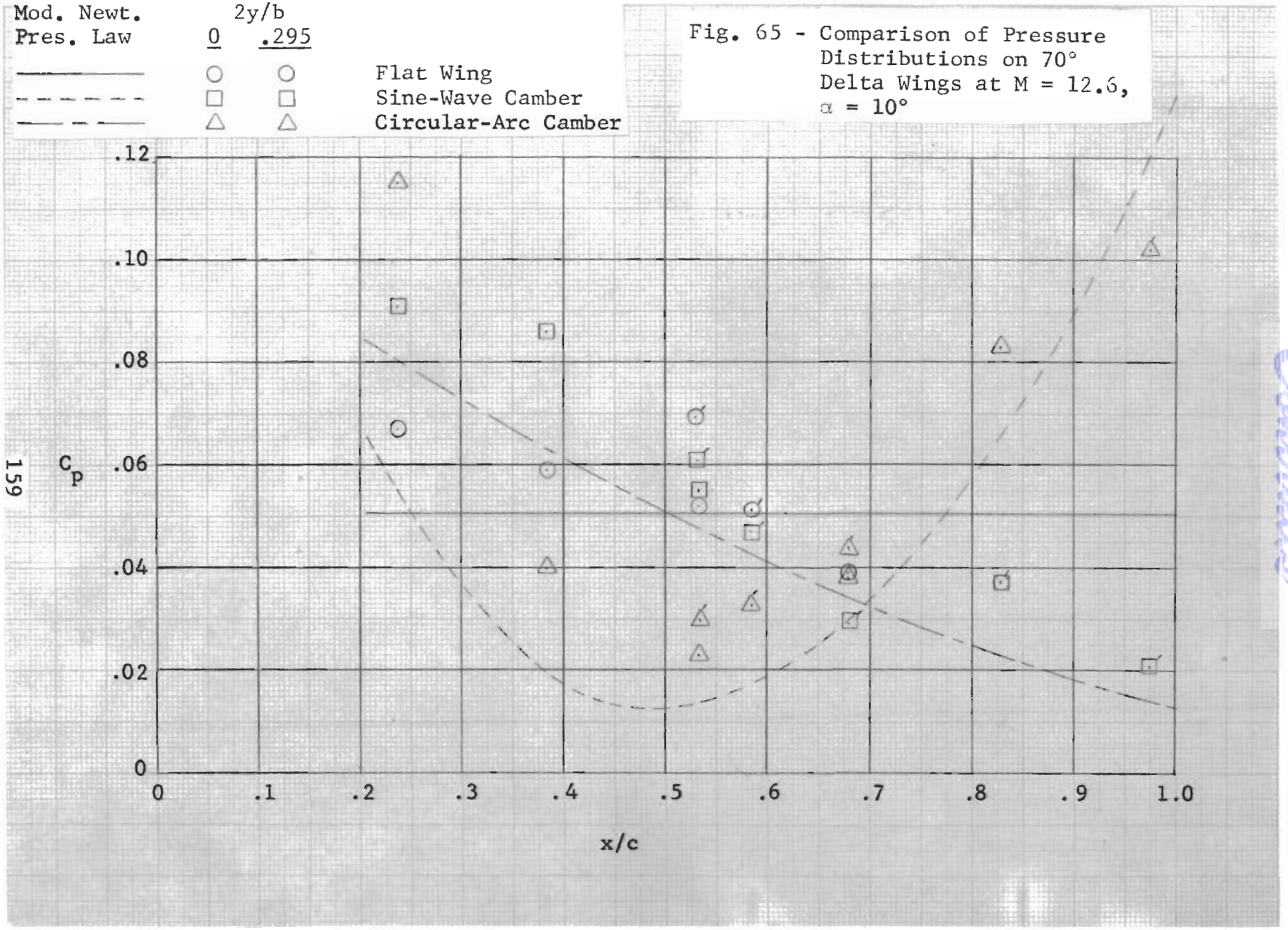

Fig. 65 - Comparison of Pressure Distributions on 70° Delta Wings at M = 12.6, α = 10°

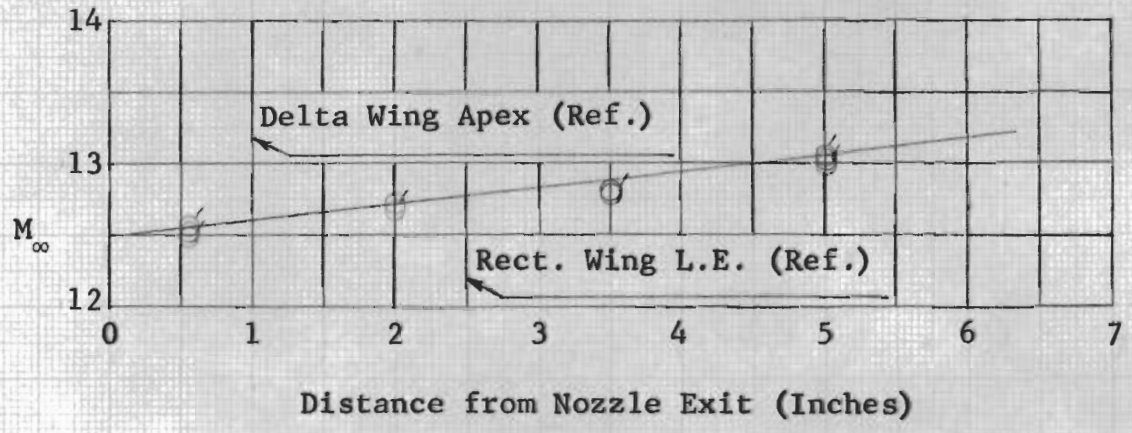

Fig. 66 - Free Stream Mach Number vs. Distance from Nozzle Exit for Initial Driver Pressure of 600 psi - M=12 Nozzle

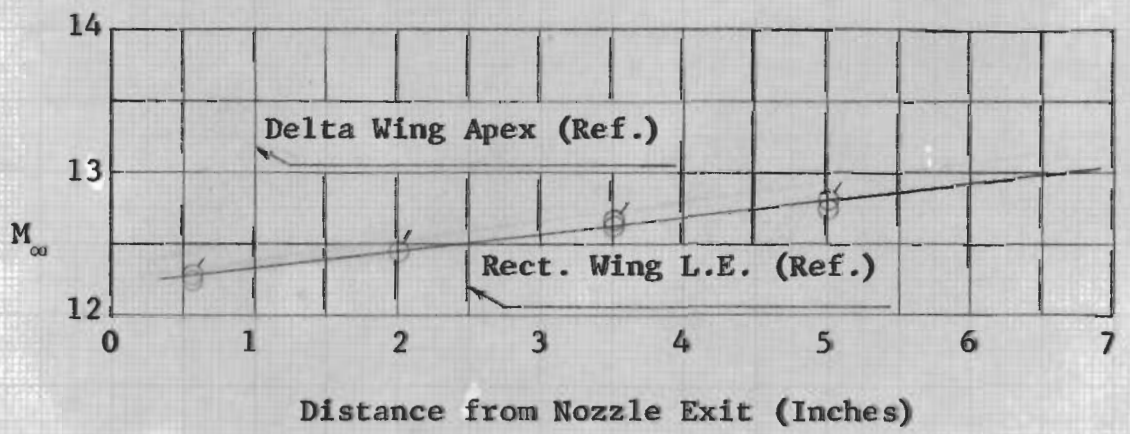

Fig. 67 - Free Stream Mach Number vs. Distance from Nozzle Exit for Initial Driver Pressure of 1200 psi - M=12 Nozzle

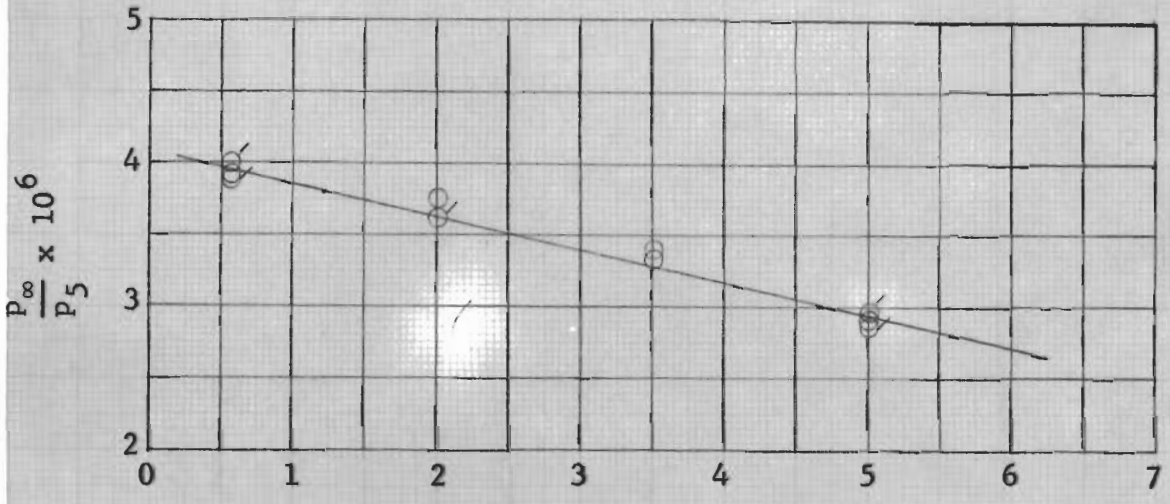

Fig. 68 - Ratio of Free-Stream Static Pressure to Tunnel Stagnation Pressure vs. Distance from Nozzle Exit for Initial Driver Pressure of 600 psi - M=12 Nozzle

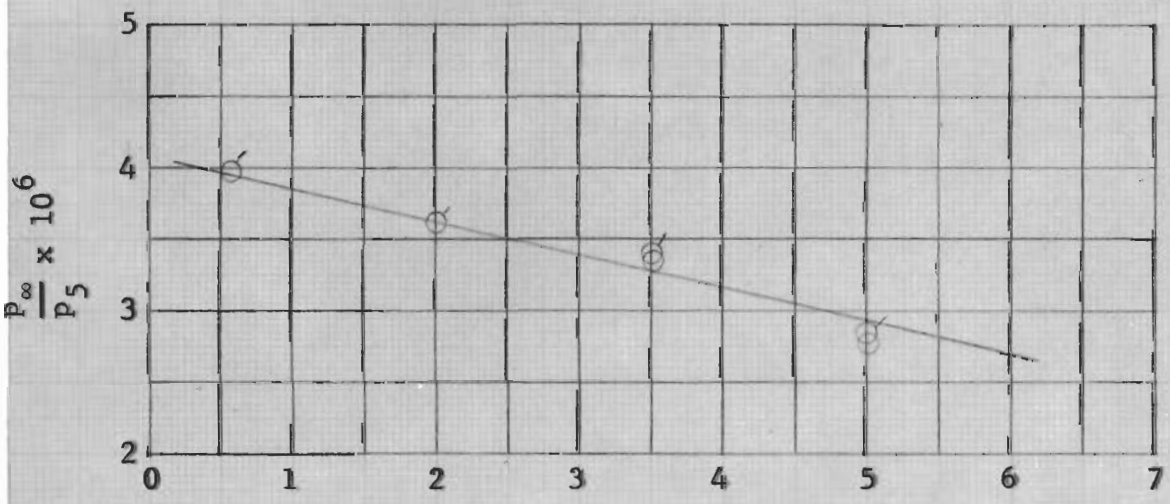

Fig. 69 - Ratio of Free-Stream Static Pressure to Tunnel Stagnation Pressure vs. Distance from Nozzle Exit for Initial Driver Pressure of 1200 psi - M=12 Nozzle

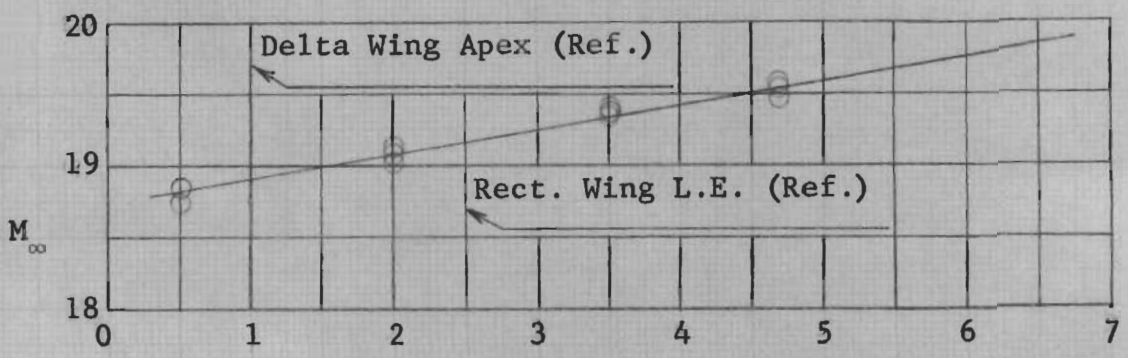

Fig. 70 - Free Stream Mach Number vs. Distance from Nozzle Exit for Initial Driver Pressure of 1300 psi - M=19 Nozzle

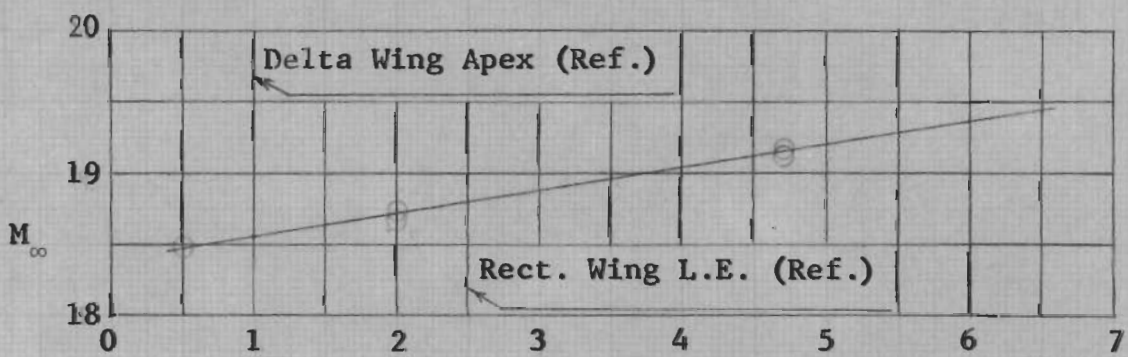

Fig. 71 - Free Stream Mach Number vs. Distance from Nozzle Exit for Initial Driver Pressure of 2000 psi - M=19 Nozzle

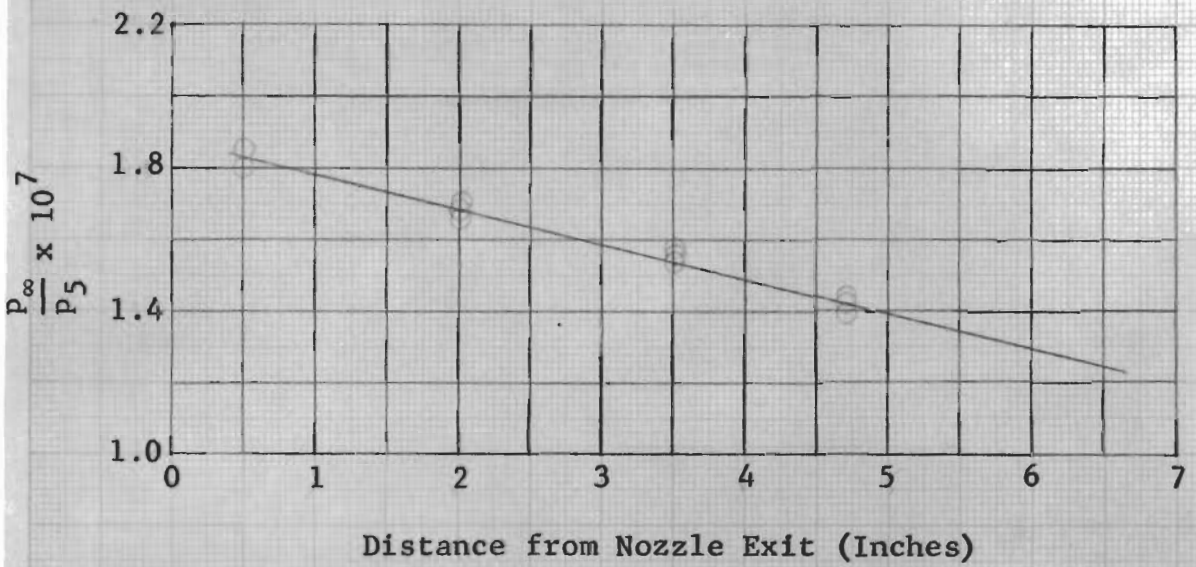

Fig. 72 - Ratio of Free-Stream Static Pressure to Tunnel Stagnation Pressure vs. Distance from Nozzle Exit for Initial Driver Pressure of 1300 psi - M=19 Nozzle

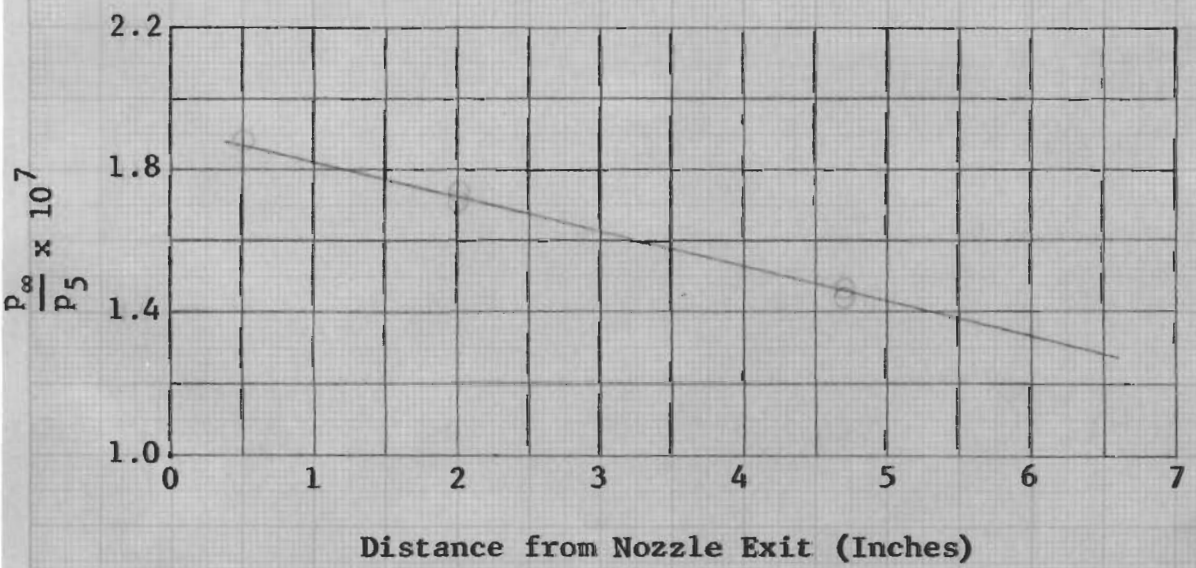

Fig. 73 - Ratio of Free-Stream Static Pressure to Tunnel Stagnation Pressure vs. Distance from Nozzle Exit for Initial Driver Pressure of 2000 psi - M=19 Nozzle

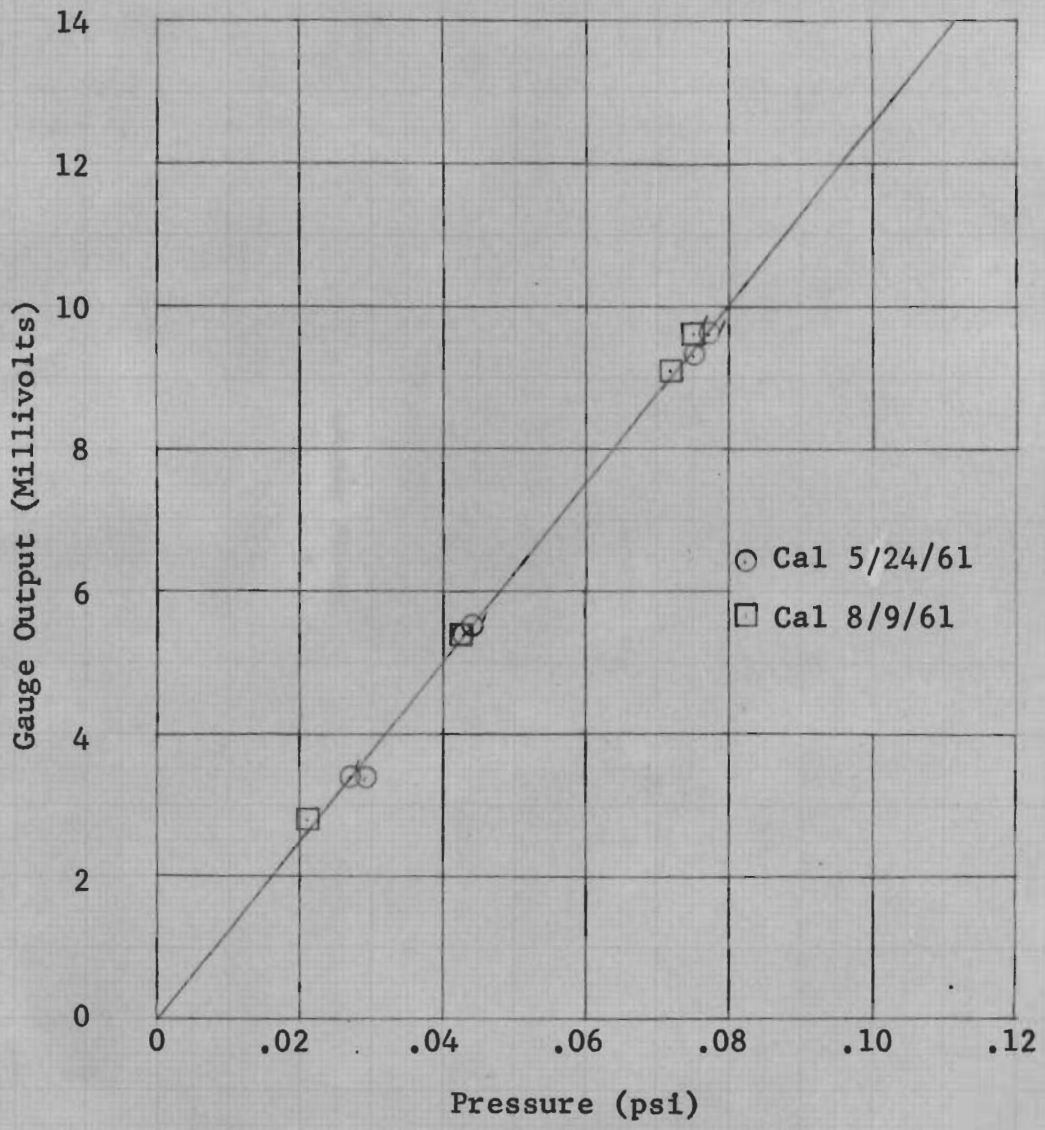

Fig. 74 - Typical Transducer Calibration